![U.S.NRC logo]

U.S.NRC

United States Nuclear Regulatory Commission

Protecting People and the Environment

Production and Testing of the VITAMIN-B7 Fine-Group and BUGLE-B7 Broad-Group Coupled Neutron/Gamma Cross-Section Libraries Derived from ENDF/B-VII.0 Nuclear Data

Office of Nuclear Reactor Regulation

AVAILABILITY OF REFERENCE MATERIALS
IN NRC PUBLICATIONS

NRC Reference Material

As of November 1999, you may electronically access NUREG-series publications and other NRC records at NRC's Public Electronic Reading Room at http://www.nrc.gov/reading-rm.html. Publicly released records include, to name a few, NUREG-series publications; *Federal Register* notices; applicant, licensee, and vendor documents and correspondence; NRC correspondence and internal memoranda; bulletins and information notices; inspection and investigative reports; licensee event reports; and Commission papers and their attachments.

NRC publications in the NUREG series, NRC regulations, and *Title 10, Energy*, in the Code of *Federal Regulations* may also be purchased from one of these two sources.
1. The Superintendent of Documents
   U.S. Government Printing Office
   Mail Stop SSOP
   Washington, DC 20402–0001
   Internet: bookstore.gpo.gov
   Telephone: 202-512-1800
   Fax: 202-512-2250
2. The National Technical Information Service
   Springfield, VA 22161–0002
   www.ntis.gov
   1–800–553–6847 or, locally, 703–605–6000

A single copy of each NRC draft report for comment is available free, to the extent of supply, upon written request as follows:
Address: U.S. Nuclear Regulatory Commission
          Office of Administration
          Publications Branch
          Washington, DC 20555-0001
E-mail: DISTRIBUTION.RESOURCE@NRC.GOV
Facsimile: 301–415–2289

Some publications in the NUREG series that are posted at NRC's Web site address http://www.nrc.gov/reading-rm/doc-collections/nuregs are updated periodically and may differ from the last printed version. Although references to material found on a Web site bear the date the material was accessed, the material available on the date cited may subsequently be removed from the site.

Non-NRC Reference Material

Documents available from public and special technical libraries include all open literature items, such as books, journal articles, and transactions, *Federal Register* notices, Federal and State legislation, and congressional reports. Such documents as theses, dissertations, foreign reports and translations, and non-NRC conference proceedings may be purchased from their sponsoring organization.

Copies of industry codes and standards used in a substantive manner in the NRC regulatory process are maintained at—
          The NRC Technical Library
          Two White Flint North
          11545 Rockville Pike
          Rockville, MD 20852–2738

These standards are available in the library for reference use by the public. Codes and standards are usually copyrighted and may be purchased from the originating organization or, if they are American National Standards, from—
          American National Standards Institute
          11 West 42nd Street
          New York, NY 10036–8002
          www.ansi.org
          212–642–4900

Legally binding regulatory requirements are stated only in laws; NRC regulations; licenses, including technical specifications; or orders, not in NUREG-series publications. The views expressed in contractor-prepared publications in this series are not necessarily those of the NRC.

The NUREG series comprises (1) technical and administrative reports and books prepared by the staff (NUREG–XXXX) or agency contractors (NUREG/CR–XXXX), (2) proceedings of conferences (NUREG/CP–XXXX), (3) reports resulting from international agreements (NUREG/IA–XXXX), (4) brochures (NUREG/BR–XXXX), and (5) compilations of legal decisions and orders of the Commission and Atomic and Safety Licensing Boards and of Directors' decisions under Section 2.206 of NRC's regulations (NUREG–0750).

Production and Testing of the VITAMIN-B7 Fine-Group and BUGLE-B7 Broad-Group Coupled Neutron/Gamma Cross-Section Libraries Derived from ENDF/B-VII.0 Nuclear Data

Prepared by
J. M. Risner, D. Wiarda, M. E. Dunn, T. M. Miller
D. E. Peplow, and B. W. Patton

Oak Ridge National Laboratory
Managed by UT-Battelle, LLC
Oak Ridge, TN 37831-6170

Bernard L. Grenier, NRC Project Manager

Office of Nuclear Reactor Regulation

ABSTRACT

New coupled neutron-gamma cross-section libraries have been developed for use in light water reactor (LWR) shielding applications, including pressure vessel dosimetry calculations. The libraries, which were generated using Evaluated Nuclear Data File/B Version VII Release 0 (ENDF/B-VII.0), use the same fine-group and broad-group energy structures as the VITAMIN-B6 and BUGLE-96 libraries. The processing methodology used to generate both libraries is based on the methods used to develop VITAMIN-B6 and BUGLE-96 and is consistent with ANSI/ANS 6.1.2. The ENDF data were first processed into the fine-group pseudo-problem-independent VITAMIN-B7 library and then collapsed into the broad-group BUGLE-B7 library. The VITAMIN-B7 library contains data for 391 nuclides. This represents a significant increase compared to the VITAMIN-B6 library, which contained data for 120 nuclides. The BUGLE-B7 library contains data for the same nuclides as BUGLE-96, and maintains the same numeric IDs for those nuclides. The broad-group data includes nuclides which are infinitely dilute and group collapsed using a concrete weighting spectrum, as well as nuclides which are self-shielded and group collapsed using weighting spectra representative of important regions of LWRs. The verification and validation of the new libraries includes a set of critical benchmark experiments, a set of regression tests that are used to evaluate multigroup cross-section libraries in the SCALE code system, and three pressure vessel dosimetry benchmarks. Results of these tests confirm that the new libraries are appropriate for use in LWR shielding analyses and meet the requirements of Regulatory Guide 1.190.

CONTENTS

CONTENTS (continued)

CONTENTS (continued)

LIST OF FIGURES

LIST OF FIGURES (continued)

LIST OF TABLES

LIST OF TABLES (continued)

ACKNOWLEDGMENTS

LIST OF ACRONYMS AND UNITS

1D	one-dimensional
ANS	American Nuclear Society
BWR	boiling water reactor
CSEWG	Cross-Section Evaluation Working Group
DORT	discrete-ordinates radiation transport
ENDF/B-VII	Version VII of the U.S. Evaluated Nuclear Data File
HBR-2	H. B. Robinson Unit 2
ICSBEP	International Handbook of Evaluated Criticality Safety Benchmark Experiments
IRDF	International Reactor Dosimetry File
LWR	light water reactor
MTR	material test reactor
NNDC	National Nuclear Data Center
ORNL	Oak Ridge National Laboratory
PCA	Pool Critical Assembly
PVWBF	pressure vessel wall benchmark facility
PWR	pressurized water reactor
SCALE	Standardized Computer Analyses for Licensing Evaluation
SGGP	SCALE Generalized Geometry Package
SNLRMLS	Sandia National Laboratories Radiation Metrology Laboratory

1 INTRODUCTION

This report describes the production and testing of revised multigroup cross-section libraries for light water reactor (LWR) shielding applications, including pressure vessel dosimetry. The new libraries, which are updates of the widely used VITAMIN-B6 and BUGLE-96 libraries [1], are based on Release 0 of ENDF/B-VII data [2]. The fine-group library, which is designated VITAMIN-B7, was prepared by processing ENDF/B-VII data into the group structure used in the VITAMIN-B6 library (199 neutron groups and 47 gamma groups). The fine-group library was then collapsed into the broad-group BUGLE-B7 library using the same group structure as BUGLE-96 (47 neutron groups and 20 gamma groups) with fine-group weighting spectra representative of various regions of pressurized water reactors (PWRs) and boiling water reactors (BWRs).

VITAMIN-B7 and BUGLE-B7 are available in AMPX and ANISN formats, respectively, for use in a range of multigroup deterministic and stochastic radiation transport codes. Although these libraries were developed primarily for use in LWR shielding applications, they may potentially be used for other types of analyses provided they are validated in an appropriate manner.

1.1   Background

Multigroup cross-section libraries used in radiation transport calculations can be generally categorized as fine group or broad group. Fine-group libraries include a sufficient number of groups such that differences between the flux spectrum used to produce the groupwise cross sections and the actual flux spectra in a given application have a negligible effect on the multigroup data. Fine-group libraries typically contain hundreds of energy groups. Broad-group libraries, which typically contain tens of groups, are produced by collapsing fine-group data using flux spectra that closely approximate the spectra that are encountered in a particular application. A broad-group library that is developed using appropriate weighting spectra for a given application can produce calculated fluxes more quickly with little loss in accuracy compared to a fine-group calculation.

As computing resources become more powerful, it is possible to use fine-group libraries more routinely. However, broad-group libraries are still useful, especially as two-dimensional models become more detailed and three-dimensional models are more commonly used. Furthermore, broad-group libraries are well-suited to parametric studies, where a large number of calculations may be run for a given model.

1.1.1   VITAMIN Libraries

The VITAMIN (Versatile Integrated Techniques using AMPX and MINX for Investigating Neutronics) multigroup cross-section library concept was originally developed to provide users of radiation transport codes with fine-group cross sections from which application-specific libraries (typically with broader energy group structures) could be derived. Temperature and resonance self-shielding corrections were provided for by including Bondarenko shielding factors in the library over a range of background cross sections.

The first VITAMIN library, VITAMIN-C [3], was produced in 1978 based on ENDF/B-IV data. The MINX [4] code system (which was the predecessor to NJOY [5]) was used to produce the neutron transport cross sections, and the AMPX [6] code system was used to produce the photon production and transport cross sections. The VITAMIN-C library contains 171 neutron

groups and 36 gamma groups. While the primary applications for which VITAMIN-C was developed were fusion and liquid-metal fast breeder reactor neutronics studies, the library was also applied to LWR shielding and RPV dosimetry applications, shipping cask design, shielding benchmarks, and air transport analyses. VITAMIN-C was released through the Radiation Shielding Information Computational Center (RSICC, which at the time was known as RSIC) as DLC-041.

The next VITAMIN library was VITAMIN-E [7], with the "E" designation representing the alphabetic equivalent of the fifth version of ENDF/B (i.e., ENDF/B-V), which was the primary source of evaluated data used to produce VITAMIN-E. Like VITAMIN-C, VITAMIN-E was generated using MINX and AMPX. The energy group structure was a slight refinement of the VITAMIN-C structure, with 174 neutron groups and 38 gamma groups. VITAMIN-E was released through RSIC as DLC-113 in 1987.

The VITAMIN-B6 library, based primarily on ENDF/B-VI Release 3, was released through RSICC as DLC-184 in 1994. The ENDF data were processed with NJOY and converted to AMPX master library format with the AMPX SMILER module. The VITAMIN-B6 group structure has 199 neutron groups and 47 photon groups. The 199 neutron groups are based on a combination of the 175 groups in VITAMIN-J (a European library based on the VITAMIN-C and VITAMIN-E structures) and the 27 groups in the SCALE [8] shielding library, with the VITAMIN-J boundaries at higher energies used when the energy values differed slightly between the VITAMIN-J and SCALE libraries. The thermal energy range, which extends to 5.043 eV, contains 36 neutron groups with upscattering. The 47 photon groups are based on a combination of the 42 photon groups in VITAMIN-J and the 18 groups in the SCALE shielding library.

1.1.2 BUGLE Libraries

The first broad-group library in the BUGLE (Broad User Group Library ENDF/B) series was created based on methodology that was being developed by the ANS 6.1 Working Group in the late 1970s. The BUGLE library, which contains 45 neutron groups and 16 gamma groups, was derived from VITAMIN-C and released through RSIC as DLC-047. Initial experience with the BUGLE library revealed that the energy group structure and the weighting technique for collapsing the fine-group library to the broad-group library were inadequate.

A new library, BUGLE-80 [9], was then developed from the same fine-group data. BUGLE-80 increased the number of energy groups to 47 neutron groups and 20 gamma groups. Specific changes were made for neutron energies above 10 MeV, in the vicinity of the 2.3-MeV minimum in the oxygen cross section and near the 25-keV minimum in the iron cross section. In addition, groups were added in the energy region below 5 eV, but no upscattering transfers were included in the thermal range. BUGLE-80 was released through RSIC as DLC-075. Following the release of BUGLE-80, the SAILOR (Shielded and Application Independent Libraries for Operating Reactors) library [10] was developed based on the analysis of pressure vessel neutron fluence levels in specific LWRs. SAILOR used the same group structure as BUGLE-80 but employed five distinct weighting spectra rather than the single energy spectrum weighting approach of BUGLE and BUGLE-80. SAILOR was released through RSIC as DLC-076, and was widely used by industry for RPV fluence calculations.

The BUGLE-96 library was developed from VITAMIN-B6 using the same multiple-weighting-spectra technique that was applied in the SAILOR library. BUGLE-96 also added cross-section sets having upscatter data for four thermal groups. The addition of the upscatter data was

intended to improve the application of BUGLE-96 for problems which require a more accurate calculation of thermal fluxes, including thermal foils in RPV surveillance capsules. BUGLE-96 also added new dosimetry response functions and kerma factors.

1.2   Evaluated Nuclear Data Files

Version VII of the U.S. Evaluated Nuclear Data File (ENDF/B-VII) was released in December 2006. Reference [2] lists the principal improvements in ENDF/B-VII relative ENDF/B-VI. Among those improvements, the following are potentially significant with respect to cross sections used for LWR shielding applications:

1. New evaluations for U, Pu, Th, Np, and Am
2. More precise standard neutron reaction cross sections for H, ^{6}Li, ^{10}B, and Au, and more precise fission cross sections for ^{235}U and ^{238}U
3. Improved thermal neutron scattering
4. An extensive set of neutron cross sections for fission products
5. New light nucleus neutron reactions

Along with these changes to the evaluated data, the formatting for the gamma yield data has changed substantially for many newer evaluations, with data being moved from Files 12 and 13 to File 6.

Although these changes are not expected to be as significant for LWR shielding applications as were the improvements to the iron evaluation in ENDF/B-VI, the availability of multigroup libraries based on ENDF/B-VII provides users of multigroup transport codes the most up-to-date data and enables adherence to Regulatory Guide 1.190 [11].

1.3   Cross-Section Processing and Testing

The methodology used to create and test the VITAMIN-B7 and BUGLE-B7 cross-section libraries is consistent with ANSI/ANS-6.1.2 [12]. VITAMIN-B7 and BUGLE-B7 represent the first of the VITAMIN/BUGLE library series to be processed entirely (with the exception of neutron and gamma kerma factors) with the AMPX code system [13]. A detailed description of the processing of the fine-group library is provided in Chapter 2. Details of the processing of the broad-group BUGLE-B7 data from the fine-group library are provided in Chapter 3. Finally, the verification and validation studies that were completed for the new libraries are described in Chapter 4.

2 FINE-GROUP LIBRARY SPECIFICATIONS

2.1 Name

The fine-group pseudo-problem-independent library is designated as VITAMIN-B7. This continues the "VITAMIN" naming convention, which started with the ENDF/B-IV-based VITAMIN-C library and continued with the ENDF/B-V-based VITAMIN-E library and ENDF/B-VI-based VITAMIN-B6 library.

2.2 Materials, Temperatures, and Background Cross Sections

A set of 391 nuclides containing fast neutron data and 18 thermal evaluations were processed for the VITAMIN-B7 library. These nuclides are listed in Table 2.1 along with the corresponding ENDF MAT numbers and SCALE library IDs. For thermal evaluations the corresponding values for the coupled fast evaluations are also listed. The final library uses the SCALE IDs to be compatible with the SCALE code system. Note that although all the nuclides listed contain neutron interaction and photon interaction data, some evaluations do not contain gamma-ray production data.

All data are based on ENDF formatted files in the ENDF/B-VII.0 library downloaded from the National Nuclear Data Center at Brookhaven National Laboratory. Table 2.1 indicates those nuclides that are contained in the VITAMIN-B6 library as well as those in VITAMIN-B7. It should be noted that ENDF/B-VII.0 provides isotopic data for some elements for which previous ENDF/B releases included only elemental data. For example, the new VITAMIN-B7 library does not include elemental titanium (which was present in ENDF/B-VI), but does include ^{46}Ti, ^{47}Ti, ^{48}Ti, ^{49}Ti, and ^{50}Ti.

The Bondarenko (f-factor) method is used for resonance self-shielding and temperature effects. Bondarenko factors are produced for evaluations that have resolved and/or unresolved resonance parameters, unless the ENDF evaluation contains isotopic data in File 2 but only elemental data in File 3. For ENDF/B-VII, the only elements for which that combination occurs are vanadium (Z = 23) and zinc (Z = 30).

All materials for which Bondarenko factors are produced were processed at temperatures of 300, 600, 1000, and 2100 K. In most cases, background cross sections (which are typically referred to as σ_0) of 10^{10}, 10^6, 10^5, 10^4, 1000, 300, 100, 50, 10, and 1 barns were used. In some cases the cross sections calculated for low values of the background cross section can become negative. (See the discussion of the AMPX FABULOUS module in Section 2.6.1.4.) In these cases, the affected values (e.g., ^{147}Pm with a background cross section σ_0 of 1 b) have been eliminated from the master library. The available values for the background cross section for each nuclide are listed in Table 2.2.

In the case of thermal moderators with $S(\alpha,\beta)$ data, scattering matrices were produced at all temperatures given in the ENDF/B-VII.0 files.

2.3   Energy Group Structure

The energy group structure of the VITAMIN-B7 library is identical to that of the VITAMIN-B6 library, with 199 neutron groups and 42 gamma groups.

The neutron energy group structure has an upper energy limit of 19.64 MeV. The thermal neutron energy range (i.e., the range of groups that include upscatter) has an upper energy boundary of 5.043 eV and includes 36 groups. The neutron groups typically have uniform lethargy widths ranging from 0.025 to 0.25 for energies above 1.445 eV, with additional boundaries to resolve resonance minima that are important for shielding calculations.

The gamma energy group structure has an upper energy limit of 30 MeV. The energy range from 14 MeV to 30 MeV is covered by two groups. From 14 MeV to 8 MeV, the group widths are uniform at 2 MeV. From 8 MeV to 1 MeV, there are group boundaries every 500 keV, with some additional boundaries in the vicinity of important source energies. Below 1 MeV, the group widths decrease in a nearly monotonic fashion from 200 keV to 10 keV. The most narrow photon group is a 2-keV group that spans the positron annihilation photon energy of 511 keV.

The group boundaries for the neutron and gamma energy group structures are given in Table 2.3 and Table 2.4, respectively.

Note that additional problem-dependent libraries can be easily derived from VITAMIN-B7 without having to repeat the fine-group averaging from the ENDF files.

2.4   Weighting Function

The weighting function used to create the fine-group neutron library is a typical combination of a fission spectrum, a 1/E slowing-down spectrum, and a Maxwellian thermal spectrum. The specific functional forms and energy ranges of these three constituents of the neutron weighting spectrum are given by the following:

Energy range	VITAMIN-B7 groups	Functional form of weighting spectrum
820.8 keV–20.0 MeV	1–66	$W(E) = C_1\sqrt{E}e^{-E/\theta}$ C_1 = 2.5625 MeV$^{-1.5}$ θ = 1.273 MeV
0.125 eV–820.8 keV	67–87	$W(E) = 1/E$
10^{-5} eV–0.125 eV	187–199	$W(E) = C_3 E e^{-E/kT}$ C_3 = 9498.4 eV^{-2} kT = 0.025 eV

The neutron weighting function is shown in Figure 2.1.

The weighting spectrum used to create the fine-group photon library consists of a 1/E spectrum for energies between 100 keV and 10 MeV, with "roll-offs" below 100 keV to represent the effect of photoelectric absorption and above 10 MeV to represent the effect of pair production. The gamma weighting function is shown in Figure 2.2.

2.5 Legendre Order of Scattering

The scattering cross sections for both neutrons and photons are provided as Legendre polynomial expansions with P_7 order for nuclides with *Z* values up to 30 (Zn), and P_5 for *Z* values above 30. These expansion orders are consistent with the VITAMIN-B6 library. The lower expansion order for higher-Z nuclides is reasonable given the trend to reduced scattering anisotropy as Z values increase. Dosimetry calculations using discrete-ordinates transport codes often employ P_5 or P_3 scattering expansion. Thermal neutron scattering expansions are P_7 for moderators with $S(\alpha,\beta)$ data, but are limited to P_3 expansions for nuclides that use the free gas model.

Table 2.1. Nuclide data in the VITAMIN-B6 and VITAMIN-B7 libraries

Z	Nuclide[a]	VITAMIN-B6 nuclide ID	VITAMIN-B7 nuclide ID	MAT[b]	Scale ID	Gamma-ray production[c]
1	H-1		h1	125	1801	X
	H-1 (H_2O)	h1(h2o)	h1 / h_h2o	125 / 1	1001	X
	H-1 (CH_2)	h1(ch2)	h1 / h_ch2	125 / 37	1901	X
	H-1 (ZrH)		h1 / h_zrh	125 / 7	1701	X
	H-1 (benzine)		h1 / benzine	125 / 40	1601	X
	H-1 (liq CH_4)		h1 / l_ch4	125 / 33	1101	X
	H-1 (solid CH_4)		h1 / s_ch4	125 / 34	1201	X
	H-1 (ortho H)		h1 / ortho_h	125 / 3	1401	X
	H-1 (para H)		h1 / para_h	125 / 2	1501	X
	H-2		h2	128	1802	X
	H-2 (D_2O)	h2(d2o)	h2 / d_d2o	128 / 11	1002	X
	H-2 (ortho D)		h2 / ortho_d	128 / 13	1402	X
	H-2 (para D)		h2 / para_d	128 / 12	1502	X
	H-3	h3	h3	131	1003	
2	He-3	he3	he3	225	2003	
	He-4	he4	he4	228	2004	
3	Li-6	li6	li6	325	3006	X
	Li-7	li7	li7	328	3007	X
4	Be-7	be7	be7	419	4007	
	Be-9	be9	be9	425	4009	X
	Be-9 (Be metal)	be9(th)	be9 / be_metal	425 / 26	4309	X
	Be-9 (BeO)		be9 / be_beo	425 / 27	4509	X
5	B-10	b10	b10	525	5010	X
	B-11	b11	b11	528	5011	X
6	C	c		600	6012	X
	C		c	600	6000	X
	C (benzine)		c / benzine	600 / 40	6500	X
	C (graphite)	c (gph)	c / graphite	600 / 31	6312	X
7	N-14	n14	n14	725	7014	X
	N-15	n15	n15	728	7015	X
8	O-16	o16	o16	825	8016	X
	O-16 (BeO)		o16 / o_beo	825 / 28	8516	X
	O-17	o17	o17	828	8017	
9	F-19	f19	f19	925	9019	X
11	Na-22		na22	1122	11022	
	Na-23	na23	na23	1125	11023	X
12	Mg	mg		1200		X
	Mg-24		mg24	1225	12025	X
	Mg-25		mg25	1228	12025	X
13	Al-27	al27	al27	1325	13027	X
	Al-27 (Al-27)		al27 / al27	1325 / 45	13701	X
14	Si	si		1400	14000	
	Si-28		si28	1425	14028	X
	Si-29		si29	1428	14029	X
	Si-30		si30	1431	14030	

Table 2.1. Nuclide data in the VITAMIN-B6 and VITAMIN-B7 libraries

Z	Nuclide[a]	VITAMIN-B6 nuclide ID	VITAMIN-B7 nuclide ID	MAT[b]	Scale ID	Gamma-ray production[c]
15	P-31	p31	p31	1525	15031	X
16	S	s		1600	16000	X
	S-32	s32	s32	1625	16032	X
	S-33		s33	1628	16033	X
	S-34		s34	1631	16034	X
	S-36		s36	1637	16036	X
17	Cl	cl (nat)		1700	17000	X
	Cl-35		cl35	1725	17035	X
	Cl-37		cl37	1731	17037	X
18	Ar-36		ar36	1825	18036	
	Ar-38		ar38	1831	18038	
	Ar-40		ar40	1837	18040	
19	K	k		1900	19000	X
	K-39		k39	1925	19039	X
	K-40		k40	1928	19040	X
	K-41		k41	1931	19041	X
20	Ca	ca		2000	20000	X
	Ca-40		ca40	2025	20040	X
	Ca-42		ca42	2031	20042	X
	Ca-43		ca43	2034	20043	X
	Ca-44		ca44	2037	20044	X
	Ca-46		ca46	2043	20046	X
	Ca-48		ca48	2049	20048	X
21	Sc-45		sc45	2125	21045	X
22	Ti	ti		2200	22000	X
	Ti-46		ti46	2225	22046	X
	Ti-47		ti47	2228	22047	X
	Ti-48		ti48	2231	22048	X
	Ti-49		ti49	2234	22049	X
	Ti-50		ti50	2237	22050	X
23	V	v	v	2300	23000	X
24	Cr-50	cr50	cr50	2425	24050	X
	Cr-52	cr52	cr52	2431	24052	X
	Cr-53	cr53	cr53	2434	24053	X
	Cr-54	cr54	cr54	2437	24054	X
25	Mn-55	mn55	mn55	2525	25055	X
26	Fe-54	fe54	fe54	2625	26054	X
	Fe-56	fe56	fe56	2631	26056	X
	Fe-56 (Fe-56)		fe56 / fe56	2631 / 56	26701	X
	Fe-57	fe57	fe57	2634	26057	X
	Fe-58	fe58	fe58	2637	26058	X
27	Co-58m		co58m	2723	27601	

Table 2.1. Nuclide data in the VITAMIN-B6 and VITAMIN-B7 libraries

Z	Nuclide[a]	VITAMIN-B6 nuclide ID	VITAMIN-B7 nuclide ID	MAT[b]	Scale ID	Gamma-ray production[c]
28	Ni-58	ni58	ni58	2825	28058	X
	Ni-59		ni59	2828	28059	X
	Ni-60	ni60	ni60	2831	28060	X
	Ni-61	ni61	ni61	2834	28061	X
	Ni-62	ni62	ni62	2837	28062	X
	Ni-64	ni64	ni64	2843	28064	X
29	Cu63	cu63	cu63	2925	29063	X
	Cu65	cu65	cu65	2931	29065	X
30	Zn		zn	3000	30000	
31	Ga	ga		3100	31000	X
	Ga-69		ga69			
	Ga-71		ga71	3131	31071	
32	Ge-70		ge70	3225	32070	X
	Ge-72		ge72	3231	32072	X
	Ge-73		ge73	3234	32073	X
	Ge-74		ge74	3237	32074	X
	Ge-76		ge76	3243	32076	X
33	As-74		as74	3322	33074	X
	As-75		as75	3325	33075	X
34	Se-74		se74	3425	34074	
	Se-76		se76	3431	34076	
	Se-77		se77	3434	34077	
	Se-78		se78	3437	34078	
	Se-79		se79	3440	34079	
	Se-80		se80	3443	34080	
	Se-82		se82	3449	34082	
35	Br-79		br79	3525	35079	
	Br-81		br81	3531	35081	
36	Kr-78		kr78	3625	36078	
	Kr-80		kr80	3631	36080	
	Kr-82		kr82	3637	36082	
	Kr-83		kr83	3640	36083	
	Kr-84		kr84	3643	36084	
	Kr-85		kr85	3646	36085	X
	Kr-86		kr86	3649	36086	
37	Rb-85		rb85	3725	37085	
	Rb-86		rb86	3728	37086	X
	Rb-87		rb87	3731	37087	
38	Sr-84		sr84	3825	38084	X
	Sr-86		sr86	3831	38086	
	Sr-87		sr87	3834	38087	
	Sr-88		sr88	3837	38088	
	Sr-89		sr89	3840	38089	
	Sr-90		sr90	3843	38090	

Table 2.1. Nuclide data in the VITAMIN-B6 and VITAMIN-B7 libraries

Z	Nuclide[a]	VITAMIN-B6 nuclide ID	VITAMIN-B7 nuclide ID	MAT[b]	Scale ID	Gamma-ray production[c]
39	Y-89	y89	y89	3925	39089	X
	Y-90		y90	3928	39090	X
	Y-91		y91	3931	39091	
40	Zr	zr		4000	40000	
	Zr-90		zr90	4025	40090	X
	Zr-90 (ZrH)		zr90 / zr_zrh	4025 / 58	40790	X
	Zr-91		zr91	4028	40091	X
	Zr-91 (ZrH)		zr91 / zr_zrh	4028 / 58	40790	X
	Zr-92		zr92	4031	40092	X
	Zr-92 (ZrH)		zr92 / zr_zrh	4031 / 58	40790	X
	Zr-93		zr93	4034	40093	
	Zr-93 (ZrH)		zr93 / zr_zrh	4034 / 58	40790	
	Zr-94		zr94	4037	40094	X
	Zr-94 (ZrH)		zr94 / zr_zrh	4037 / 58	40790	X
	Zr-95		zr95	4040	40095	
	Zr-95 (ZrH)		zr95 / zr_zrh	4040 / 58	40790	
	Zr-96		zr96	4043	40096	X
	Zr-96 (ZrH)		zr96 / zr_zrh	4043 / 58	40790	X
41	Nb-93	nb93	nb93	4125	41093	X
	Nb-94		nb94	4128	41094	
	Nb-95		nb95	4131	41095	
42	Mo	mo		4200	42000	X
	Mo-92		mo92	4225	42092	X
	Mo-94		mo94	4231	42094	X
	Mo-95		mo95	4234	42095	X
	Mo-96		mo96	4237	42096	X
	Mo-97		mo97	4240	42097	X
	Mo-98		mo98	4243	42098	X
	Mo-99		mo99	4246	42099	
	Mo-100		mo100	4249	42100	
43	Tc-99		tc99	4325	43099	X
44	Ru-96		ru96	4425	44096	
	Ru-98		ru98	4431	44098	
	Ru-99		ru99	4434	44099	
	Ru-100		ru100	4437	44100	
	Ru-101		ru101	4440	44101	X
	Ru-102		ru102	4443	44102	
	Ru-103		ru103	4446	44103	
	Ru-104		ru104	4449	44104	
	Ru-105		ru105	4452	44105	
	Ru-106		ru106	4455	44106	
45	Rh-103		rh103	4525	45103	X
	Rh-105		rh105	4531	45105	

Table 2.1. Nuclide data in the VITAMIN-B6 and VITAMIN-B7 libraries

Z	Nuclide[a]	VITAMIN-B6 nuclide ID	VITAMIN-B7 nuclide ID	MAT[b]	Scale ID	Gamma-ray production[c]
46	Pd-102		pd102	4625	46102	X
	Pd-104		pd104	4631	46104	X
	Pd-105		pd105	4634	46105	X
	Pd-106		pd106	4637	46106	X
	Pd-107		pd107	4640	46107	
	Pd-108		pd108	4643	46108	X
	Pd-110		pd110	4649	46110	X
47	Ag-107	ag107	ag107	4725	47107	X
	Ag-109	ag109	ag109	4731	47109	X
	Ag-110m		ag110m	4735	47601	
	Ag-111		ag111	4737	47111	X
48	Cd	cd (nat)		4800	48000	
	Cd-106		cd106	4825	48106	X
	Cd-108		cd108	4831	48108	
	Cd-110		cd110	4837	48110	
	Cd-111		cd111	4840	48111	X
	Cd-112		cd112	4843	48112	
	Cd-113		cd113	4846	48113	
	Cd-114		cd114	4849	48114	
	Cd-115m		cd115m	4853	48601	X
	Cd-116		cd116	4855	48116	
49	In	in (nat)		4900	49000	
	In-113		in113	4925	49113	
	In-115		in115	4931	49115	
50	Sn	sn (nat)		5000	50000	
	Sn-112		sn112	5025	50112	
	Sn-113		sn113	5028	50113	X
	Sn-114		sn114	5031	50114	
	Sn-115		sn115	5034	50115	
	Sn-116		sn116	5037	50116	
	Sn-117		sn117	5040	50117	
	Sn-118		sn118	5043	50118	
	Sn-119		sn119	5046	50119	
	Sn-120		sn120	5049	50120	
	Sn-122		sn122	5055	50122	
	Sn-123		sn123	5058	50123	
	Sn-124		sn124	5061	50124	
	Sn-125		sn125	5064	50125	X
	Sn-126		sn126	5067	50126	
51	Sb-121		sb121	5125	51121	
	Sb-123		sb123	5131	51123	
	Sb-124		sb124	5134	51124	
	Sb-125		sb125	5137	51125	
	Sb-126		sb126	5140	51126	X

Table 2.1. Nuclide data in the VITAMIN-B6 and VITAMIN-B7 libraries

Z	Nuclide[a]	VITAMIN-B6 nuclide ID	VITAMIN-B7 nuclide ID	MAT[b]	Scale ID	Gamma-ray production[c]
52	Te-120		te120	5225	52120	
	Te-122		te122	5231	52122	
	Te-123		te123	5234	52123	
	Te-124		te124	5237	52124	
	Te-125		te125	5240	52125	
	Te-126		te126	5243	52126	
	Te-127m		te127m	5247	52601	
	Te-128		te128	5249	52128	
	Te-129m		te129m	5253	52611	
	Te-130		te130	5255	52130	
	Te-132		te132	5261	52132	X
53	I-127		i127	5325	53127	X
	I-129		i129	5331	53129	
	I-130		i130	5334	53130	X
	I-131		i131	5337	53131	
	I-135		i135	5349	53135	
54	Xe-123		xe123	5422	54123	
	Xe-124		xe124	5425	54124	
	Xe-126		xe126	5431	54126	
	Xe-128		xe128	5437	54128	
	Xe-129		xe129	5440	54129	
	Xe-130		xe130	5443	54130	
	Xe-131		xe131	5446	54131	X
	Xe-132		xe132	5449	54132	
	Xe-133		xe133	5452	54133	
	Xe-134		xe134	5455	54134	
	Xe-135		xe135	5458	54135	
	Xe-136		xe136	5461	54136	
55	Cs-133		cs133	5525	55133	X
	Cs-134		cs134	5528	55134	
	Cs-135		cs135	5531	55135	
	Cs-136		cs136	5534	55136	
	Cs-137		cs137	5537	55137	
56	Ba-130		ba130	5625	56130	
	Ba-132		ba132	5631	56132	
	Ba-133		ba133	5634	56133	X
	Ba-134		ba134	5637	56134	
	Ba-135		ba135	5640	56135	
	Ba-136		ba136	5643	56136	
	Ba-137		ba137	5646	56137	
	Ba-138	ba138	ba138	5649	56138	
	Ba-140		ba139	5655	56140	
57	La-138		la138	5725	57138	
	La-139		la139	5728	57139	
	La-140		la140	5731	57140	X

Table 2.1. Nuclide data in the VITAMIN-B6 and VITAMIN-B7 libraries

Z	Nuclide[a]	VITAMIN-B6 nuclide ID	VITAMIN-B7 nuclide ID	MAT[b]	Scale ID	Gamma-ray production[c]
58	Ce-136		cd136	5825	58136	X
	Ce-138		ce138	5831	58138	X
	Ce-139		ce139	5834	58139	X
	Ce-140		ce140	5837	58140	
	Ce-141		ce141	5840	58141	
	Ce-142		ce142	5843	58142	
	Ce-143		ce143	5846	58143	X
	Ce-144		ce144	5849	58144	
59	Pr-141		pr141	5925	59141	X
	Pr-142		pr142	5928	59142	X
	Pr-143		pr143	5931	59143	
60	Nd-142		nd142	6025	60142	X
	Nd-143		nd143	6028	60143	X
	Nd-144		nd144	6031	60144	X
	Nd-145		nd145	6034	60145	X
	Nd-146		nd146	6037	60146	X
	Nd-147		nd147	6040	60147	X
	Nd-148		nd148	6043	60148	X
	Nd-150		nd150	6049	60150	X
61	Pm-147		pm147	6149	61147	
	Pm-148		pm148	6152	61148	
	Pm-148m		pm148m	6153	61601	
	Pm-149		pm149	6155	61149	
	Pm-151		pm151	6161	61151	X
62	Sm-144		sm144	6225	62144	X
	Sm-147		sm147	6234	62147	X
	Sm-148		sm148	6237	62148	X
	Sm-149		sm149	6240	62149	X
	Sm-150		sm150	6243	62150	X
	Sm-151		sm151	6246	62151	X
	Sm-152		sm152	6249	62152	X
	Sm-153		sm153	6252	62153	X
	Sm-154		sm154	6255	62154	X
63	Eu-151	eu151	eu151	6325	63151	
	Eu-152	eu152	eu152	6328	63152	
	Eu-153	eu153	eu153	6331	63153	X
	Eu-154	eu154	eu154	6334	63154	
	Eu-155	eu155	eu155	6337	63155	
	Eu-156		eu156	6340	63156	
	Eu-157		eu157	6343	63157	X
64	Gd-152		gd152	6425	64152	X
	Gd-153		gd153	6428	64153	X
	Gd-154		gd154	6431	64154	X
	Gd-155		gd155	6434	64155	X
	Gd-156		gd156	6437	64156	X
	Gd-157		gd157	6440	64157	X
	Gd-158		gd158	6443	64158	X
	Gd-160		gd159	6449	64160	X

Table 2.1. Nuclide data in the VITAMIN-B6 and VITAMIN-B7 libraries

Z	Nuclide[a]	VITAMIN-B6 nuclide ID	VITAMIN-B7 nuclide ID	MAT[b]	Scale ID	Gamma-ray production[c]
65	Tb-159		tb159	6525	65159	
	Tb-160		tb160	6528	65160	X
66	Dy-156		dy156	6625	66156	X
	Dy-158		dy158	6631	66158	X
	Dy-160		dy160	6637	66160	X
	Dy-161		dy161	6640	66161	X
	Dy-162		dy162	6643	66162	X
	Dy-163		dy163	6646	66163	X
	Dy-164		dy164	6649	66164	X
67	Ho-165		ho165	6725	67165	X
	Ho-166m		ho166m	6729	67601	X
68	Er-162		er162	6825	68162	X
	Er-164		er164	6831	68164	X
	Er-166		er166	6837	68166	X
	Er-167		er167	6840	68167	X
	Er-168		er168	6843	68168	X
	Er-170		er170	6849	68170	X
71	Lu-175		lu175	7125	71175	
	Lu-176		lu176	7128	71176	
72	Hf-174	hf174	hf174	7225	72174	
	Hf-176	hf176	hf176	7231	72176	
	Hf-177	hf177	hf177	7234	72177	
	Hf-178	hf178	hf178	7237	72178	
	Hf-179	hf179	hf179	7240	72179	
	Hf-180	hf180	hf180	7243	72180	
73	Ta-181	ta181	ta181	7328	73181	X
	Ta-182	ta182	ta182	7331	73182	
74	W-182	w182	w182	7431	74182	X
	W-183	w183	w183	7434	74183	X
	W-184	w184	w184	7437	74184	X
	W-186	w186	w186	7443	74186	X
75	Re-185	re185	re185	7525	75185	
	Re-187	re187	re187	7531	75187	
77	Ir-191		ir191	7725	77191	X
	Ir-193		ir193	7731	77193	X
79	Au-197	au197	au197	7925	79197	X
80	Hg-196		hg196	8025	80196	X
	Hg-198		hg198	8031	80198	X
	Hg-199		hg199	8034	80199	X
	Hg-200		hg200	8037	80200	X
	Hg-201		hg201	8040	80201	X
	Hg-202		hg202	8043	80202	X
	Hg-204		hg204	8049	80204	X

15

Table 2.1. Nuclide data in the VITAMIN-B6 and VITAMIN-B7 libraries

Z	Nuclide[a]	VITAMIN-B6 nuclide ID	VITAMIN-B7 nuclide ID	MAT[b]	Scale ID	Gamma-ray production[c]
82	Pb-204		pb204	8225	82204	X
	Pb-206	pb206	pb206	8231	82206	X
	Pb-207	pb207	pb207	8234	82207	X
	Pb-208	pb208	pb208	8237	82208	X
83	Bi-209	bi209	bi209	8325	83209	X
88	Ra-223		ra223	8825	88223	
	Ra-224		ra224	8828	88224	
	Ra-225		ra225	8831	88225	
	Ra-226		ra226	8834	88226	
89	Ac-225		ac225	8925	89225	
	Ac-226		ac226	8928	89226	
	Ac-227		ac227	8931	89227	
90	Th-227		th227	9025	90227	
	Th-228		th228	9028	90228	
	Th-229		th229	9031	90229	
	Th-230	th230	th230	9034	90230	
	Th-232	th232	th232	9040	90232	X
	Th-233		th233	9043	90233	
	Th-234		th234	9046	90234	
91	Pa-231	pa231	pa231	9131	91231	X
	Pa-232		pa232	9134	91232	
	Pa-233	pa233	pa233	9137	91233	X
92	U-232	u232	u232	9219	92232	X
	U-233	u233	u233	9222	92233	X
	U-234	u234	u234	9225	92234	X
	U-235	u235	u235	9228	92235	X
	U-236	u236	u236	9231	92236	X
	U-237	u237	u237	9234	92237	X
	U-238	u238	u238	9237	92238	X
	U-239		u239	9240	92239	X
	U-240		u240	9243	92240	X
	U-241		u241	9246	92241	X
93	Np-235		np235	9340	93235	
	Np-236		np236	9343	93236	
	Np-237	np237	np237	9346	93237	X
	Np-238	np238	np238	9349	93238	
	Np-239	np239	np239	9352	93239	
94	Pu-236	pu236	pu236	9428	94236	
	Pu-237	pu237	pu237	9431	94237	
	Pu-238	pu238	pu238	9434	94238	
	Pu-239	pu239	pu239	9437	94239	X
	Pu-240	pu240	pu240	9440	94240	X
	Pu-241	pu241	pu241	9443	94241	X
	Pu-242	pu242	pu242	9446	94242	X
	Pu-243	pu243	pu243	9449	94243	X
	Pu-244	pu244	pu244	9452	94244	
	Pu-246		pu246	9458	94246	

Table 2.1. Nuclide data in the VITAMIN-B6 and VITAMIN-B7 libraries

Z	Nuclide[a]	VITAMIN-B6 nuclide ID	VITAMIN-B7 nuclide ID	MAT[b]	Scale ID	Gamma-ray production[c]
95	Am-241	am241	am241	9543	95241	X
	Am-242	am242	am242	9546	95242	
	Am-242m	am242m	am242m	9547	95601	
	Am-243	am243	am243	9549	95243	X
	Am-244		am244	9552	95244	
	Am-244m		am244m	9553	95611	
96	Cm-241	cm241	cm241	9628	96241	
	Cm-242	cm242	cm242	9631	96242	X
	Cm-243	cm243	cm243	9634	96243	
	Cm-244	cm244	cm244	9637	96244	
	Cm-245	cm245	cm245	9640	96245	
	Cm-246	cm246	cm246	9643	96246	
	Cm-247	cm247	cm247	9646	96247	
	Cm-248	cm248	cm248	9649	96248	X
	Cm-249		cm249	9652	96249	
	Cm-250		cm250	9655	96250	
97	Bk-249		bk249	9752	97249	
	Bk-250		bk250	9755	97250	
98	Cf-249		cf249	9852	98249	
	Cf-250		cf250	9855	98250	X
	Cf-251		cf251	9858	98251	X
	Cf-252		cf252	9861	98252	X
	Cf-253		cf253	9864	98253	
	Cf-254		cf254	9867	98254	
99	Es-253		es253	9913	99253	
	Es-254		es254	9914	99254	
	Es-255		es255	9915	99255	
100	Fm-255		fm255	9936	100255	

[a] For nuclides with thermal moderator data, the nuclide ID for the fast evaluation is given, followed by the nuclide ID for the moderator.

[b] For thermal moderators the ENDF MAT number for the moderator is given followed by the ENDF MAT number of the fast evaluation.

[c] For nuclides with thermal moderator data, the nuclide ID for the fast evaluation is given, followed by the nuclide ID for the moderator.

Table 2.2. Background cross-section values at which Bondarenko factors are tabulated in the Vitamin-B7 library

(All nuclides were processed at 300, 600, 1000 and 2100 K)

Nuclide[a]	Background cross sections (barns)										Legendre order
	10^{10}	10^6	10^5	10^4	1000	300	100	50	10	1	
H-1	X	X	X	X	X	X	X	X	X	X	7
H-1 (H_2O)	X	X	X	X	X	X	X	X	X	X	7
H-1 (CH_2)	X	X	X	X	X	X	X	X	X	X	7
H-1 (ZrH)	X	X	X	X	X	X	X	X	X	X	7
H-1 (benzine)	X	X	X	X	X	X	X	X	X	X	7
H-1 (liq CH_4)	X	X	X	X	X	X	X	X	X	X	7
H-1 (solid CH_4)	X	X	X	X	X	X	X	X	X	X	7
H-1 (ortho H)	X	X	X	X	X	X	X	X	X	X	7
H-1 (para H)	X	X	X	X	X	X	X	X	X	X	7
H-2	X	X	X	X	X	X	X	X	X	X	7
H-2 (D_2O)	X	X	X	X	X	X	X	X	X	X	7
H-2 (ortho D)	X	X	X	X	X	X	X	X	X	X	7
H-2 (para D)	X	X	X	X	X	X	X	X	X	X	7
H-3	X	X	X	X	X	X	X	X	X	X	7
He-3	X	X	X	X	X	X	X	X	X	X	7
He-4	X	X	X	X	X	X	X	X	X	X	7
Li-6	X	X	X	X	X	X	X	X	X	X	7
Li-7	X	X	X	X	X	X	X	X	X	X	7
Be-7	X	X	X	X	X	X	X	X	X	X	7
Be-9	X	X	X	X	X	X	X	X	X	X	7
Be-9 (Be metal)	X	X	X	X	X	X	X	X	X	X	7
Be-9 (BeO)	X	X	X	X	X	X	X	X	X	X	7
B10	X	X	X	X	X	X	X	X	X	X	7
B11	X	X	X	X	X	X	X	X	X	X	7
C	X	X	X	X	X	X	X	X	X	X	7
C (benzene)	X	X	X	X	X	X	X	X	X	X	7
C (graphite)	X	X	X	X	X	X	X	X	X	X	7
N-14	X	X	X	X	X	X	X	X	X	X	7
N-15	X	X	X	X	X	X	X	X	X	X	7
O-16	X	X	X	X	X	X	X	X	X	X	7
O-16 (BeO)	X	X	X	X	X	X	X	X	X	X	7
O-17	X	X	X	X	X	X	X	X	X	X	7
F-19	X	X	X	X	X	X	X	X	X	X	7
Na-23	X	X	X	X	X	X	X	X	X	X	7
Mg-24	X	X	X	X	X	X	X	X	X	X	7
Mg-25	X	X	X	X	X	X	X	X	X	X	7
Mg-26	X	X	X	X	X	X	X	X	X	X	7
Al-27	X	X	X	X	X	X	X	X	X	X	7
Al-27 (Al-27)	X	X	X	X	X	X	X	X	X	X	7
Si-28	X	X	X	X	X	X	X	X	X	X	7
Si-29	X	X	X	X	X	X	X	X	X	X	7
Si-30	X	X	X	X	X	X	X	X	X	X	7
P-31	X	X	X	X	X	X	X	X	X	X	7
S-32	X	X	X	X	X	X	X	X	X	X	7
S-33	X	X	X	X	X	X	X	X	X	X	7
S-34	X	X	X	X	X	X	X	X	X	X	7
S-36	X	X	X	X	X	X	X	X	X	X	7

Table 2.2. Background cross-section values at which Bondarenko factors are tabulated in the Vitamin-B7 library

(All nuclides were processed at 300, 600, 1000 and 2100 K)

Nuclide[a]	Background cross sections (barns)										Legendre order
	10^{10}	10^6	10^5	10^4	1000	300	100	50	10	1	
Cl-35	X	X	X	X	X	X	X	X	X	X	7
Cl-37	X	X	X	X	X	X	X	X	X	X	7
Ar-36	X	X	X	X	X	X	X	X	X	X	7
Ar-38	X	X	X	X	X	X	X	X	X	X	7
Ar-40	X	X	X	X	X	X	X	X	X	X	7
K-39	X	X	X	X	X	X	X	X	X	X	7
K-40	X	X	X	X	X	X	X	X	X	X	7
K-41	X	X	X	X	X	X	X	X	X	X	7
Ca-40	X	X	X	X	X	X	X	X	X	X	7
Ca-42	X	X	X	X	X	X	X	X	X	X	7
Ca-43	X	X	X	X	X	X	X	X	X	X	7
Ca-44	X	X	X	X	X	X	X	X	X	X	7
Ca-46	X	X	X	X	X	X	X	X	X	X	7
Ca-48	X	X	X	X	X	X	X	X	X	X	7
Sc-45	X	X	X	X	X	X	X	X	X	X	7
Ti-46	X	X	X	X	X	X	X	X	X	X	7
Ti-47	X	X	X	X	X	X	X	X	X	X	7
Ti-48	X	X	X	X	X	X	X	X	X	X	7
Ti-49	X	X	X	X	X	X	X	X	X	X	7
Ti-50	X	X	X	X	X	X	X	X	X	X	7
V											7
Cr-50	X	X	X	X	X	X	X	X	X	X	7
Cr-52	X	X	X	X	X	X	X	X	X	X	7
Cr-53	X	X	X	X	X	X	X	X	X	X	7
Cr-54	X	X	X	X	X	X	X	X	X	X	7
Mn-55	X	X	X	X	X	X	X	X	X	X	7
Fe-54	X	X	X	X	X	X	X	X	X	X	7
Fe-56	X	X	X	X	X	X	X	X	X	X	7
Fe-56 (Fe-56)	X	X	X	X	X	X	X	X	X	X	7
Fe-57	X	X	X	X	X	X	X	X	X	X	7
Fe-58	X	X	X	X	X	X	X	X	X	X	7
Co-58m	X	X	X	X	X	X	X	X	X	X	7
Co-59	X	X	X	X	X	X	X	X	X	X	7
Ni-58	X	X	X	X	X	X	X	X	X	X	7
Ni-59	X	X	X	X	X	X	X	X	X	X	7
Ni-60	X	X	X	X	X	X	X	X	X	X	7
Ni-61	X	X	X	X	X	X	X	X	X	X	7
Ni-62	X	X	X	X	X	X	X	X	X	X	7
Ni-64	X	X	X	X	X	X	X	X	X	X	7
Cu-63	X	X	X	X	X	X	X	X	X	X	7
Cu-65	X	X	X	X	X	X	X	X	X	X	7
Zn											7
Ga-69	X	X	X	X	X	X	X	X	X	X	5
Ga-71	X	X	X	X	X	X	X	X	X	X	5
Ge-70	X	X	X	X	X	X	X	X	X	X	5
Ge-72	X	X	X	X	X	X	X	X	X	X	5
Ge-73	X	X	X	X	X	X	X	X	X	X	5

Table 2.2. Background cross-section values at which Bondarenko factors are tabulated in the Vitamin-B7 library

(All nuclides were processed at 300, 600, 1000 and 2100 K)

Nuclide[a]	Background cross sections (barns)										Legendre order
	10^{10}	10^6	10^5	10^4	1000	300	100	50	10	1	
Ge-74	X	X	X	X	X	X	X	X	X	X	5
Ge-76	X	X	X	X	X	X	X	X	X	X	5
As-74	X	X	X	X	X	X	X	X	X	X	5
As-75	X	X	X	X	X	X	X	X	X	X	5
Se-74	X	X	X	X	X	X	X	X	X	X	5
Se-76	X	X	X	X	X	X	X	X	X	X	5
Se-77	X	X	X	X	X	X	X	X	X	X	5
Se-78	X	X	X	X	X	X	X	X	X	X	5
Se-79	X	X	X	X	X	X	X	X	X	X	5
Se-80	X	X	X	X	X	X	X	X	X	X	5
Se-82	X	X	X	X	X	X	X	X	X	X	5
Br-79	X	X	X	X	X	X	X	X	X	X	5
Br-81	X	X	X	X	X	X	X	X	X	X	5
Kr-78	X	X	X	X	X	X	X	X	X	X	5
Kr-80	X	X	X	X	X	X	X	X	X	X	5
Kr-82	X	X	X	X	X	X	X	X	X	X	5
Kr-83	X	X	X	X	X	X	X	X	X	X	5
Kr-84	X	X	X	X	X	X	X	X	X	X	5
Kr-85	X	X	X	X	X	X	X	X	X	X	5
Kr-86	X	X	X	X	X	X	X	X	X	X	5
Rb-85	X	X	X	X	X	X	X	X	X	X	5
Rb-86	X	X	X	X	X	X	X	X	X	X	5
Rb-87	X	X	X	X	X	X	X	X	X	X	5
Sr-84	X	X	X	X	X	X	X	X	X	X	5
Sr-86	X	X	X	X	X	X	X	X	X	X	5
Sr-87	X	X	X	X	X	X	X	X	X	X	5
Sr-88	X	X	X	X	X	X	X	X	X	X	5
Sr-89	X	X	X	X	X	X	X	X	X	X	5
Sr-90	X	X	X	X	X	X	X	X	X	X	5
Y-89	X	X	X	X	X	X	X	X	X	X	5
Y-90	X	X	X	X	X	X	X	X	X	X	5
Y-91	X	X	X	X	X	X	X	X	X	X	5
Zr-90	X	X	X	X	X	X	X	X	X	X	5
Zr-90 (ZrH)	X	X	X	X	X	X	X	X	X	X	5
Zr-91	X	X	X	X	X	X	X	X	X	X	5
Zr-91 (ZrH)	X	X	X	X	X	X	X	X	X	X	5
Zr-92	X	X	X	X	X	X	X	X	X	X	5
Zr-92 (ZrH)	X	X	X	X	X	X	X	X	X	X	5
Zr-93	X	X	X	X	X	X	X	X	X	X	5
Zr-93 (ZrH)	X	X	X	X	X	X	X	X	X	X	5
Zr-94	X	X	X	X	X	X	X	X	X	X	5
Zr-94 (ZrH)	X	X	X	X	X	X	X	X	X	X	5
Zr-95	X	X	X	X	X	X	X	X	X	X	5
Zr-95 (ZrH)	X	X	X	X	X	X	X	X	X	X	5
Zr-96	X	X	X	X	X	X	X	X	X	X	5
Zr-96 (ZrH)	X	X	X	X	X	X	X	X	X	X	5
Nb-93	X	X	X	X	X	X	X	X	X	X	5

Table 2.2. Background cross-section values at which Bondarenko factors are tabulated in the Vitamin-B7 library

(All nuclides were processed at 300, 600, 1000 and 2100 K)

Nuclide[a]	Background cross sections (barns)										Legendre order
	10^{10}	10^6	10^5	10^4	1000	300	100	50	10	1	
Nb-94	X	X	X	X	X	X	X	X	X	X	5
Nb-95	X	X	X	X	X	X	X	X	X	X	5
Mo-92	X	X	X	X	X	X	X	X	X	X	5
Mo-94	X	X	X	X	X	X	X	X	X	X	5
Mo-95	X	X	X	X	X	X	X	X	X	X	5
Mo-96	X	X	X	X	X	X	X	X	X	X	5
Mo-97	X	X	X	X	X	X	X	X	X	X	5
Mo-98	X	X	X	X	X	X	X	X	X	X	5
Mo-99	X	X	X	X	X	X	X	X	X	X	5
Mo-100	X	X	X	X	X	X	X	X	X	X	5
Tc-99	X	X	X	X	X	X	X	X	X	X	5
Ru-96	X	X	X	X	X	X	X	X	X	X	5
Ru-98	X	X	X	X	X	X	X	X	X	X	5
Ru-99	X	X	X	X	X	X	X	X	X	X	5
Ru-100	X	X	X	X	X	X	X	X	X	X	5
Ru-101	X	X	X	X	X	X	X	X	X	X	5
Ru-102	X	X	X	X	X	X	X	X	X	X	5
Ru-103	X	X	X	X	X	X	X	X	X	X	5
Ru-104	X	X	X	X	X	X	X	X	X	X	5
Ru-105	X	X	X	X	X	X	X	X	X	X	5
Ru-106	X	X	X	X	X	X	X	X	X	X	5
Rh-103	X	X	X	X	X	X	X	X	X	X	5
Rh-105	X	X	X	X	X	X	X	X	X	X	5
Pd-102	X	X	X	X	X	X	X	X	X	X	5
Pd-104	X	X	X	X	X	X	X	X	X	X	5
Pd-105	X	X	X	X	X	X	X	X	X	X	5
Pd-106	X	X	X	X	X	X	X	X	X	X	5
Pd-107	X	X	X	X	X	X	X	X	X	X	5
Pd-108	X	X	X	X	X	X	X	X	X	X	5
Pd-110	X	X	X	X	X	X	X	X	X	X	5
Ag-107	X	X	X	X	X	X	X	X	X	X	5
Ag-109	X	X	X	X	X	X	X	X	X	X	5
Ag-110m	X	X	X	X	X	X	X	X	X	X	5
Ag-111	X	X	X	X	X	X	X	X	X	X	5
Cd-106	X	X	X	X	X	X	X	X	X	X	5
Cd-108	X	X	X	X	X	X	X	X	X	X	5
Cd-110	X	X	X	X	X	X	X	X	X	X	5
Cd-111	X	X	X	X	X	X	X	X	X	X	5
Cd-112	X	X	X	X	X	X	X	X	X	X	5
Cd-113	X	X	X	X	X	X	X	X	X	X	5
Cd-114	X	X	X	X	X	X	X	X	X	X	5
Cd-115m	X	X	X	X	X	X	X	X	X	X	5
Cd-116	X	X	X	X	X	X	X	X	X	X	5
In-113	X	X	X	X	X	X	X	X	X	X	5
In-115	X	X	X	X	X	X	X	X	X	X	5
Sn-112	X	X	X	X	X	X	X	X	X	X	5
Sn-113	X	X	X	X	X	X	X	X	X	X	5

Table 2.2. Background cross-section values at which Bondarenko factors are tabulated in the Vitamin-B7 library

(All nuclides were processed at 300, 600, 1000 and 2100 K)

Nuclide[a]	Background cross sections (barns)										Legendre order
	10^{10}	10^6	10^5	10^4	1000	300	100	50	10	1	
Sn-114	X	X	X	X	X	X	X	X	X	X	5
Sn-115	X	X	X	X	X	X	X	X	X	X	5
Sn-116	X	X	X	X	X	X	X	X	X	X	5
Sn-117	X	X	X	X	X	X	X	X	X	X	5
Sn-118	X	X	X	X	X	X	X	X	X	X	5
Sn-119	X	X	X	X	X	X	X	X	X	X	5
Sn-120	X	X	X	X	X	X	X	X	X	X	5
Sn-122	X	X	X	X	X	X	X	X	X	X	5
Sn-123	X	X	X	X	X	X	X	X	X	X	5
Sn-124	X	X	X	X	X	X	X	X	X	X	5
Sn-125	X	X	X	X	X	X	X	X	X	X	5
Sn-126	X	X	X	X	X	X	X	X	X	X	5
Sb-121	X	X	X	X	X	X	X	X	X	X	5
Sb-123	X	X	X	X	X	X	X	X	X	X	5
Sb-124	X	X	X	X	X	X	X	X	X	X	5
Sb-125	X	X	X	X	X	X	X	X	X	X	5
Sb-126	X	X	X	X	X	X	X	X	X	X	5
Te-120	X	X	X	X	X	X	X	X	X	X	5
Te-122	X	X	X	X	X	X	X	X	X	X	5
Te-123	X	X	X	X	X	X	X	X	X	X	5
Te-124	X	X	X	X	X	X	X	X	X	X	5
Te-125	X	X	X	X	X	X	X	X	X	X	5
Te-126	X	X	X	X	X	X	X	X	X	X	5
Te-127m	X	X	X	X	X	X	X	X	X	X	5
Te-128	X	X	X	X	X	X	X	X	X	X	5
Te-129m	X	X	X	X	X	X	X	X	X	X	5
Te-130	X	X	X	X	X	X	X	X	X	X	5
Te-132	X	X	X	X	X	X	X	X	X	X	5
I-127	X	X	X	X	X	X	X	X	X	X	5
I-129	X	X	X	X	X	X	X	X	X	X	5
I-130	X	X	X	X	X	X	X	X	X	X	5
I-131	X	X	X	X	X	X	X	X	X	X	5
I-135	X	X	X	X	X	X	X	X	X	X	5
Xe-123	X	X	X	X	X	X	X	X	X	X	5
Xe-124	X	X	X	X	X	X	X	X	X	X	5
Xe-126	X	X	X	X	X	X	X	X	X	X	5
Xe-128	X	X	X	X	X	X	X	X	X	X	5
Xe-129	X	X	X	X	X	X	X	X	X	X	5
Xe-130	X	X	X	X	X	X	X	X	X	X	5
Xe-131	X	X	X	X	X	X	X	X	X	X	5
Xe-132	X	X	X	X	X	X	X	X	X	X	5
Xe-133	X	X	X	X	X	X	X	X	X	X	5
Xe-134	X	X	X	X	X	X	X	X	X	X	5
Xe-135	X	X	X	X	X	X	X	X	X	X	5
Xe-136	X	X	X	X	X	X	X	X	X	X	5
Cs-133	X	X	X	X	X	X	X	X	X	X	5
Cs-134	X	X	X	X	X	X	X	X	X	X	5

Table 2.2. Background cross-section values at which Bondarenko factors are tabulated in the Vitamin-B7 library

(All nuclides were processed at 300, 600, 1000 and 2100 K)

Nuclide[a]	Background cross sections (barns)										Legendre order
	10^{10}	10^6	10^5	10^4	1000	300	100	50	10	1	
Cs-135	X	X	X	X	X	X	X	X	X	X	5
Cs-136	X	X	X	X	X	X	X	X	X	X	5
Cs-137	X	X	X	X	X	X	X	X	X	X	5
Ba-130	X	X	X	X	X	X	X	X	X	X	5
Ba-132	X	X	X	X	X	X	X	X	X	X	5
Ba-133	X	X	X	X	X	X	X	X	X	X	5
Ba-134	X	X	X	X	X	X	X	X	X	X	5
Ba-135	X	X	X	X	X	X	X	X	X	X	5
Ba-136	X	X	X	X	X	X	X	X	X	X	5
Ba-137	X	X	X	X	X	X	X	X	X	X	5
Ba-138	X	X	X	X	X	X	X	X	X	X	5
Ba-140	X	X	X	X	X	X	X	X	X	X	5
La-138	X	X	X	X	X	X	X	X	X	X	5
La-139	X	X	X	X	X	X	X	X	X	X	5
La-140	X	X	X	X	X	X	X	X	X	X	5
Ce-136	X	X	X	X	X	X	X	X	X	X	5
Ce-138	X	X	X	X	X	X	X	X	X	X	5
Ce-139	X	X	X	X	X	X	X	X	X	X	5
Ce-140	X	X	X	X	X	X	X	X	X	X	5
Ce-141	X	X	X	X	X	X	X	X	X	X	5
Ce-142	X	X	X	X	X	X	X	X	X	X	5
Ce-143	X	X	X	X	X	X	X	X	X	X	5
Ce-144	X	X	X	X	X	X	X	X	X	X	5
Pr-141	X	X	X	X	X	X	X	X	X	X	5
Pr-142	X	X	X	X	X	X	X	X	X	X	5
Pr-143	X	X	X	X	X	X	X	X	X	X	5
Nd-142	X	X	X	X	X	X	X	X	X	X	5
Nd-143	X	X	X	X	X	X	X	X	X	X	5
Nd-144	X	X	X	X	X	X	X	X	X	X	5
Nd-145	X	X	X	X	X	X	X	X	X	X	5
Nd-146	X	X	X	X	X	X	X	X	X	X	5
Nd-147	X	X	X	X	X	X	X	X	X	X	5
Nd-148	X	X	X	X	X	X	X	X	X	X	5
Nd-150	X	X	X	X	X	X	X	X	X	X	5
Pm-147	X	X	X	X	X	X	X	X	X		5
Pm-148	X	X	X	X	X	X	X	X			5
Pm-148m	X	X	X	X	X	X	X	X	X	X	5
Pm-149	X	X	X	X	X	X	X	X	X		5
Pm-151	X	X	X	X	X	X	X	X	X	X	5
Sm-144	X	X	X	X	X	X	X	X	X	X	5
Sm-147	X	X	X	X	X	X	X	X	X	X	5
Sm-148	X	X	X	X	X	X	X	X	X	X	5
Sm-149	X	X	X	X	X	X	X	X	X	X	5
Sm-150	X	X	X	X	X	X	X	X	X	X	5
Sm-151	X	X	X	X	X	X	X	X	X	X	5
Sm-152	X	X	X	X	X	X	X	X	X	X	5
Sm-153	X	X	X	X	X	X	X	X	X	X	5

Table 2.2. Background cross-section values at which Bondarenko factors are tabulated in the Vitamin-B7 library

(All nuclides were processed at 300, 600, 1000 and 2100 K)

Nuclide[a]	Background cross sections (barns)										Legendre order
	10^{10}	10^6	10^5	10^4	1000	300	100	50	10	1	
Sm-154	X	X	X	X	X	X	X	X	X	X	5
Eu-151	X	X	X	X	X	X	X	X	X		5
Eu-152	X	X	X	X	X	X	X	X	X		5
Eu-153	X	X	X	X	X	X	X	X	X	X	5
Eu-154	X	X	X	X	X	X	X	X			5
Eu-155	X	X	X	X	X	X	X	X			5
Eu-156	X	X	X	X	X	X	X	X	X	X	5
Eu-157	X	X	X	X	X	X	X	X	X	X	5
Gd-152	X	X	X	X	X	X	X	X	X	X	5
Gd-153	X	X	X	X	X	X	X	X	X	X	5
Gd-154	X	X	X	X	X	X	X	X	X	X	5
Gd-155	X	X	X	X	X	X	X	X	X	X	5
Gd-156	X	X	X	X	X	X	X	X	X	X	5
Gd-157	X	X	X	X	X	X	X	X	X	X	5
Gd-158	X	X	X	X	X	X	X	X	X	X	5
Gd-160	X	X	X	X	X	X	X	X	X	X	5
Tb-159	X	X	X	X	X	X	X	X	X	X	5
Tb-160	X	X	X	X	X	X	X	X	X	X	5
Dy-156	X	X	X	X	X	X	X	X	X		5
Dy-158	X	X	X	X	X	X	X	X	X	X	5
Dy-160	X	X	X	X	X	X	X	X	X	X	5
Dy-161	X	X	X	X	X	X	X	X	X	X	5
Dy-162	X	X	X	X	X	X	X	X	X	X	5
Dy-163	X	X	X	X	X	X	X	X	X	X	5
Dy-164	X	X	X	X	X	X	X	X	X	X	5
Ho-165	X	X	X	X	X	X	X	X	X	X	5
Ho-166m	X	X	X	X	X	X	X	X	X	X	5
Er-162	X	X	X	X	X	X	X	X	X	X	5
Er-164	X	X	X	X	X	X	X	X	X	X	5
Er-166	X	X	X	X	X	X	X	X	X	X	5
Er-167	X	X	X	X	X	X	X	X	X	X	5
Er-168	X	X	X	X	X	X	X	X	X	X	5
Er-170	X	X	X	X	X	X	X	X	X	X	5
Lu-175	X	X	X	X	X	X	X	X	X	X	5
Lu-176	X	X	X	X	X	X	X	X	X	X	5
Hf-174	X	X	X	X	X	X	X	X	X	X	5
Hf-176	X	X	X	X	X	X	X	X	X	X	5
Hf-177	X	X	X	X	X	X	X	X	X	X	5
Hf-178	X	X	X	X	X	X	X	X	X	X	5
Hf-179	X	X	X	X	X	X	X	X	X	X	5
Hf-180	X	X	X	X	X	X	X	X	X	X	5
Ta-181	X	X	X	X	X	X	X	X	X	X	5
Ta-182	X	X	X	X	X	X	X	X	X	X	5
W-182	X	X	X	X	X	X	X	X	X	X	5
W-183	X	X	X	X	X	X	X	X	X	X	5
W-184	X	X	X	X	X	X	X	X	X	X	5
W-186	X	X	X	X	X	X	X	X	X	X	5

Table 2.2. Background cross-section values at which Bondarenko factors are tabulated in the Vitamin-B7 library

(All nuclides were processed at 300, 600, 1000 and 2100 K)

Nuclide[a]	Background cross sections (barns)										Legendre order
	10^{10}	10^6	10^5	10^4	1000	300	100	50	10	1	
Re-185	X	X	X	X	X	X	X	X	X	X	5
Re-187	X	X	X	X	X	X	X	X	X	X	5
Ir-191	X	X	X	X	X	X	X	X	X	X	5
Ir-193	X	X	X	X	X	X	X	X	X	X	5
Au-197	X	X	X	X	X	X	X	X	X	X	5
Hg-196	X	X	X	X	X	X	X	X	X	X	5
Hg-198	X	X	X	X	X	X	X	X	X	X	5
Hg-199	X	X	X	X	X	X	X	X	X	X	5
Hg-200	X	X	X	X	X	X	X	X	X	X	5
Hg-201	X	X	X	X	X	X	X	X	X	X	5
Hg-202	X	X	X	X	X	X	X	X	X	X	5
Hg-204	X	X	X	X	X	X	X	X	X	X	5
Pb-204	X	X	X	X	X	X	X	X	X	X	5
Pb-206	X	X	X	X	X	X	X	X	X	X	5
Pb-207	X	X	X	X	X	X	X	X	X	X	5
Pb-208	X	X	X	X	X	X	X	X	X	X	5
Bi-209	X	X	X	X	X	X	X	X	X	X	5
Ra-223	X	X	X	X	X	X	X	X	X	X	5
Ra-224	X	X	X	X	X	X	X	X	X	X	5
Ra-225	X	X	X	X	X	X	X	X	X	X	5
Ra-226	X	X	X	X	X	X	X	X	X	X	5
Ac-225	X	X	X	X	X	X	X	X	X	X	5
Ac-226	X	X	X	X	X	X	X	X	X	X	5
Ac-227	X	X	X	X	X	X	X	X	X	X	5
Th-227	X	X	X	X	X	X	X	X	X	X	5
Th-228	X	X	X	X	X	X	X	X	X	X	5
Th-229	X	X	X	X	X	X	X	X	X	X	5
Th-230	X	X	X	X	X	X	X	X	X	X	5
Th-232	X	X	X	X	X	X	X	X	X	X	5
Th-233	X	X	X	X	X	X	X	X	X	X	5
Th-234	X	X	X	X	X	X	X	X	X	X	5
Pa-231	X	X	X	X	X	X	X	X	X	X	5
Pa-232	X	X	X	X	X	X	X	X	X	X	5
Pa-233	X	X	X	X	X	X	X	X	X	X	5
U-232	X	X	X	X	X	X	X	X	X	X	5
U-233	X	X	X	X	X	X	X	X	X	X	5
U-234	X	X	X	X	X	X	X	X	X	X	5
U-235	X	X	X	X	X	X	X	X	X	X	5
U-236	X	X	X	X	X	X	X	X	X	X	5
U-237	X	X	X	X	X	X	X	X	X	X	5
U-238	X	X	X	X	X	X	X	X	X	X	5
U-239	X	X	X	X	X	X	X	X	X	X	5
U-240	X	X	X	X	X	X	X	X	X	X	5
U-241	X	X	X	X	X	X	X	X	X	X	5
Np-235	X	X	X	X	X	X	X	X	X	X	5
Np-236	X	X	X	X	X	X	X	X	X	X	5
Np-237	X	X	X	X	X	X	X	X	X	X	5

Table 2.2. Background cross-section values at which Bondarenko factors are tabulated in the Vitamin-B7 library

(All nuclides were processed at 300, 600, 1000 and 2100 K)

Nuclide[a]	Background cross sections (barns)										Legendre order
	10^{10}	10^6	10^5	10^4	1000	300	100	50	10	1	
Np-238	X	X	X	X	X	X	X	X	X	X	5
Np-239	X	X	X	X	X	X	X	X	X	X	5
Pu-236	X	X	X	X	X	X	X	X			5
Pu-237	X	X	X	X	X	X	X	X	X	X	5
Pu-238	X	X	X	X	X	X	X	X	X	X	5
Pu-239	X	X	X	X	X	X	X	X	X	X	5
Pu-240	X	X	X	X	X	X	X	X	X	X	5
Pu-241	X	X	X	X	X	X	X	X	X	X	5
Pu-242	X	X	X	X	X	X	X	X	X	X	5
Pu-243	X	X	X	X	X	X	X	X	X	X	5
Pu-244	X	X	X	X	X	X	X	X	X	X	5
Pu-246	X	X	X	X	X	X	X	X	X	X	5
Am-241	X	X	X	X	X	X	X	X	X	X	5
Am-242	X	X	X	X	X	X	X	X	X	X	5
Am-242m	X	X	X	X	X	X	X	X			5
Am-243	X	X	X	X	X	X	X	X	X	X	5
Am-244	X	X	X	X	X	X	X	X	X	X	5
Am-244m	X	X	X	X	X	X	X	X	X	X	5
Cm-241	X	X	X	X	X	X	X	X	X	X	5
Cm-242	X	X	X	X	X	X	X	X	X	X	5
Cm-243	X	X	X	X	X	X	X	X	X	X	5
Cm-244	X	X	X	X	X	X	X	X	X	X	5
Cm-245	X	X	X	X	X	X	X	X	X	X	5
Cm-246	X	X	X	X	X	X	X	X	X	X	5
Cm-247	X	X	X	X	X	X	X	X	X		5
Cm-248	X	X	X	X	X	X	X	X	X	X	5
Cm-249	X	X	X	X	X	X	X	X	X	X	5
Cm-250	X	X	X	X	X	X	X	X	X	X	5
Bk-249	X	X	X	X	X	X	X	X	X	X	5
Bk-250	X	X	X	X	X	X	X	X	X	X	5
Cf-249	X	X	X	X	X	X	X	X	X	X	5
Cf-250	X	X	X	X	X	X	X	X	X	X	5
Cf-251	X	X	X	X	X	X	X	X	X	X	5
Cf-252	X	X	X	X	X	X	X	X	X	X	5
Cf-253	X	X	X	X	X	X	X	X			5
Cf-254	X	X	X	X	X	X	X	X	X	X	5
Es-253	X	X	X	X	X	X	X	X	X	X	5
Es-254	X	X	X	X	X	X	X	X	X	X	5
Es-255	X	X	X	X	X	X	X	X	X	X	5
Fm-255	X	X	X	X	X	X	X	X	X	X	5

[a] For nuclides with thermal moderator data, the nuclide ID for the fast evaluation is given, followed by the nuclide ID for the moderator.

Table 2.3. Neutron group energy boundaries for the VITAMIN-B7 library

| Grp no.	Upper energy (eV)	Lethargy width	Grp no.	Upper energy (eV)	Lethargy width	Grp No.	Upper energy (eV)	Lethargy width
1	1.9640E+07	0.1250	68	7.8082E+05	0.0500	135	3.0354E+03	0.1000
2	1.7332E+07	0.0249	69	7.4274E+05	0.0500	136	2.7465E+03	0.0500
3	1.6905E+07	0.0250	70	7.0651E+05	0.0500	137	2.6126E+03	0.0500
4	1.6487E+07	0.0500	71	6.7206E+05	0.0500	138	2.4852E+03	0.1000
5	1.5683E+07	0.0500	72	6.3928E+05	0.0500	139	2.2487E+03	0.1000
6	1.4918E+07	0.0250	73	6.0810E+05	0.0500	140	2.0347E+03	0.2500
7	1.4550E+07	0.0250	74	5.7844E+05	0.0500	141	1.5846E+03	0.2500
8	1.4191E+07	0.0250	75	5.5023E+05	0.0500	142	1.2341E+03	0.2500
9	1.3840E+07	0.0249	76	5.2340E+05	0.0500	143	9.6112E+02	0.2500
10	1.3499E+07	0.0501	77	4.9787E+05	0.1000	144	7.4852E+02	0.2500
11	1.2840E+07	0.0250	78	4.5049E+05	0.1000	145	5.8295E+02	0.2500
12	1.2523E+07	0.0250	79	4.0762E+05	0.0500	146	4.5400E+02	0.2500
13	1.2214E+07	0.0500	80	3.8774E+05	0.0500	147	3.5357E+02	0.2500
14	1.1618E+07	0.0499	81	3.6883E+05	0.1000	148	2.7536E+02	0.2500
15	1.1052E+07	0.0500	82	3.3373E+05	0.1000	149	2.1445E+02	0.2500
16	1.0513E+07	0.0500	83	3.0197E+05	0.0116	150	1.6702E+02	0.2500
17	1.0000E+07	0.0500	84	2.9849E+05	0.0043	151	1.3007E+02	0.2500
18	9.5123E+06	0.0500	85	2.9721E+05	0.0091	152	1.0130E+02	0.2500
19	9.0484E+06	0.0500	86	2.9452E+05	0.0250	153	7.8893E+01	0.2500
20	8.6071E+06	0.0500	87	2.8725E+05	0.0500	154	6.1442E+01	0.2500
21	8.1873E+06	0.0500	88	2.7324E+05	0.1000	155	4.7851E+01	0.2500
22	7.7880E+06	0.0500	89	2.4724E+05	0.0500	156	3.7266E+01	0.2500
23	7.4082E+06	0.0500	90	2.3518E+05	0.0500	157	2.9023E+01	0.2500
24	7.0469E+06	0.0500	91	2.2371E+05	0.0500	158	2.2603E+01	0.2500
25	6.7032E+06	0.0167	92	2.1280E+05	0.0500	159	1.7604E+01	0.2500
26	6.5924E+06	0.0333	93	2.0242E+05	0.0500	160	1.3710E+01	0.2500
27	6.3763E+06	0.0500	94	1.9255E+05	0.0500	161	1.0677E+01	0.2500
28	6.0653E+06	0.0500	95	1.8316E+05	0.0500	162	8.3153E+00	0.2500
29	5.7695E+06	0.0500	96	1.7422E+05	0.0500	163	6.4760E+00	0.2500
30	5.4881E+06	0.0500	97	1.6573E+05	0.0500	164	5.0435E+00	0.2500
31	5.2205E+06	0.0500	98	1.5764E+05	0.0499	165	3.9279E+00	0.2500
32	4.9659E+06	0.0500	99	1.4996E+05	0.0500	166	3.0590E+00	0.2500
33	4.7237E+06	0.0500	100	1.4264E+05	0.0500	167	2.3824E+00	0.2500
34	4.4933E+06	0.1000	101	1.3569E+05	0.0500	168	1.8554E+00	0.2500
35	4.0657E+06	0.1000	102	1.2907E+05	0.0500	169	1.4450E+00	0.1057
36	3.6788E+06	0.1000	103	1.2277E+05	0.0499	170	1.3000E+00	0.1442
37	3.3287E+06	0.0500	104	1.1679E+05	0.0500	171	1.1253E+00	0.0412
38	3.1664E+06	0.0500	105	1.1109E+05	0.1250	172	1.0800E+00	0.0377
39	3.0119E+06	0.0500	106	9.8037E+04	0.1250	173	1.0400E+00	0.0392
40	2.8651E+06	0.0500	107	8.6517E+04	0.0475	174	1.0000E+00	0.1319
41	2.7253E+06	0.0500	108	8.2503E+04	0.0371	175	8.7643E-01	0.0912
42	2.5924E+06	0.0500	109	7.9499E+04	0.0991	176	8.0000E-01	0.1588
43	2.4660E+06	0.0333	110	7.1998E+04	0.0663	177	6.8256E-01	0.0880
44	2.3852E+06	0.0084	111	6.7379E+04	0.1750	178	6.2506E-01	0.1620
45	2.3653E+06	0.0083	112	5.6562E+04	0.0750	179	5.3158E-01	0.0612
46	2.3457E+06	0.0167	113	5.2475E+04	0.1250	180	5.0000E-01	0.1888
47	2.3069E+06	0.0333	114	4.6309E+04	0.1250	181	4.1399E-01	0.1210
48	2.2313E+06	0.0500	115	4.0868E+04	0.1750	182	3.6680E-01	0.1210
49	2.1225E+06	0.0500	116	3.4307E+04	0.0750	183	3.2500E-01	0.1671
50	2.0190E+06	0.0500	117	3.1828E+04	0.1104	184	2.7500E-01	0.2007

Table 2.3. Neutron group energy boundaries for the VITAMIN-B7 library

Grp no.	Upper energy (eV)	Lethargy width	Grp no.	Upper energy (eV)	Lethargy width	Grp No.	Upper energy (eV)	Lethargy width
51	1.9205E+06	0.0500	118	2.8501E+04	0.0541	185	2.2500E-01	0.2012
52	1.8268E+06	0.0500	119	2.7000E+04	0.0355	186	1.8400E-01	0.2043
53	1.7377E+06	0.0500	120	2.6058E+04	0.0500	187	1.5000E-01	0.1823
54	1.6530E+06	0.0500	121	2.4788E+04	0.0250	188	1.2500E-01	0.2231
55	1.5724E+06	0.0500	122	2.4176E+04	0.0250	189	1.0000E-01	0.3567
56	1.4957E+06	0.0500	123	2.3579E+04	0.0750	190	7.0000E-02	0.3365
57	1.4227E+06	0.0499	124	2.1875E+04	0.1250	191	5.0000E-02	0.2231
58	1.3534E+06	0.0500	125	1.9305E+04	0.2500	192	4.0000E-02	0.2877
59	1.2874E+06	0.0500	126	1.5034E+04	0.2500	193	3.0000E-02	0.3567
60	1.2246E+06	0.0501	127	1.1709E+04	0.1000	194	2.1000E-02	0.3704
61	1.1648E+06	0.0500	128	1.0595E+04	0.1500	195	1.4500E-02	0.3716
62	1.1080E+06	0.1000	129	9.1188E+03	0.2500	196	1.0000E-02	0.6931
63	1.0026E+06	0.0417	130	7.1017E+03	0.2500	197	5.0000E-03	0.9163
64	9.6164E+05	0.0583	131	5.5308E+03	0.2500	198	2.0000E-03	1.3863
65	9.0718E+05	0.0500	132	4.3074E+03	0.1500	199	5.0000E-04	3.9120
66	8.6294E+05	0.0500	133	3.7074E+03	0.1000		1.0000E-05	
67	8.2085E+05	0.0500	134	3.3546E+03	0.1000			

Note: The groups shaded in gray (groups 164–199) are the thermal groups.

Table 2.4. Photon group energy boundaries for the VITAMIN-B7 library

Grp no.	Upper energy (eV)		Grp no.	Upper energy (eV)	Grp no.	Upper energy (eV)
1	3.00E+07		16	3.00E+06	31	3.00E+05
2	2.00E+07		17	2.50E+06	32	2.00E+05
3	1.40E+07		18	2.00E+06	33	1.50E+05
4	1.20E+07		19	1.66E+06	34	1.00E+05
5	1.00E+07		20	1.50E+06	35	7.50E+04
6	8.00E+06		21	1.34E+06	36	7.00E+04
7	7.50E+06		22	1.33E+06	37	6.00E+04
8	7.00E+06		23	1.00E+06	38	4.50E+04
9	6.50E+06		24	8.00E+05	39	4.00E+04
10	6.00E+06		25	7.00E+05	40	3.00E+04
11	5.50E+06		26	6.00E+05	41	2.00E+04
12	5.00E+06		27	5.12E+05	42	1.00E+04
13	4.50E+06		28	5.10E+05		1.00E+03
14	4.00E+06		29	4.50E+05		
15	3.50E+06		30	4.00E+05		
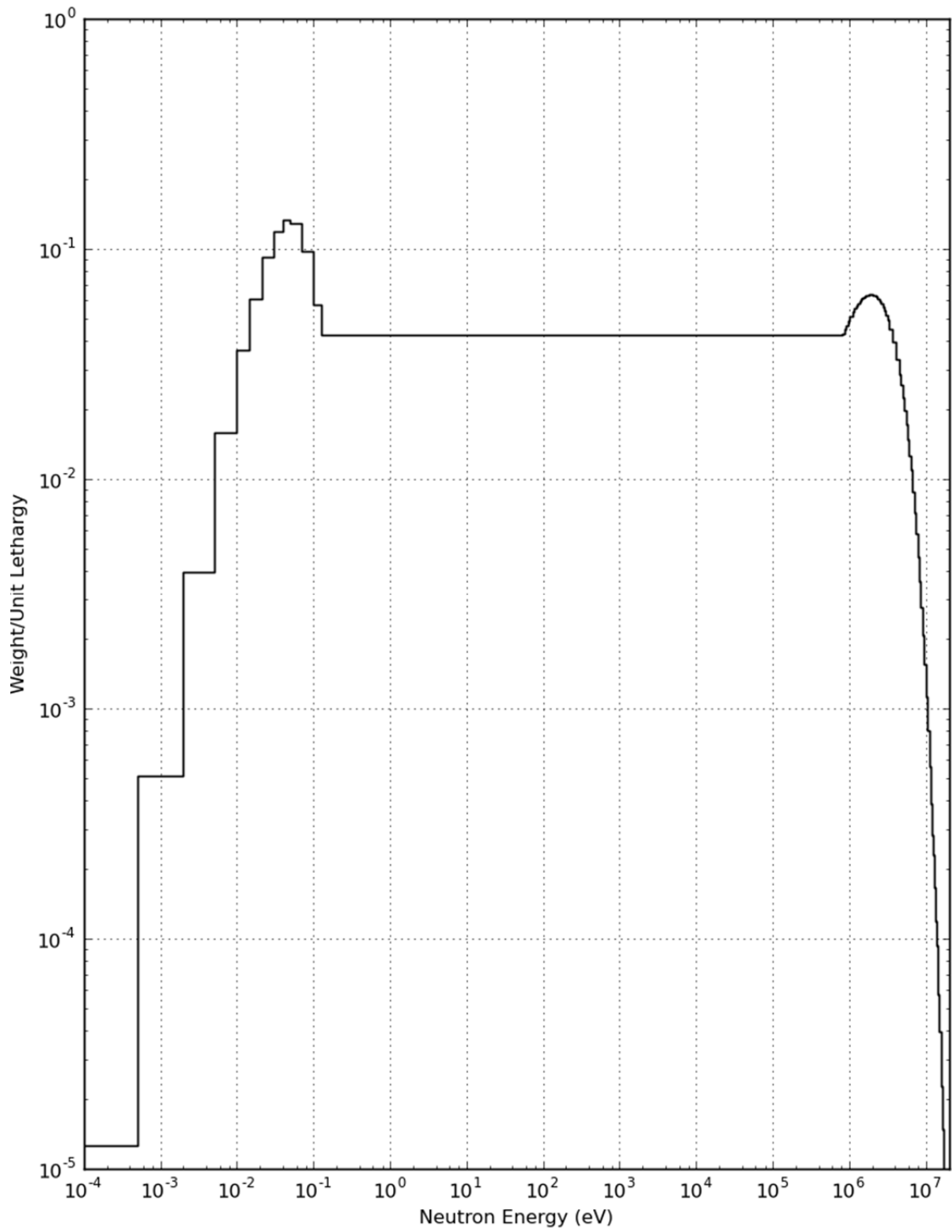
Figure 2.1. Neutron weighting spectrum used to create the fine-group VITAMIN-B7 neutron library.
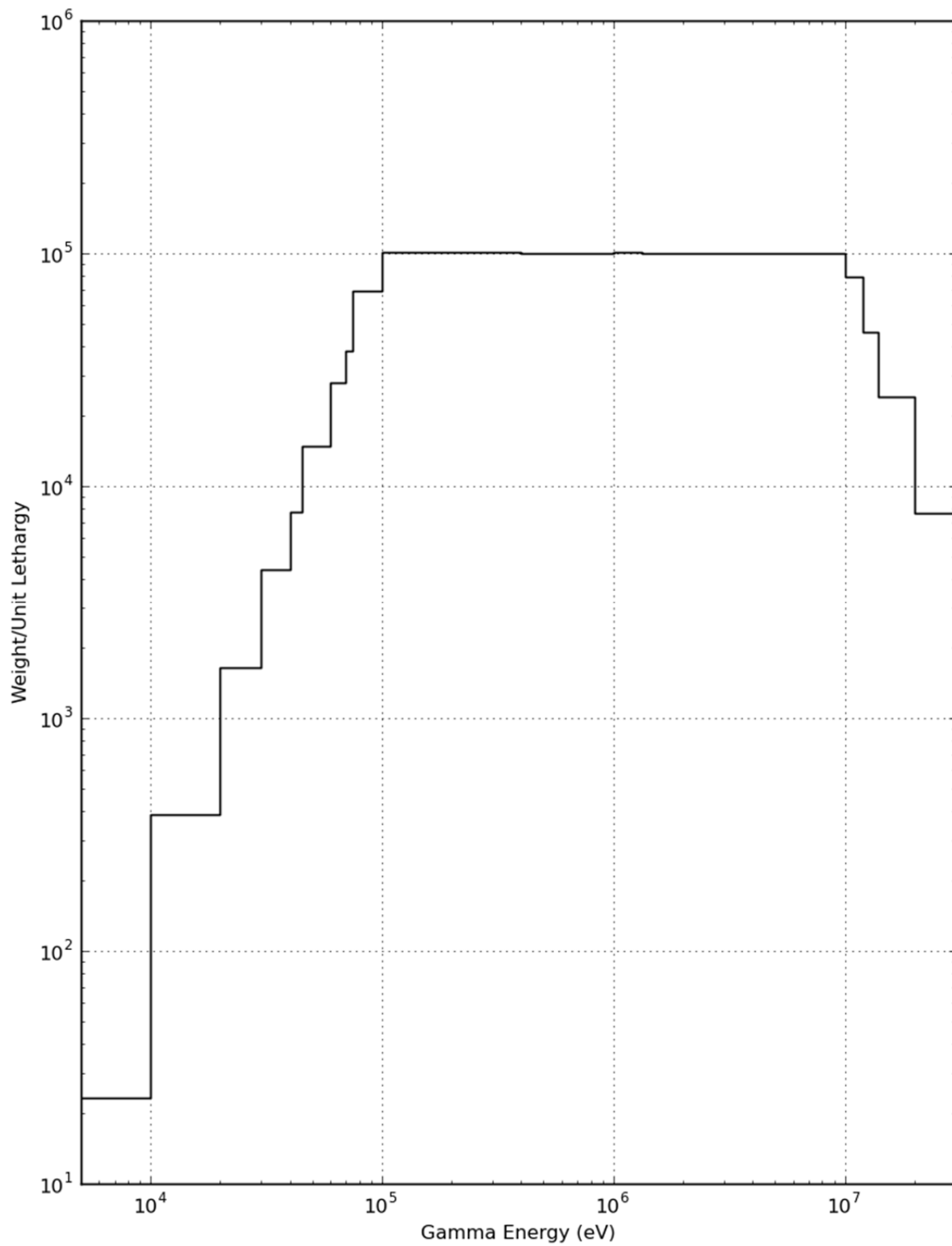
Figure 2.2. Gamma weighting spectrum used to create the fine-group VITAMIN-B7 gamma library.

2.6 Processing Codes and Procedures

The AMPX code system was used to generate pointwise and multigroup data in AMPX master library format. Input files were generated using an XML listing of the desired evaluations and XML templates. The XML listings for each evaluation were generated by a Java program that scans a directory tree of ENDF files and writes the relevant information to a file. The input listings for each evaluation are included in the D00245MNYCP00 data package available from the Radiation Safety Information Computational Center (RSICC).

Relevant XML templates were processed with the EXSITE program to produce input files for AMPX. The input files for all cases are provided on the accompanying CD.

2.6.1 AMPX Execution Sequences for Neutron and Gamma-Ray Yield Processing

The AMPX processing system contains more than 100 distinct modules that can be used to perform a wide range of nuclear data processing functions. The specific modules needed to process a cross-section evaluation and generate a pointwise or multigroup cross-section library depend upon the data specified in the nuclide evaluation. For example, a resonance nuclide will require more modules to be executed than will a non-resonance nuclide. If the evaluation is a thermal moderator material with $S(\alpha,\beta)$ data, the AMPX execution sequence will be different because the final cross-section data will be a mixture of data from one evaluation for energies above the thermal cutoff and from another evaluation in the thermal range.

The general procedure to generate multigroup neutron cross-section data is outlined in Figure 2.3. The flow chart to produce the coupled part of the library is depicted in Figure 2.4.

The ENDF/B-VII.0 cross-section evaluations were downloaded from the National Nuclear Data Center (NNDC) Web page [14]. The thermal evaluations for $U(UO_2)$ and $O(UO_2)$ were excluded because some inconsistencies in the ENDF evaluations prevent the AMPX Y12 module from processing the data.

2.6.1.1 Processing of Pointwise Cross-Section Data

POLIDENT

Whether cross sections are being prepared for continuous energy or multigroup applications, the first module that is executed is POLIDENT. For resonance nuclides, POLIDENT determines a point energy mesh in the resolved resonance region and calculates the cross sections on that energy mesh. An analogous procedure is performed for nuclides having unresolved resonance data. For each nuclide, POLIDENT combines the resonance parameter data (if present) with the smooth cross-section data from the ENDF/B File 3 point data file to produce linearized cross-section functions. The combined data functions are written out in a standard AMPX tabular data format that is based on the ENDF/B TAB1 format.
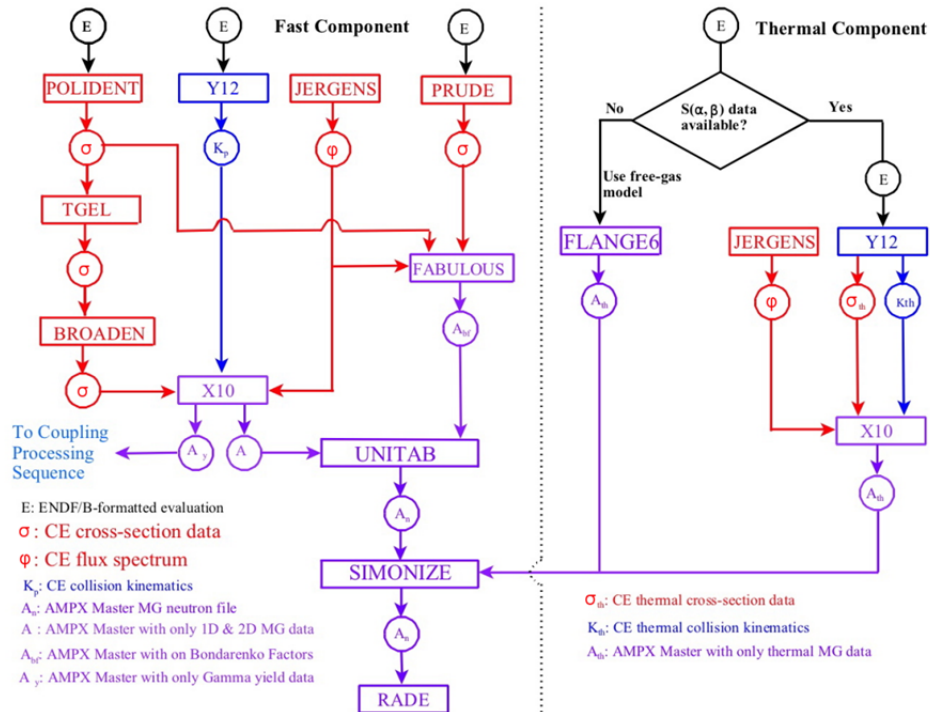
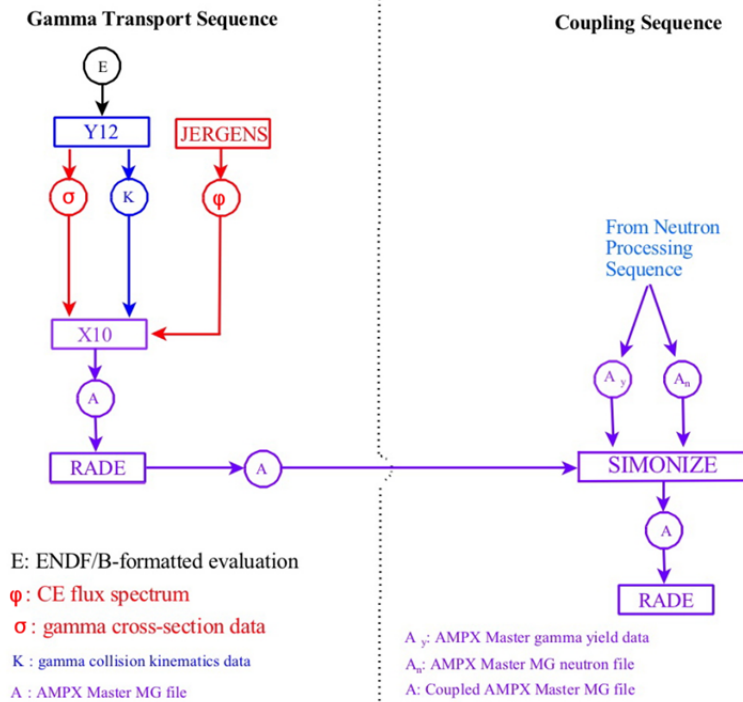**Figure 2.3. AMPX sequence for producing neutron multigroup data.**

Figure 2.4. AMPX sequence to generate coupled neutron–gamma multigroup data.

TGEL

One of the primary reasons to linearize cross-section data is to produce internally consistent datasets. When all of the cross-section data are produced on a linear–linear grid, the sum of a group of linear functions is itself linear; however, simply applying the interpolation method (e.g., lin-log, log-log) given in an evaluation does not necessarily lead to this consistency. To ensure consistency, the total cross section and other "redundant" reactions (e.g., fission, inelastic scatter) are formed by summing the linearized partial values. The TGEL module is used to ensure all redundant reactions are equal to the sum of the partial reactions. The output is written in the same tabular format that is used by POLIDENT.

BROADEN

Many applications, especially those dealing with reactors, require cross sections that vary as a function of temperature. The point cross sections can be Doppler broadened by a numerical treatment used in the BROADEN module. This module adds additional points as needed to describe the broadened resonance structure. Unnecessary grid points are omitted. The output data from BROADEN are exported in an AMPX tabular format.

JERGENS

The production of multigroup cross sections from pointwise data requires a weighting function to collapse the pointwise data to the multigroup energy structure. The JERGENS module provides a variety of options for generating weighting spectra. JERGENS has options for calculating weighting spectra that may use point cross sections from POLIDENT. The output is written in an AMPX tabular format. For the pointwise neutron cross-section data of the coupled library generation task, JERGENS was used to produce a "smooth" weighting spectrum that has the form of a Maxwellian —1/E— fission spectrum as described in Section 2.4.

2.6.1.2 Neutron and Gamma Yield Processing

Y12

A unique feature of the AMPX system is the Y12 module, which reads an ENDF/B evaluation and produces tabular collision kinematics data for all reactions. The functions produced by Y12 describe what particles are produced and at what energies and directions when a reaction is encountered at some source energy. The output from Y12 is an AMPX tabular kinematics file.

X10

The X10 module reads tabular point cross sections, a tabular weighting spectrum, and the tabular kinematics data file and uses these three files to produce group-averaged cross sections and group-to-group transfer matrices. This code contains no programming related to the physics of any reaction and is programmed in a manner that treats neutron data, gamma-ray data, or gamma-ray yield data. The output from X10 is a set of group cross sections that are written on a file in AMPX master library format.

When a cross-section evaluation contains gamma-production data, either in ENDF File 6 or in the special Files 12, 13, 14 and 15, the kinematics data file produced by Y12 and the point data files from POLIDENT and JERGENS are passed to X10 to produce gamma-ray yield transfer matrices. The gamma yield matrices indicate where gamma rays are produced as a function of

neutron reaction. The yield data are exported from X10 in an AMPX master library format. After the gamma transport data are processed in a separate AMPX sequence, the gamma yield data are coupled with the multigroup neutron and gamma-ray data.

2.6.1.3 Thermal Neutron Processing

FLANGE6

If a nuclide does not have $S(\alpha,\beta)$ data given in ENDF, the FLANGE6 module is used to produce thermal scattering matrices at the desired temperatures based on the free gas–scattering model. The matrices are exported in AMPX master library format. As noted in Section 2.5, thermal scattering matrices based on the free gas model are limited to a P_3 expansion order.

JERGENS, Y12, and X10

If a nuclide is a bound moderator material (e.g., hydrogen bound in water, carbon in graphite), the ENDF/B thermal scattering law evaluations are processed by the Y12 module to produce thermal kinematics data as a function of temperatures provided in the ENDF/B evaluation. In addition, the Y12 module produces thermal pointwise cross-section data. The resulting thermal kinematics file and thermal pointwise data file are passed to the X10 module, along with the JERGENS weighting spectrum, to produce a special thermal AMPX master library.

In many of the ENDF/B thermal evaluations, the cross sections for the principal isotope in a compound can be isolated. For example, the thermal data for water gives the scattering law data for hydrogen in a manner that describes the specific binding effects for hydrogen present in a water molecule. The file then specifies that oxygen should simply be treated by the free gas model. This treatment allows one to produce a set of full-range cross sections for water-bound hydrogen by collecting together the thermal hydrogen values and combining them with the values from the fast-neutron hydrogen evaluation. For other moderators, such as BeO, it is not possible to separate the elemental data (e.g., the Be in BeO) out of the data for the molecule. In those cases the scattering law data are given for the molecule as a combined unit. There are several ways to deal with this situation. The one that was chosen to be analogous to the water-bound hydrogen case was to couple the data from the fast neutron evaluation for Be with the thermal BeO data, and call this set "Be bound in BeO." For the oxygen component, a special set was prepared and called "O bound in BeO." For the case of O in BeO, the oxygen data were prepared from the fast neutron evaluation without any thermal data (i.e., no thermal scattering data as would normally be present from a free gas calculation by the FLANGE6 module).

2.6.1.4 Generation of Full-Range Bondarenko Factors and Thermal Data

PRUDE

For nuclides with unresolved resonance data, the PRUDE module is used to produce point "averaged" cross sections that are a function of temperature and background cross section. The background cross section is simply defined as the cross section per unit atom of a nuclide of the mixture (other than the nuclide itself) in which the nuclide is mixed. The cross sections are written out in an AMPX tabular file. This module can be run only for monoisotopic evaluations. In ENDF/B-VII, the only neutron evaluations that are not monoisotopic are those for vanadium ($Z = 23$) and zinc ($Z = 30$). Those evaluations contain elemental data in File 3 but have data for multiple isotopes in File 2.

FABULOUS

For all nuclides, the point data from POLIDENT and from PRUDE (if applicable) are passed to the FABULOUS module, along with the weighting spectrum file from JERGENS. FABULOUS uses the same temperatures and background cross sections described for PRUDE to Doppler broaden the functions outside the unresolved region to the temperatures at which the nuclides were processed, after which the functions are spliced together with the appropriate unresolved functions. These spliced functions are then used in a numerical scheme that calculates Bondarenko factors for all nuclides for elastic scattering, capture, fission, and total cross sections. The Bondarenko factors can be used in resonance self-shielding calculations.

For low values of the background cross section σ_0, the unresolved cross-section data can become negative. Calculation of the "total" Bondarenko factor is given by

$$\frac{\int \frac{\phi \sigma_T}{\left(\sigma_T + \sigma_0\right)^2}}{\int \frac{\phi}{\left(\sigma_T + \sigma_0\right)^2}} \tag{2.1}$$

In some cases, the value of $\left(\sigma_T + \sigma_0\right)$ can become negative. The NJOY manual [5] describes how this calculation is performed in the UNRESR module, which is similar to the AMPX PRUDE module. Reference [5] states that for materials with strong resonance overlaps, the approximation used in calculating this quantity can produce negative shielded cross-section data for lower values of σ_0. If this happens, FABULOUS omits the relevant value of σ_0 from the AMPX master library. The nuclides for which this occurs are indicated in Table 2.2 by the absence of Bondarenko data for some σ_0 values.

2.6.1.5 Gamma Processing

The processing of gamma-ray cross-section data is much simpler than that of neutron data. The following processes are included in the processing of the gamma-ray data from the ENDF evaluations: incoherent (Compton) scattering, coherent (Rayleigh) scattering, pair production in the electric field of the nucleus, pair production in the electric field of an electron (also known as triplet production), and photoelectric absorption. Note that unlike neutron cross sections, photon cross sections are elemental rather than isotopic.

JERGENS

The JERGENS module is used to produce a weighting spectrum for use in generating multigroup gamma-ray cross sections. The gamma spectrum is typically a 1/E spectrum with "roll-offs" that account for significant absorption of the gamma rays due to photoelectric absorption at low energies and pair production at high energies. As with the neutron evaluations, the weighting spectrum is written out in a pointwise AMPX tabular file based on the ENDF/B TAB1 format.

Y12

The Y12 module produces a tabular kinematics file that describes coherent (Rayleigh) and incoherent (Compton) scattering along with pair production. In addition, Y12 produces a pointwise data file for all of these processes. The pointwise file is exported in an AMPX tabular format.

X10

The tabular files from JERGENS and Y12 are passed to X10, along with the tabular kinematics file. X10 produces a group-averaged AMPX master library for gamma-ray interactions.

2.6.1.6 Creating the Master Library

After all the neutron and gamma data have been processed as described above, a master library containing data for all the nuclides is created. The input files for this process are included in the D00245MNYCP00 data package available from RSICC.

3 BROAD-GROUP LIBRARY SPECIFICATIONS

3.1 Name

The problem-dependent broad-group cross-section library that was developed from the VITAMIN-B7 pseudo-problem-independent fine-group library is designated as BUGLE-B7. This naming convention maintains consistency with the previous BUGLE libraries while using a suffix that is consistent with that of the fine-group library.

3.2 Materials and Energy Group Structure

The BUGLE-B7 library contains a subset of the nuclides present in the VITAMIN-B7 fine-group library (see Table 2.1). The contents of the BUGLE-B7 library are described in Section 3.5. Some nuclides appear multiple times (with distinct identifiers in each case) because of the use of different resonance self-shielding and distinct flux weighting spectra for specific regions of typical PWR and BWR reactor shielding applications. These self-shielding and spectral weighting effects are discussed in Section 3.3.

The BUGLE-B7 neutron and gamma group structures are identical to those used in the BUGLE-96 library. The energy group boundaries for the 47 neutron groups are provided in Table 3.1. The energy group boundaries for the 20 gamma groups are provided in Table 3.2**.**

3.3 Self-Shielding and Group Collapsing of the Broad-Group Library

While broad-group libraries such as BUGLE-B7 allow the users of transport codes to run calculations more rapidly and with fewer computer resources compared with the use of fine-group libraries, the accuracy of the results is dependent upon using broad-group data that have been collapsed from the fine-group library using appropriate weighting spectra. As with previous BUGLE libraries, the BUGLE-B7 library was developed for in-vessel and reactor cavity analyses for LWRs (both PWRs and BWRs). The validity of the BUGLE-B7 data would need to be explicitly demonstrated to justify its use for any other application. Even for LWR applications, it is important that properly self-shielded and collapsed data sets are selected for specific regions of the reactor plant geometry in transport models.

The BUGLE-B7 library was produced by self-shielding nuclides from the VITAMIN-B7 library in representative materials, adjusting to the appropriate temperature, and then group collapsing using weighting spectra from key regions of one-dimensional (1D) PWR and BWR models.

3.3.1 Self-Shielding Calculations

The self-shielding was performed using the BONAMI code in SCALE. In the core region, nuclides in the fuel, cladding, and coolant were self-shielded and temperature corrected using PWR and BWR fuel-clad-moderator pin cell models. In the coolant regions outside the core, hydrogen, oxygen, and boron were self-shielded in an infinite water medium. The constituents of carbon steel and stainless steel were self-shielded in infinite media of carbon steel (A533-B) and stainless steel (SS-304). The constituents of concrete were self-shielded in an infinite medium of Type 04 concrete. Details of the BONAMI parameters for these calculations are provided in Sections 3.3.1.1–3.3.1.5.

Table 3.1. Neutron group energy boundaries for the BUGLE-B7 library

Grp no.	Upper energy (eV)	Lethargy width	VITAMIN-B7 groups
1	1.7332E+07	0.1999	2-7
2	1.4191E+07	0.1500	8-12
3	1.2214E+07	0.2000	13-16
4	1.0000E+07	0.1500	17-19
5	8.6071E+06	0.1500	20-22
6	7.4082E+06	0.2000	23-27
7	6.0653E+06	0.2000	28-31
8	4.9658E+06	0.3000	32-35
9	3.6788E+06	0.2000	36-38
10	3.0119E+06	0.1000	39-40
11	2.7253E+06	0.1000	41-42
12	2.4660E+06	0.0417	43-44
13	2.3652E+06	0.0083	45
14	2.3457E+06	0.0500	46-47
15	2.2313E+06	0.1500	48-50
16	1.9205E+06	0.1500	51-53
17	1.6530E+06	0.2000	54-57
18	1.3534E+06	0.3000	58-62
19	1.0026E+06	0.2000	63-66
20	8.2085E+05	0.1000	67-68
21	7.4274E+05	0.2000	69-72
22	6.0810E+05	0.2000	73-76
23	4.9787E+05	0.3000	77-80
24	3.6883E+05	0.2159	81-84
25	2.9721E+05	0.4841	85-94
26	1.8316E+05	0.5000	95-104
27	1.1109E+05	0.5000	105-110
28	6.7379E+04	0.5000	111-114
29	4.0868E+04	0.2500	115-116
30	3.1828E+04	0.2000	117-119
31	2.6058E+04	0.0750	120-121
32	2.4176E+04	0.1000	122-123
33	2.1875E+04	0.3750	124-125
34	1.5034E+04	0.7500	126-129
35	7.1017E+03	0.7500	130-133
36	3.3546E+03	0.7500	134-140
37	1.5846E+03	1.2500	141-145
38	4.5400E+02	0.7500	146-148
39	2.1445E+02	0.7500	149-151
40	1.0130E+02	1.0000	152-155
41	3.7267E+01	1.2500	156-160
42	1.0677E+01	0.7500	161-163
43	5.0435E+00	1.0000	164-167
44	1.8554E+00	0.7500	168-174
45	8.7643E-01	0.7500	175-180
46	4.1399E-01	1.4207	181-188
47	1.0000E-01	9.2103	189-199
	1.0000E-05		

Note: The groups shaded in gray are the thermal groups. See Sections 3.4 and 3.5 for a discussion of upscatter in the thermal energy range.

Table 3.2. Gamma group energy boundaries for the BUGLE-B7 library

Grp No.	Upper Energy (eV)	VITAMIN-B7 Groups
1	1.40E+07	3-4
2	1.00E+07	5
3	8.00E+06	6-7
4	7.00E+06	8-9
5	6.00E+06	10-11
6	5.00E+06	12-13
7	4.00E+06	14-15
8	3.00E+06	16-17
9	2.00E+06	18-19
10	1.50E+06	20-22
11	1.00E+06	23
12	8.00E+05	24
13	7.00E+05	25
14	6.00E+05	26-29
15	4.00E+05	30-31
16	2.00E+05	32-33
17	1.00E+05	34-36
18	6.00E+04	37-39
19	3.00E+04	40
20	2.00E+04	41
	1.00E+04	

3.3.1.1 PWR Fuel Cell Self-Shielding

The PWR pin cell model, as described in Table 3.3, is based on the description in Table 3.6 of [1]. The coolant temperature was corrected to 583 K, which is incorrectly listed as the BWR coolant temperature in Table 3.6 of [1]. The Zircaloy-4 composition was modified to be consistent with the composition of Zircaloy-4 in the SCALE standard composition library, with the addition of a trace (0.01 wt %) of nickel, which is not present in Zircaloy-4. The nickel was added to provide cross-section data for nickel self-shielded in cladding to maintain consistency with the self-shielded nuclides provided in the BUGLE-96 library.

PWR pin cell calculations run with Zirlo cladding rather than Zircaloy-4 resulted in almost no difference in the self-shielded cross sections for the major isotopes in the cladding. Thus, the VITAMIN-B7 and BUGLE-B7 libraries are considered to be appropriate for PWR cores with Zr-Nb cladding (such as ZIRLO and M5) as well as Zircaloy-4.

Geometry: Cylinder
Number of zones: 3
Mixing table length: 40
Dancoff factor: Cylindrical cell (Sauer's method) square lattice with clad
Temperature: 1000 K for zone 1, 600 K for zones 2 and 3

Table 3.3. Description of mixtures used for self-shielding nuclides in the PWR pin cell model

Zone no.	Mixture no.	Nuclide	Concentration (atoms/b-cm)	Outer radius (cm)	Temperature (K)	Zone type
1	1	U-235 U-238 O-16	6.325×10^{-4} 2.166×10^{-2} 4.465×10^{-2}	0.41783	921	Fuel
2	2^a	Zr Sn Fe Cr Ni Hf	4.254×10^{-2} 4.825×10^{-4} 1.486×10^{-4} 7.598×10^{-5} 6.731×10^{-6} 2.213×10^{-6}	0.47498	672	Cladding
3	3	H-1^b O-16 B-10	4.714×10^{-2} 2.357×10^{-2} 4.200×10^{-6}	0.71079	583	Moderator

^{a} The isotopic number densities in the BONAMI input are based on the element number densities listed here and isotopic abundances from [15].
^{b} H-1 in H_2O.

3.3.1.2 BWR Fuel Cell Self-Shielding

The BWR pin cell model, as described in Table 3.4, is based on the description in Table 3.6 of [1]. The coolant temperature was corrected to 551 K, which is incorrectly listed as the PWR coolant temperature in Table 3.6 of [1]. The Zircaloy-4 composition was modified to be consistent with the composition of Zircaloy-4 in the SCALE standard composition library, with the addition of a trace (0.01 wt %) of nickel, which is not present in Zircaloy-4. The nickel was added to provide cross-section data for nickel self-shielded in cladding to maintain consistency with the self-shielded nuclides provided in the BUGLE-96 library.

Geometry: Cylinder
Number of zones: 3
Mixing table length: 39
Dancoff factor: Cylindrical cell (Sauer's method) square lattice with clad
Temperature: 1000 K for zone 1, 600 K for zones 2 and 3

Table 3.4. Description of mixtures used for self-shielding nuclides in the BWR pin cell model

Zone no.	Mixture no.	Nuclide	Concentration (atoms/b-cm)	Outer radius (cm)	Temperature (K)	Zone type
1	1	U-235 U-238 O-16	4.959×10^{-4} 2.177×10^{-2} 4.455×10^{-2}	0.53213	921	Fuel
2	2[a]	Zr Sn Fe Cr Ni Hf	4.254×10^{-2} 4.825×10^{-4} 1.486×10^{-4} 7.598×10^{-5} 6.731×10^{-6} 2.213×10^{-6}	0.6134	672	Cladding
3	3	H-1[b] O-16	2.475×10^{-2} 1.2375×10^{-2}	0.9174	551	Moderator

[a] The isotopic number densities in the BONAMI input are based on the element number densities listed here and isotopic abundances from [15].
[b] H-1 in H_2O.

3.3.1.3 Coolant Self-Shielding

The coolant self-shielding model, as described in Table 3.5, is based on the PWR coolant composition in Table 3.3 of [1].

Geometry:　　　　　　Slab
Number of zones:　　2
Mixing table length:　3
Dancoff factor:　　　Homogeneous (σ_e = 0.0)
Temperature:　　　　600 K

Table 3.5.　Description of mixtures used for self-shielding nuclides in the coolant model

Zone no.	Mixture no.	Nuclide	Concentration (atoms/b-cm)	Outer radius (cm)	Temperature (K)	Zone type
1	1	H-1[a] O-16 B-10	4.714×10^{-2} 2.357×10^{-2} 4.2×10^{-6}	10.0	600	Moderator

[a] H-1 in H_2O.

3.3.1.4 Carbon Steel and Stainless Steel Self-Shielding

The carbon steel (A533-B) and stainless steel (SS-304) self-shielding model, as described in Table 3.6, is based on the description in Table 3.3 of [1]. Note that this includes the silicon in the steel, which was present in the XSDRNPM models of [1] but not in the BONAMI input. The silicon has been included in the BONAMI input for consistency between the BONAMI and XSDRNPM models.

Geometry:　　　　　　Slab
Number of zones:　　2
Mixing table length:　36
Dancoff factor:　　　Homogeneous (σ_e = 0.0)
Temperature:　　　　600 K

Table 3.6.　Description of mixtures used for self-shielding nuclides in the steel models

Zone no.	Mixture no.	Nuclide	Concentration (atoms/b-cm)	Outer radius (cm)	Temperature (K)	Zone type
1 (A533-B)	1[a]	Fe Cr Ni Mn C Si	8.19×10^{-2} 1.27×10^{-4} 4.44×10^{-4} 1.12×10^{-3} 9.81×10^{-4} 3.74×10^{-4}	10.0	600	Moderator
2 (SS-304)	2[a]	Fe Cr Ni Mn C Si	5.83×10^{-2} 1.74×10^{-2} 8.55×10^{-3} 1.52×10^{-3} 2.37×10^{-4} 8.93×10^{-4}	20.0	600	Moderator

[a] The isotopic number densities in the BONAMI input are based on the element number densities listed here and isotopic abundances from [15].

3.3.1.5 Concrete Self-Shielding

The concrete self-shielding model, as described in Table 3.7, is based on the composition of Type 04 concrete from [16]. A trace (0.01 wt %) of carbon, which is not present in Type 04 concrete, was added to the mixture to provide cross-section data for carbon self-shielded in concrete. This addition maintains consistency with the self-shielded nuclides provided in the BUGLE-96 library.

Geometry: Slab
Number of zones: 1
Mixing table length: 28
Dancoff factor: Homogeneous (σ_e = 0.0)
Temperature: 300 K

Table 3.7. Description of mixtures used for self-shielding nuclides in the concrete model

Zone no.	Mixture no.	Nuclide	Concentration (atoms/b-cm)	Outer radius (cm)	Temperature (K)	Zone type
		H-1[a]	7.767×10^{-3}			
		O-16	4.408×10^{-2}			
		Si	1.591×10^{-2}			
		Ca	2.915×10^{-3}			
		Na	1.048×10^{-3}			
1	1[b]	Mg	1.487×10^{-4}	100.0	300	Moderator
		Al	2.388×10^{-3}			
		S	5.634×10^{-5}			
		K	6.931×10^{-4}			
		Fe	3.127×10^{-4}			
		C	1.178×10^{-5}			

[a] H-1 in H_2O.
[b] The isotopic number densities in the BONAMI input are based on the element number densities listed here and isotopic abundances from [15].

3.3.2 Fine-Group Spectra Used for Group Collapsing

The self-shielded fine-group cross sections were group collapsed to the BUGLE group structure using weighting spectra at the following locations of the 1D PWR and BWR reactor plant models: (1) off-center in the core region of the BWR model, (2) off-center in the core region of the PWR model, (3) the downcomer region in the PWR model, (4) within the PWR pressure vessel at one-fourth the vessel thickness, and (5) within the PWR concrete biological shield. The weighting spectra were generated using the 1D XSDRNPM discrete-ordinates transport code in SCALE. Details of the 1D PWR and BWR models are provided in Sections 3.3.2.1 and 3.3.2.2.

The calculated neutron flux spectra are shown in Figure 3.3 and listed in Table 3.10. The gamma spectra are shown in Figure 3.4 and listed in Table 3.11. In addition to these self-shielded nuclides with distinct weighting spectra, many of the nuclides in the VITAMIN-B7 library were collapsed to the BUGLE group structure using the flux spectrum calculated within the concrete shield. These nuclides are infinitely dilute (i.e., they are not self-shielded).

3.3.2.1 BWR XSDRNPM Model for Weighting Spectra

The geometry of the 1D BWR reactor plant model is shown in Figure 3.1. The compositions of the homogenized core region and the coolant regions outside the core are provided in Table 3.8. The compositions of the remaining regions (SS-304, A533-B, and concrete) are the same as those used in the BONAMI cases. The nuclides used in each region are those that were self-shielded in the equivalent BONAMI cases. For the core region, nuclide identifiers ending in "21" are self-shielded in the fuel, those ending in "22" are self-shielded in the cladding, and those ending in "23" are self-shielded in the coolant.
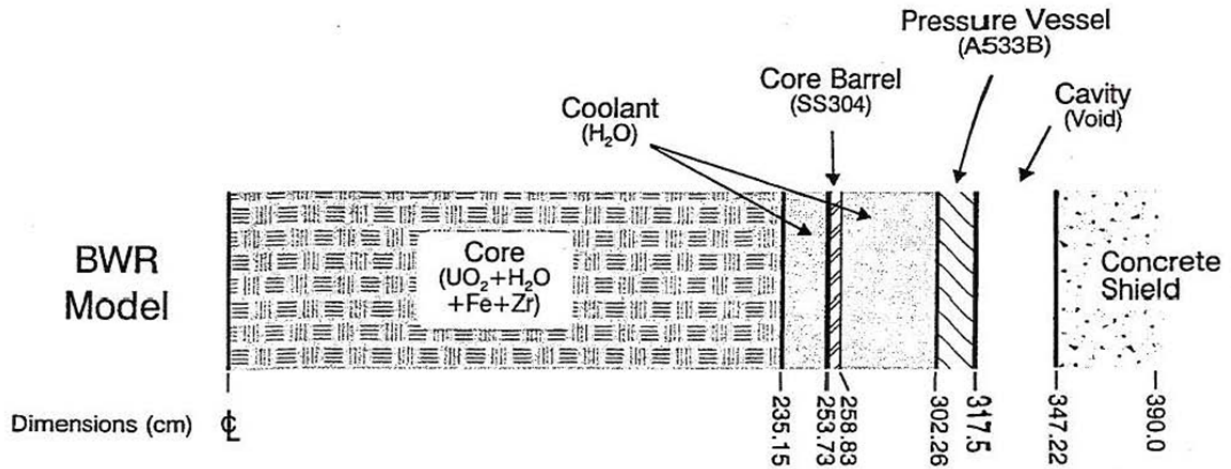
Figure 3.1. One-dimensional BWR reactor plant model used to generate weighting spectra for group collapsing BUGLE-B7 cross sections from VITAMIN-B7 data (from Ref. [1]).

Table 3.8. Description of the homogenized core and coolant mixtures used in the 1D BWR reactor plant model

(The remaining mixtures are equivalent to those in the BONAMI descriptions of Sections 3.3.1.4 and 3.3.1.5)

Mixture no.	Description	Nuclide	Nuclide identifier	Concentration (atoms/b-cm)
1	Homogenized BWR core	H-1	100123	1.5354×10^{-2}
		O-16	801623	7.677×10^{-3}
		Zr-90	4009022	2.99609×10^{-3}
		Zr-91	4009122	6.46833×10^{-4}
		Zr-92	4009222	9.88697×10^{-4}
		Zr-94	4009422	1.00196×10^{-3}
		Zr-96	4009622	1.61420×10^{-4}
		Fe-54	2605422	1.1818×10^{-6}
		Fe-56	2605622	1.83715×10^{-5}
		Fe-57	2605722	4.206×10^{-7}
		Fe-58	2605822	5.61×10^{-8}
		U-235	9223521	1.2125×10^{-4}
		U-238	9223821	5.322×10^{-3}
		O-16	801621	1.0884×10^{-2}
2	Coolant	H-1	100131	4.950×10^{-2}
		O-16	801631	2.475×10^{-2}

3.3.2.2 PWR XSDRNPM Model for Weighting Spectra

The geometry of the 1D PWR reactor plant model is shown in Figure 3.2. The compositions of the homogenized core region and the coolant regions outside the core are provided in Table 3.9. The compositions of the remaining regions (SS-304, A533-B, and concrete) are the same as those used in the BONAMI cases. The nuclides used in each region are those that were self-shielded in the equivalent BONAMI cases. For the core region, nuclide identifiers ending in "11" are self-shielded in the fuel, those ending in "12"are self-shielded in the cladding, and those ending in "13" are self-shielded in the coolant.
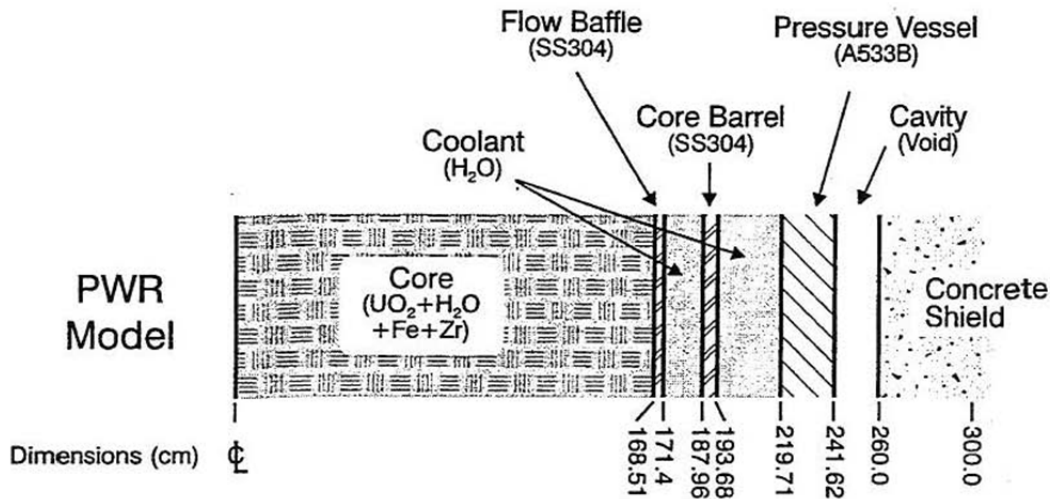
Figure 3.2. One-dimensional PWR reactor plant model used to generate weighting spectra for group collapsing BUGLE-B7 cross sections from VITAMIN-B7 data (from Ref. [1]).

Table 3.9. Description of the homogenized core and coolant mixtures used in the 1D PWR reactor plant model
(The remaining mixtures are equivalent to those in the BONAMI descriptions of Sections 3.3.1.4 and 3.3.1.5)

Mixture no.	Description	Nuclide	Nuclide identifier	Concentration (atoms/b-cm)
1	Homogenized PWR core	H-1	100113	2.768×10^{-2}
		O-16	801613	1.384×10^{-2}
		B-10	501013	2.466×10^{-6}
		Zr-90	4009012	2.19023×10^{-3}
		Zr-91	4009112	4.77635×10^{-4}
		Zr-92	4009212	7.30075×10^{-4}
		Zr-94	4009412	7.39867×10^{-4}
		Zr-96	4009612	1.19196×10^{-4}
		Fe-54	2605412	8.5196×10^{-7}
		Fe-56	2605612	1.32444×10^{-5}
		Fe-57	2605712	3.0324×10^{-7}
		Fe-58	2605812	4.0432×10^{-8}
		U-235	9223511	1.903×10^{-4}
		U-238	9223811	6.515×10^{-3}
		O-16	801611	1.343×10^{-2}
2	Coolant	H-1	100131	4.714×10^{-2}
		O-16	801631	2.357×10^{-2}
		B-10	501031	4.200×10^{-6}
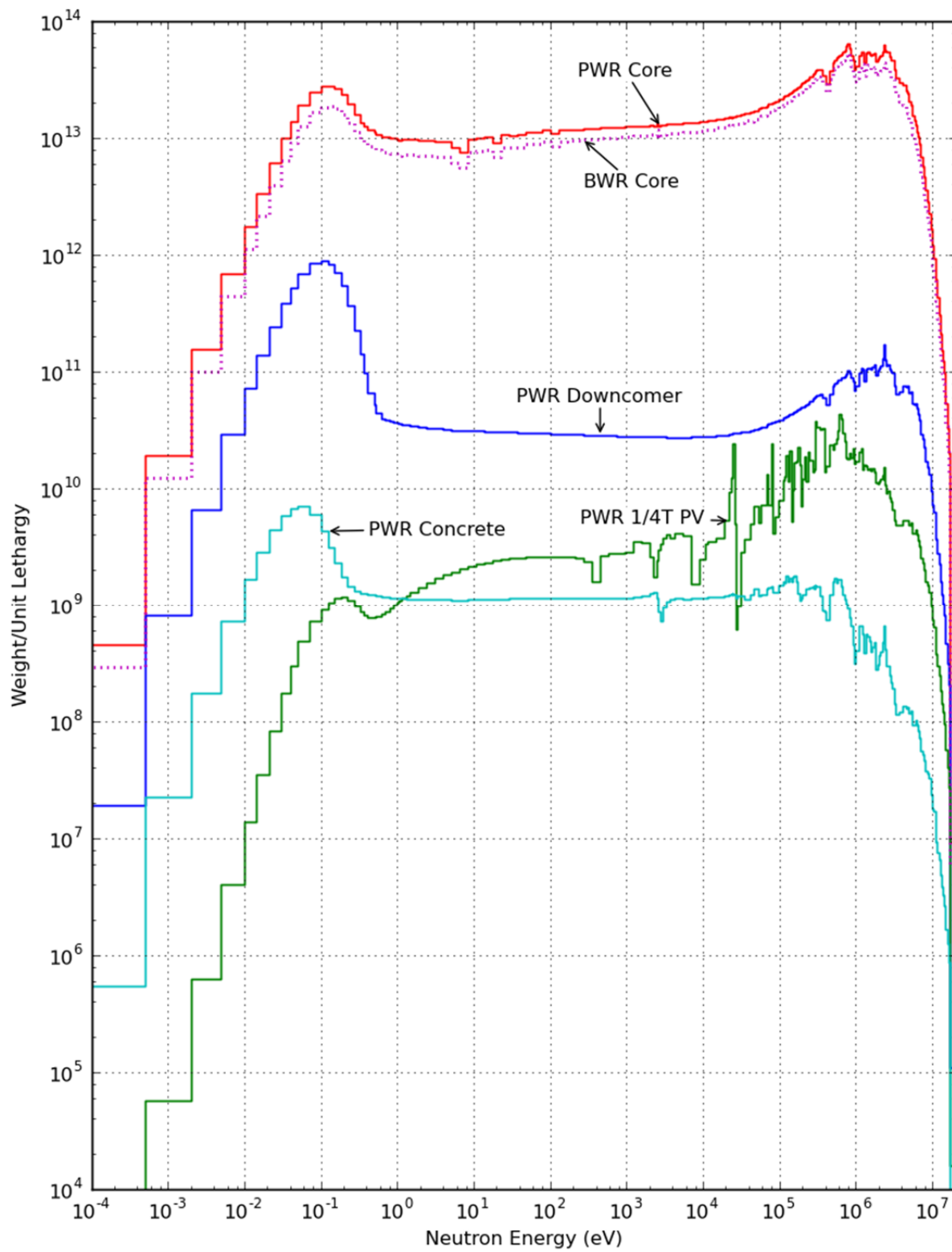
Figure 3.3. Fine-group neutron weighting spectra from the 1D BWR and PWR models.

Table 3.10. Fine-group neutron weighting spectra from the 1D BWR and PWR models

Fine group	BWR core	PWR core	PWR downcomer	PWR 1/4T pressure vessel	PWR concrete
1	7.4034E+05	1.1652E+06	1.3689E+04	1.9840E+03	7.2613E+01
2	2.8348E+08	4.3737E+08	3.4877E+06	4.1141E+05	1.1445E+04
3	3.1895E+08	4.9821E+08	5.1197E+06	6.7461E+05	2.1537E+04
4	1.0541E+09	1.6354E+09	1.5503E+07	2.0159E+06	6.3624E+04
5	1.7355E+09	2.6795E+09	2.3267E+07	2.8704E+06	8.4169E+04
6	1.2327E+09	1.8984E+09	1.5693E+07	1.8803E+06	5.3037E+04
7	1.5787E+09	2.4352E+09	2.0224E+07	2.4039E+06	6.6197E+04
8	1.9935E+09	3.0750E+09	2.5339E+07	2.9915E+06	8.2124E+04
9	2.4650E+09	3.7954E+09	3.0405E+07	3.5454E+06	9.6953E+04
10	6.7912E+09	1.0425E+10	7.9712E+07	9.1150E+06	2.4370E+05
11	5.0383E+09	7.7160E+09	5.6083E+07	6.2334E+06	1.6565E+05
12	5.2018E+09	7.9778E+09	6.0638E+07	6.8372E+06	1.8448E+05
13	1.4361E+10	2.1786E+10	1.4042E+08	1.4953E+07	3.8116E+05
14	2.0364E+10	3.0770E+10	1.8482E+08	1.8765E+07	4.6688E+05
15	3.0735E+10	4.6945E+10	3.1298E+08	3.2407E+07	8.4803E+05
16	4.0259E+10	6.0834E+10	3.5899E+08	3.6893E+07	9.0410E+05
17	5.5065E+10	8.3267E+10	4.8276E+08	4.8719E+07	1.1951E+06
18	7.4767E+10	1.1329E+11	6.5538E+08	6.4877E+07	1.6252E+06
19	9.4952E+10	1.4288E+11	7.5819E+08	7.3429E+07	1.7946E+06
20	1.1929E+11	1.7846E+11	8.6205E+08	8.0158E+07	1.8780E+06
21	1.5525E+11	2.3294E+11	1.1258E+09	1.0075E+08	2.3070E+06
22	1.9219E+11	2.8800E+11	1.3218E+09	1.1627E+08	2.5898E+06
23	2.3238E+11	3.4640E+11	1.4744E+09	1.2641E+08	2.7759E+06
24	2.9512E+11	4.4199E+11	1.9114E+09	1.6081E+08	3.5913E+06
25	1.1260E+11	1.6889E+11	7.1988E+08	6.0067E+07	1.3928E+06
26	2.5152E+11	3.7720E+11	1.6337E+09	1.3582E+08	3.1327E+06
27	4.2894E+11	6.4243E+11	2.6646E+09	2.2157E+08	5.1116E+06
28	4.7381E+11	7.0131E+11	2.5788E+09	2.0881E+08	4.6578E+06
29	5.3265E+11	7.8521E+11	2.6482E+09	2.0629E+08	4.6384E+06
30	6.4612E+11	9.6079E+11	3.3779E+09	2.5305E+08	6.2228E+06
31	7.0308E+11	1.0388E+12	3.2904E+09	2.4088E+08	5.8598E+06
32	8.1088E+11	1.2002E+12	3.7656E+09	2.6499E+08	6.5489E+06
33	8.5463E+11	1.2551E+12	3.6693E+09	2.6636E+08	6.4273E+06
34	1.9370E+12	2.8282E+12	7.5263E+09	5.3062E+08	1.3642E+07
35	2.0759E+12	2.9834E+12	6.7056E+09	4.9100E+08	1.1938E+07
36	2.2960E+12	3.2612E+12	6.4363E+09	4.8393E+08	1.1400E+07
37	1.3611E+12	1.9341E+12	3.7710E+09	2.6612E+08	7.0454E+06
38	1.6110E+12	2.3020E+12	4.8869E+09	3.3192E+08	9.4936E+06
39	1.6246E+12	2.3028E+12	4.9872E+09	3.8484E+08	1.0667E+07
40	1.7513E+12	2.4746E+12	5.2588E+09	4.1583E+08	1.2380E+07
41	1.9182E+12	2.7033E+12	5.7562E+09	4.7781E+08	1.5014E+07
42	1.9311E+12	2.7061E+12	5.6114E+09	4.5397E+08	1.5058E+07
43	1.3380E+12	1.8738E+12	4.2353E+09	3.5762E+08	1.3683E+07
44	3.6292E+11	5.1067E+11	1.3065E+09	1.1141E+08	4.2002E+06

Table 3.10. Fine-group neutron weighting spectra from the 1D BWR and PWR models

Fine group	BWR core	PWR core	PWR downcomer	PWR 1/4T pressure vessel	PWR concrete
45	3.7059E+11	5.2125E+11	1.4303E+09	1.2501E+08	5.4672E+06
46	7.2871E+11	1.0175E+12	2.4588E+09	2.0222E+08	8.9979E+06
47	1.3277E+12	1.8268E+12	4.3055E+09	4.3190E+08	1.5657E+07
48	1.8683E+12	2.5485E+12	5.6681E+09	6.0272E+08	1.9632E+07
49	1.8160E+12	2.4622E+12	5.3208E+09	5.7392E+08	1.8294E+07
50	1.7709E+12	2.3880E+12	5.1263E+09	5.5508E+08	1.5305E+07
51	1.7033E+12	2.2811E+12	4.6866E+09	5.5973E+08	1.3896E+07
52	2.0165E+12	2.6985E+12	5.7552E+09	6.9216E+08	2.4030E+07
53	1.9678E+12	2.6029E+12	5.4552E+09	7.4819E+08	2.1839E+07
54	1.9144E+12	2.5209E+12	5.1811E+09	7.1039E+08	1.9868E+07
55	2.0032E+12	2.6273E+12	5.3326E+09	7.4358E+08	2.4080E+07
56	2.1002E+12	2.7369E+12	5.3660E+09	7.1873E+08	2.6627E+07
57	2.0562E+12	2.6588E+12	5.2589E+09	7.6846E+08	2.7606E+07
58	1.7172E+12	2.2071E+12	4.1276E+09	8.0072E+08	1.9045E+07
59	2.1402E+12	2.7532E+12	5.2048E+09	7.2908E+08	2.8223E+07
60	2.1494E+12	2.7339E+12	5.3453E+09	1.0972E+09	3.3087E+07
61	1.9991E+12	2.5273E+12	4.8444E+09	1.0321E+09	3.2701E+07
62	3.2889E+12	4.1520E+12	7.6215E+09	1.7021E+09	4.0242E+07
63	1.2881E+12	1.6229E+12	2.8549E+09	6.7632E+08	1.3089E+07
64	2.1573E+12	2.6952E+12	4.8049E+09	1.2719E+09	2.6598E+07
65	2.0823E+12	2.5687E+12	4.4237E+09	9.0783E+08	3.2951E+07
66	2.4022E+12	2.9289E+12	4.8882E+09	9.9454E+08	3.8374E+07
67	2.6672E+12	3.2138E+12	5.0901E+09	8.8520E+08	4.6651E+07
68	2.5545E+12	3.0408E+12	4.7773E+09	9.0662E+08	5.1140E+07
69	2.3821E+12	2.8187E+12	4.5885E+09	1.2637E+09	5.6060E+07
70	2.2967E+12	2.7104E+12	4.4566E+09	1.4812E+09	6.2259E+07
71	2.2357E+12	2.6308E+12	4.4009E+09	1.9916E+09	7.1873E+07
72	2.1751E+12	2.5536E+12	4.2913E+09	2.1566E+09	8.2835E+07
73	2.1151E+12	2.4794E+12	4.2139E+09	1.5470E+09	8.4246E+07
74	2.0546E+12	2.4056E+12	4.0724E+09	1.3153E+09	7.7597E+07
75	1.9945E+12	2.3333E+12	3.9410E+09	1.2173E+09	8.4693E+07
76	1.9157E+12	2.2411E+12	3.7900E+09	1.0836E+09	8.0072E+07
77	3.1915E+12	3.7632E+12	6.5006E+09	2.3478E+09	1.2367E+08
78	2.4525E+12	2.9360E+12	5.2166E+09	1.5580E+09	7.3697E+07
79	1.4408E+12	1.7268E+12	3.0279E+09	6.8903E+08	4.3161E+07
80	1.4439E+12	1.7207E+12	3.0149E+09	1.6381E+09	4.5030E+07
81	3.2869E+12	3.8611E+12	6.4222E+09	3.2368E+09	1.1971E+08
82	3.3507E+12	3.8896E+12	6.3385E+09	3.3818E+09	1.4396E+08
83	3.7462E+11	4.3239E+11	7.0691E+08	4.4117E+08	1.6897E+07
84	1.3773E+11	1.5895E+11	2.6040E+08	1.4508E+08	6.3249E+06
85	2.8933E+11	3.3400E+11	5.4775E+08	2.3122E+08	1.2996E+07
86	7.8566E+11	9.0719E+11	1.4859E+09	3.6386E+08	3.4904E+07
87	1.5319E+12	1.7677E+12	2.8983E+09	6.9973E+08	7.2281E+07
88	2.9140E+12	3.3594E+12	5.5549E+09	1.7596E+09	1.4144E+08
89	1.3910E+12	1.6027E+12	2.6734E+09	1.0177E+09	6.9762E+07

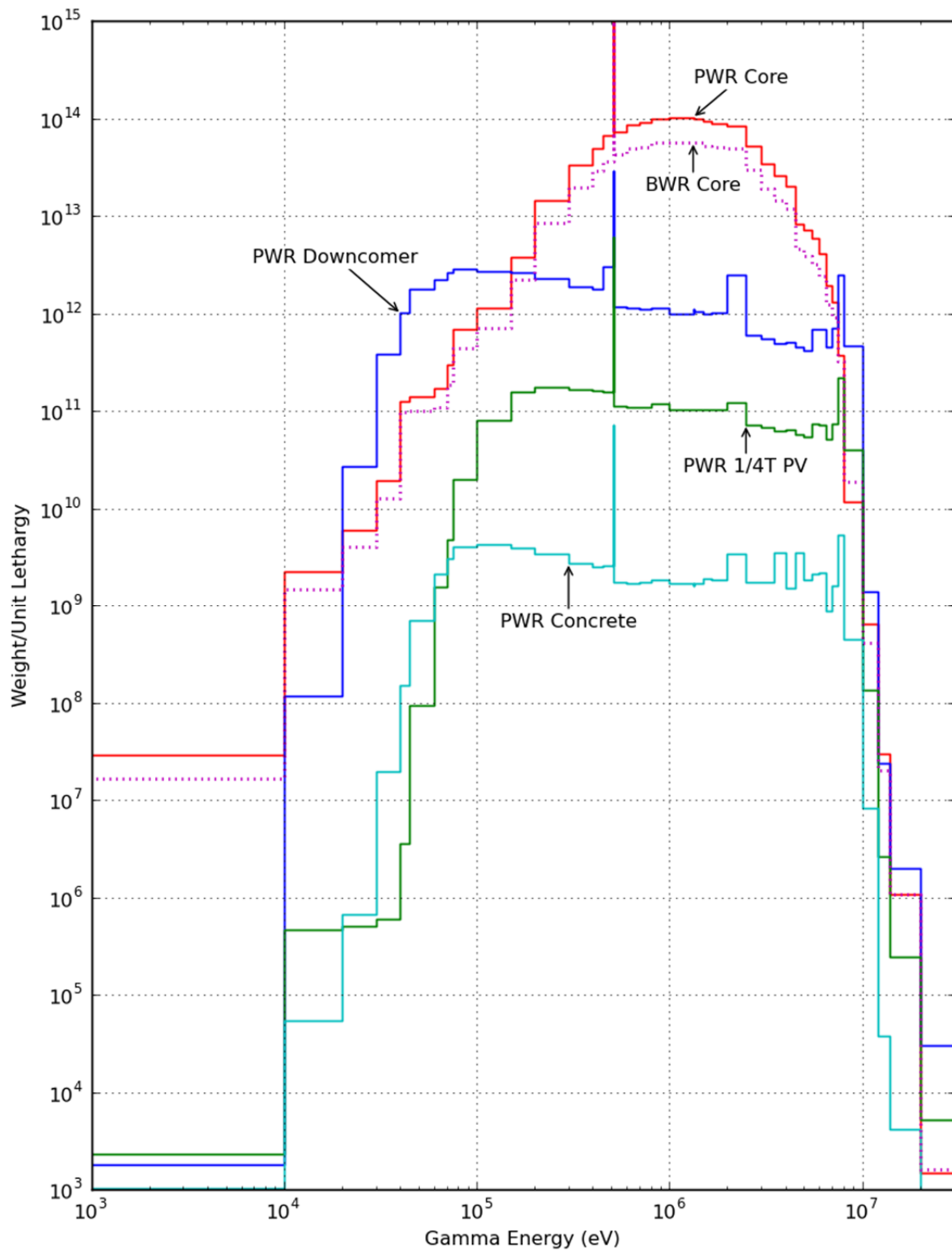**Table 3.10. Fine-group neutron weighting spectra from the 1D BWR and PWR models**

Fine group	BWR core	PWR core	PWR downcomer	PWR 1/4T pressure vessel	PWR concrete
90	1.3457E+12	1.5530E+12	2.6105E+09	5.8077E+08	6.9327E+07
91	1.3093E+12	1.5126E+12	2.5600E+09	9.2774E+08	6.2300E+07
92	1.2783E+12	1.4780E+12	2.5134E+09	5.9753E+08	6.0962E+07
93	1.2461E+12	1.4421E+12	2.4633E+09	3.5654E+08	5.7686E+07
94	1.2121E+12	1.4034E+12	2.4090E+09	7.9281E+08	5.5178E+07
95	1.1826E+12	1.3700E+12	2.3641E+09	1.1297E+09	6.3833E+07
96	1.1517E+12	1.3354E+12	2.3124E+09	8.5419E+08	7.8954E+07
97	1.1272E+12	1.3078E+12	2.2742E+09	8.3562E+08	8.9362E+07
98	1.0988E+12	1.2763E+12	2.2311E+09	4.9196E+08	8.6548E+07
99	1.0742E+12	1.2490E+12	2.1908E+09	2.5833E+08	7.9384E+07
100	1.0485E+12	1.2188E+12	2.1438E+09	1.0576E+09	8.5262E+07
101	1.0257E+12	1.1928E+12	2.1067E+09	5.8177E+08	7.8929E+07
102	1.0037E+12	1.1681E+12	2.0706E+09	9.6342E+08	8.9268E+07
103	9.8082E+11	1.1422E+12	2.0307E+09	6.2906E+08	7.8103E+07
104	9.6313E+11	1.1224E+12	2.0017E+09	5.8502E+08	7.9068E+07
105	2.3263E+12	2.7157E+12	4.8721E+09	9.8982E+08	1.8685E+08
106	2.2137E+12	2.5932E+12	4.6998E+09	7.1494E+08	1.6321E+08
107	8.2928E+11	9.6456E+11	1.7430E+09	1.9605E+08	6.1852E+07
108	6.1885E+11	7.3178E+11	1.3525E+09	8.9514E+08	5.4065E+07
109	1.6602E+12	1.9371E+12	3.5295E+09	7.1066E+08	1.3947E+08
110	1.0546E+12	1.2482E+12	2.3140E+09	8.8534E+08	9.1425E+07
111	2.7534E+12	3.2181E+12	5.9313E+09	1.2755E+09	2.1530E+08
112	1.1314E+12	1.3295E+12	2.4708E+09	3.8644E+08	9.0173E+07
113	1.8223E+12	2.1533E+12	4.0405E+09	8.8147E+08	1.7182E+08
114	1.7415E+12	2.0794E+12	3.9487E+09	6.2868E+08	1.5480E+08
115	2.4648E+12	2.8758E+12	5.3928E+09	6.4109E+08	1.9616E+08
116	1.0162E+12	1.1953E+12	2.2672E+09	2.1258E+08	9.0193E+07
117	1.4692E+12	1.7302E+12	3.2921E+09	1.0792E+08	1.3436E+08
118	7.0469E+11	8.3395E+11	1.5981E+09	3.2966E+07	6.2731E+07
119	4.6046E+11	5.4385E+11	1.0517E+09	1.7637E+08	4.3321E+07
120	6.4545E+11	7.6143E+11	1.4763E+09	1.2172E+09	6.1346E+07
121	3.1618E+11	3.7644E+11	7.3564E+08	5.9378E+08	3.1251E+07
122	3.1397E+11	3.7475E+11	7.3110E+08	3.1150E+08	3.0834E+07
123	9.5796E+11	1.1290E+12	2.1799E+09	6.9480E+08	9.1506E+07
124	1.5321E+12	1.8347E+12	3.5907E+09	6.5949E+08	1.4999E+08
125	3.0774E+12	3.6337E+12	7.0826E+09	9.3190E+08	2.9548E+08
126	2.9742E+12	3.5351E+12	7.0031E+09	8.7233E+08	2.9222E+08
127	1.1678E+12	1.3921E+12	2.7821E+09	3.3123E+08	1.1590E+08
128	1.7224E+12	2.0628E+12	4.1520E+09	3.6833E+08	1.7098E+08
129	2.8150E+12	3.3881E+12	6.8822E+09	3.7791E+08	2.8689E+08
130	2.8204E+12	3.3649E+12	6.8697E+09	9.8607E+08	2.8322E+08
131	2.7559E+12	3.3112E+12	6.8618E+09	1.0295E+09	2.8562E+08
132	1.6343E+12	1.9691E+12	4.1184E+09	5.5869E+08	1.6840E+08
133	1.0920E+12	1.3130E+12	2.7490E+09	4.0615E+08	1.0833E+08
134	1.0745E+12	1.2996E+12	2.7507E+09	3.8060E+08	9.6542E+07

Table 3.10. Fine-group neutron weighting spectra from the 1D BWR and PWR models

Fine group	BWR core	PWR core	PWR downcomer	PWR 1/4T pressure vessel	PWR concrete
135	1.0471E+12	1.2827E+12	2.7526E+09	3.3591E+08	7.2082E+07
136	5.0545E+11	6.2941E+11	1.3758E+09	1.4741E+08	4.3914E+07
137	5.8435E+11	6.7638E+11	1.3758E+09	1.2083E+08	5.7623E+07
138	1.0466E+12	1.2716E+12	2.7534E+09	1.7560E+08	1.2982E+08
139	1.0779E+12	1.2988E+12	2.7637E+09	2.5952E+08	1.2528E+08
140	2.6025E+12	3.1702E+12	6.9325E+09	8.5679E+08	3.0272E+08
141	2.5938E+12	3.1603E+12	6.9582E+09	8.6975E+08	2.9377E+08
142	2.5886E+12	3.1562E+12	6.9856E+09	7.0789E+08	2.9019E+08
143	2.5382E+12	3.1102E+12	7.0227E+09	6.9958E+08	2.8935E+08
144	2.5032E+12	3.0779E+12	7.0590E+09	6.8924E+08	2.8915E+08
145	2.4749E+12	3.0530E+12	7.0969E+09	6.6231E+08	2.8910E+08
146	2.4533E+12	3.0362E+12	7.1279E+09	3.9652E+08	2.8857E+08
147	2.4255E+12	3.0138E+12	7.1828E+09	5.9109E+08	2.8856E+08
148	2.3763E+12	2.9627E+12	7.2245E+09	6.2887E+08	2.8843E+08
149	2.3656E+12	2.9537E+12	7.2650E+09	6.4364E+08	2.8818E+08
150	2.3261E+12	2.9196E+12	7.3094E+09	6.5075E+08	2.8798E+08
151	2.1287E+12	2.7186E+12	7.3504E+09	6.5300E+08	2.8752E+08
152	2.3217E+12	2.9142E+12	7.3936E+09	6.5287E+08	2.8706E+08
153	2.2008E+12	2.7881E+12	7.4367E+09	6.5064E+08	2.8651E+08
154	2.2039E+12	2.7967E+12	7.4797E+09	6.4605E+08	2.8588E+08
155	2.0972E+12	2.6976E+12	7.5227E+09	6.3879E+08	2.8518E+08
156	2.0546E+12	2.6313E+12	7.5644E+09	6.2900E+08	2.8437E+08
157	2.0795E+12	2.6752E+12	7.6067E+09	6.1637E+08	2.8351E+08
158	1.7398E+12	2.2970E+12	7.6466E+09	6.0102E+08	2.8250E+08
159	1.9647E+12	2.5578E+12	7.6886E+09	5.8279E+08	2.8150E+08
160	1.9410E+12	2.5249E+12	7.7261E+09	5.6292E+08	2.8036E+08
161	1.8821E+12	2.4617E+12	7.7562E+09	5.3813E+08	2.7900E+08
162	1.3821E+12	1.8895E+12	7.7880E+09	5.1095E+08	2.7757E+08
163	1.5255E+12	2.0917E+12	7.8204E+09	4.8177E+08	2.7607E+08
164	1.7361E+12	2.3269E+12	8.0473E+09	4.5827E+08	2.8036E+08
165	1.7358E+12	2.3237E+12	8.1219E+09	4.2504E+08	2.7772E+08
166	1.7669E+12	2.3641E+12	8.2442E+09	3.9069E+08	2.7859E+08
167	1.7774E+12	2.3817E+12	8.3982E+09	3.5591E+08	2.7968E+08
168	1.8023E+12	2.4170E+12	8.5658E+09	3.2486E+08	2.8115E+08
169	7.6709E+11	1.0319E+12	3.7014E+09	1.2885E+08	1.1962E+08
170	1.0409E+12	1.4008E+12	5.1174E+09	1.6523E+08	1.6428E+08
171	2.9056E+11	3.9221E+11	1.4623E+09	4.4951E+07	4.6847E+07
172	2.6869E+11	3.6279E+11	1.3487E+09	4.0260E+07	4.3050E+07
173	2.8371E+11	3.8373E+11	1.4290E+09	4.0745E+07	4.4855E+07
174	9.6750E+11	1.3053E+12	4.8306E+09	1.3067E+08	1.5173E+08
175	6.8130E+11	9.2215E+11	3.4488E+09	8.5179E+07	1.0591E+08
176	1.2083E+12	1.6330E+12	6.1481E+09	1.3911E+08	1.8629E+08
177	6.7008E+11	9.0790E+11	3.5097E+09	7.2979E+07	1.0393E+08
178	1.2859E+12	1.7436E+12	7.1731E+09	1.2836E+08	1.9454E+08
179	5.0940E+11	6.9543E+11	3.2058E+09	4.7441E+07	7.5270E+07

Table 3.10. Fine-group neutron weighting spectra from the 1D BWR and PWR models

Fine group	BWR core	PWR core	PWR downcomer	PWR 1/4T pressure vessel	PWR concrete
180	1.6203E+12	2.2133E+12	1.2427E+10	1.4692E+08	2.3248E+08
181	1.1136E+12	1.5368E+12	1.1960E+10	9.8701E+07	1.5140E+08
182	1.1896E+12	1.6559E+12	1.7076E+10	1.0605E+08	1.5126E+08
183	1.8814E+12	2.6572E+12	3.7321E+10	1.6323E+08	2.1925E+08
184	2.7266E+12	3.9199E+12	7.3722E+10	2.1999E+08	2.9307E+08
185	3.2258E+12	4.7111E+12	1.0916E+11	2.3430E+08	3.5321E+08
186	3.6594E+12	5.4140E+12	1.4474E+11	2.3376E+08	4.6719E+08
187	3.4197E+12	5.1174E+12	1.5120E+11	1.8940E+08	5.6715E+08
188	4.1202E+12	6.2160E+12	1.9807E+11	2.0177E+08	9.6181E+08
189	5.8834E+12	8.9272E+12	3.0547E+11	2.5952E+08	2.1568E+09
190	4.2281E+12	6.4532E+12	2.3451E+11	1.6286E+08	2.3951E+09
191	2.0300E+12	3.1130E+12	1.1748E+11	6.5982E+07	1.5131E+09
192	1.8542E+12	2.8539E+12	1.1072E+11	4.9697E+07	1.6982E+09
193	1.4149E+12	2.1843E+12	8.6955E+10	2.9774E+07	1.5654E+09
194	8.0702E+11	1.2493E+12	5.0856E+10	1.2906E+07	1.0466E+09
195	4.2120E+11	6.5357E+11	2.7046E+10	5.1424E+06	6.1392E+08
196	3.0781E+11	4.7853E+11	2.0073E+10	2.7927E+06	4.9546E+08
197	9.1821E+10	1.4306E+11	6.0675E+09	5.8151E+05	1.6107E+08
198	1.7008E+10	2.6548E+10	1.1289E+09	7.9657E+04	3.1250E+07
199	1.1410E+09	1.7814E+09	7.5436E+07	4.4364E+03	2.1357E+06

Figure 3.4. Fine-group gamma weighting spectra from the 1D BWR and PWR models.

Table 3.11. Fine-group gamma weighting spectra from the 1D BWR and PWR models

Fine group	BWR core	PWR core	PWR downcomer	PWR 1/4T pressure vessel	PWR concrete
1	6.5625E+02	6.0659E+02	1.2340E+04	2.0883E+03	4.5662E+01
2	3.8697E+05	3.8075E+05	7.0004E+05	8.6233E+04	1.4901E+03
3	3.0811E+06	4.5177E+06	3.6753E+06	4.0796E+05	5.7632E+03
4	7.3879E+07	1.1705E+08	2.5340E+08	2.4284E+07	1.5185E+06
5	4.2255E+09	2.6380E+09	1.0215E+11	8.8743E+09	9.7966E+07
6	2.0652E+10	2.3818E+10	1.5940E+11	1.4294E+10	3.3993E+08
7	6.3363E+10	9.1133E+10	4.8905E+10	5.0100E+09	1.1066E+08
8	9.2640E+10	1.4474E+11	3.3782E+10	3.8429E+09	6.4522E+07
9	1.9306E+11	3.2867E+11	5.4526E+10	5.7934E+09	1.7301E+08
10	2.7373E+11	5.1008E+11	5.9217E+10	6.4439E+09	1.8634E+08
11	3.6621E+11	6.7757E+11	3.9188E+10	5.1374E+09	1.7496E+08
12	4.8172E+11	8.6989E+11	4.7531E+10	6.0754E+09	3.7454E+08
13	1.3998E+12	2.3963E+12	5.9742E+10	7.4576E+09	1.8038E+08
14	1.9455E+12	3.4019E+12	6.5233E+10	8.4190E+09	4.7152E+08
15	2.9489E+12	5.2058E+12	8.5363E+10	1.0486E+10	2.6937E+08
16	5.4454E+12	9.5606E+12	1.0778E+11	1.3055E+10	3.1449E+08
17	1.0896E+13	1.8731E+13	5.5368E+11	2.6988E+10	7.6379E+08
18	9.5278E+12	1.6421E+13	1.8974E+11	1.9285E+10	3.4869E+08
19	5.2995E+12	9.3788E+12	1.0037E+11	1.0331E+10	1.9397E+08
20	6.2922E+12	1.1200E+13	1.1766E+11	1.1653E+10	1.9011E+08
21	4.2595E+11	7.6561E+11	8.2820E+09	7.7874E+08	1.2177E+07
22	1.6054E+13	2.8722E+13	2.8397E+11	2.9300E+10	4.8943E+08
23	1.2606E+13	2.1996E+13	2.5588E+11	2.6068E+10	4.1545E+08
24	6.8086E+12	1.2120E+13	1.4718E+11	1.4343E+10	2.3374E+08
25	7.6130E+12	1.3389E+13	1.7329E+11	1.6832E+10	2.6329E+08
26	6.6842E+12	1.1575E+13	1.8426E+11	1.7673E+10	2.7884E+08
27	3.9421E+12	6.7731E+12	1.1253E+11	2.3384E+10	2.8219E+08
28	4.4756E+12	8.3124E+12	3.8183E+11	1.9738E+10	3.2562E+08
29	3.3769E+12	5.8446E+12	2.0854E+11	1.8669E+10	2.9277E+08
30	5.5828E+12	9.5714E+12	5.4382E+11	4.6990E+10	7.8313E+08
31	3.4384E+12	5.7836E+12	9.1767E+11	7.1222E+10	1.3853E+09
32	6.4196E+11	1.0683E+12	7.4570E+11	4.5103E+10	1.1372E+09
33	2.8565E+11	4.5359E+11	1.0878E+12	3.2230E+10	1.7310E+09
34	1.2480E+11	1.9858E+11	8.1060E+11	5.6950E+09	1.1695E+09
35	1.2878E+10	2.0266E+10	1.7867E+11	3.2536E+08	2.1199E+08
36	1.6623E+10	2.5910E+10	3.4271E+11	2.4270E+08	3.2498E+08
37	2.8897E+10	3.9736E+10	5.1089E+11	2.6484E+07	2.0151E+08
38	1.1308E+10	1.4875E+10	1.1802E+11	4.2032E+05	1.7484E+07
39	3.6878E+09	5.4675E+09	1.1007E+11	1.7072E+05	5.6426E+06
40	1.6152E+09	2.4150E+09	1.0967E+10	2.0718E+05	2.6908E+05
41	1.0354E+09	1.5679E+09	8.1821E+07	3.2258E+05	3.7104E+04
42	3.7997E+07	6.5722E+07	4.1407E+03	5.3263E+03	2.3838E+03

3.4   Processing Codes and Procedures

All the processing of the fine-group VITAMIN-B7 library into the broad-group BUGLE-B7 library was performed using modules of the AMPX code system. The names and a brief description of each module are provided in Table 3.12. Figure 3.5 illustrates the steps that were performed to self-shield the fine-group data and create the fine-group weighting spectra. Figure 3.6 illustrates the steps that were used to collapse the fine-group data using the PWR- and BWR-specific flux spectra.

The treatment of upscatter in the thermal groups was handled in two ways. In many shielding applications, accurate calculation of the thermal flux is relatively unimportant, because neutron transport is dominated by higher-energy neutrons. When the thermal flux is unimportant, the transport calculations can be run more rapidly by ignoring upscatter and hence eliminating the need to perform outer iterations to converge the flux.

The method used to remove the upscatter terms in the BUGLE-B7 library is consistent with that used in BUGLE-96. In the MALOCS processing step illustrated in Figure 3.6, the upscatter between two groups is set to zero and the downscatter is reduced by an equivalent amount to preserve the net transfer rate between the two groups. The in-group scattering terms for both groups are increased by a corresponding amount to preserve the total scattering rate. This approach is referred to as the "ANISN upscatter" approximation. Although this adjustment provides an acceptable solution in most circumstances, it can lead to negative downscatter terms if the upscatter is greater than the downscatter between two groups.

The final processing sequence used in creating the BUGLE-B7, shown in Figure 3.7, was the creation of a full set of infinitely dilute cross sections collapsed with the concrete weighting spectrum. These nuclides can be used for general purposes where the problem-specific self-shielded and weighted data sets are not appropriate.

3.5   Library Format and Content

The BUGLE-B7 data library contains two major parts:

1. BUGLE-B7: a complete replacement for all the data contained in BUGLE-96. This library uses the "ANISN upscatter" approximation to remove the upscatter cross sections
2. BUGLE-B7T: the same cross sections as BUGLE-B7 with the inclusion of the thermal upscatter cross sections

The BUGLE-B7 library package is available in ANISN card image format and AMPX working library format. The table width of the ANISN-formatted files for BUGLE-B7 is 67, and the table length is 70. For BUGLE-B7T the table width is 67, and the table length is 74.

Table positions 1 through 3 are defined in the normal manner as follows:

1. absorption cross section (σ_a)
2. fission cross section multiplied by the average number of neutrons per fission ($\nu\sigma_f$)
3. total cross section (σ_t)

For the BUGLE-B7 data, position 4 is the in-group scattering cross section, and positions 5 through 70 are the downscatter cross sections. For the BUGLE-B7T, data positions 4 through 7

54

are the upscatter cross sections, position 8 is the in-group scattering cross section, and positions 9 through 74 are the downscatter cross sections.

Listings of the library contents for BUGLE-B7 are given in Table 3.13 and Table 3.14. Table 3.13 lists the materials that were processed as infinitely dilute (i.e., with no self-shielding) and collapsed using the concrete weighting spectrum. Table 3.14 lists the materials that were self-shielded and collapsed using the PWR and BWR spectra described in Section 3.3.

Table 3.12. AMPX modules used to self-shield and group collapse fine-group cross sections into the BUGLE-B7 library

Module name	Function
AIM	Converts AMPX master libraries between binary and BCD formats
AJAX	Merges and deletes nuclides from AMPX master libraries
ALPO	Produces an ANISN library from an AMPX working library
BONAMI	Performs interpolation on Bondarenko factors to self-shield reaction cross sections
MALOCS	Collapses data in an AMPX master library to a coarser group structure based on a specified weighting spectrum
NITAWL	Converts a master library to working library format
PALEALE	Lists data contained in AMPX master and working libraries
WORKER	Prepares working libraries for use in transport calculations. Interpolates thermal scattering matrices, which is particularly useful for nuclides with upscattering
XSDRNPM	Performs 1D discrete-ordinates transport calculations using cross sections from an AMPX working library
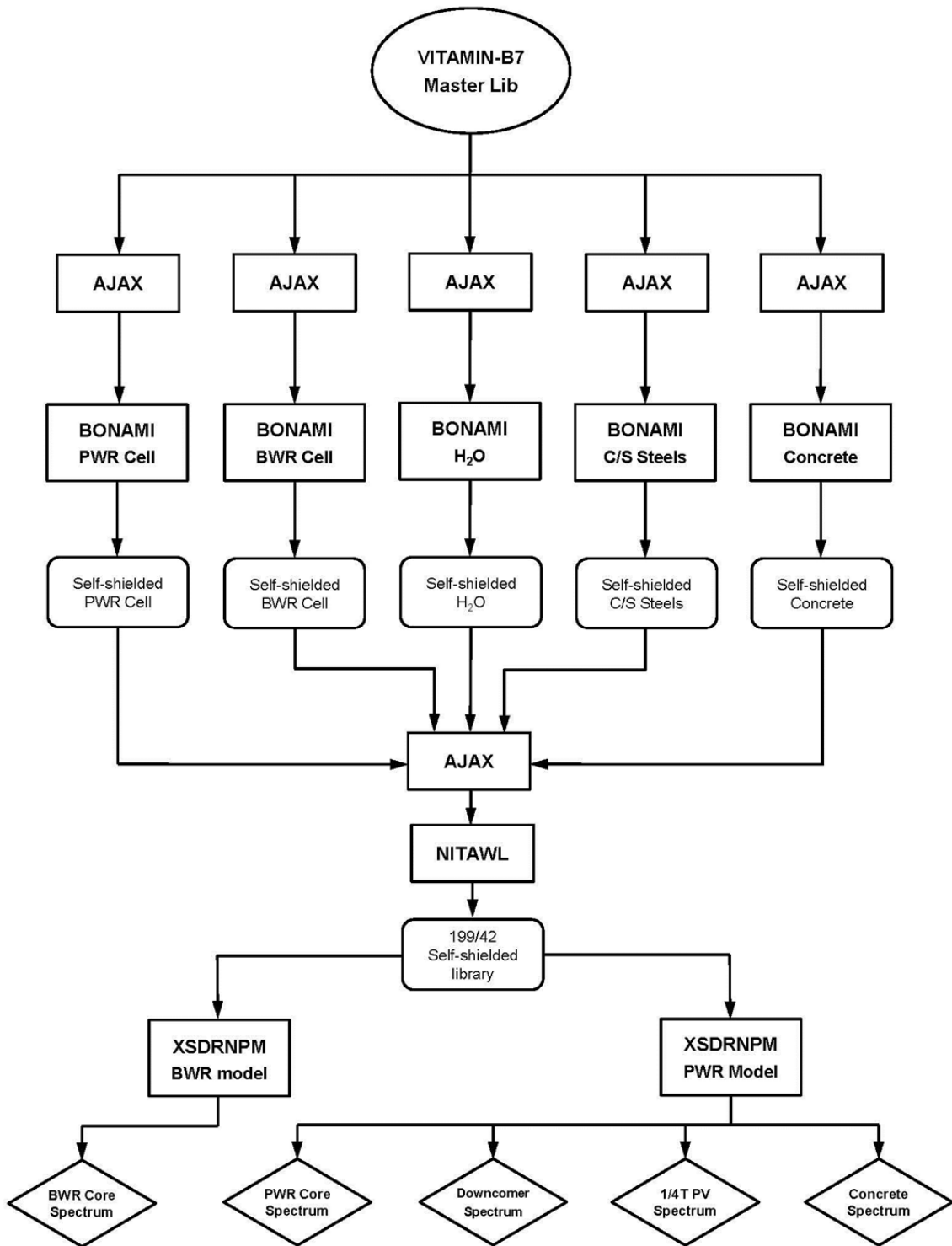
Figure 3.5. Procedure for self-shielding nuclide data and calculating BWR- and PWR-specific flux spectra.
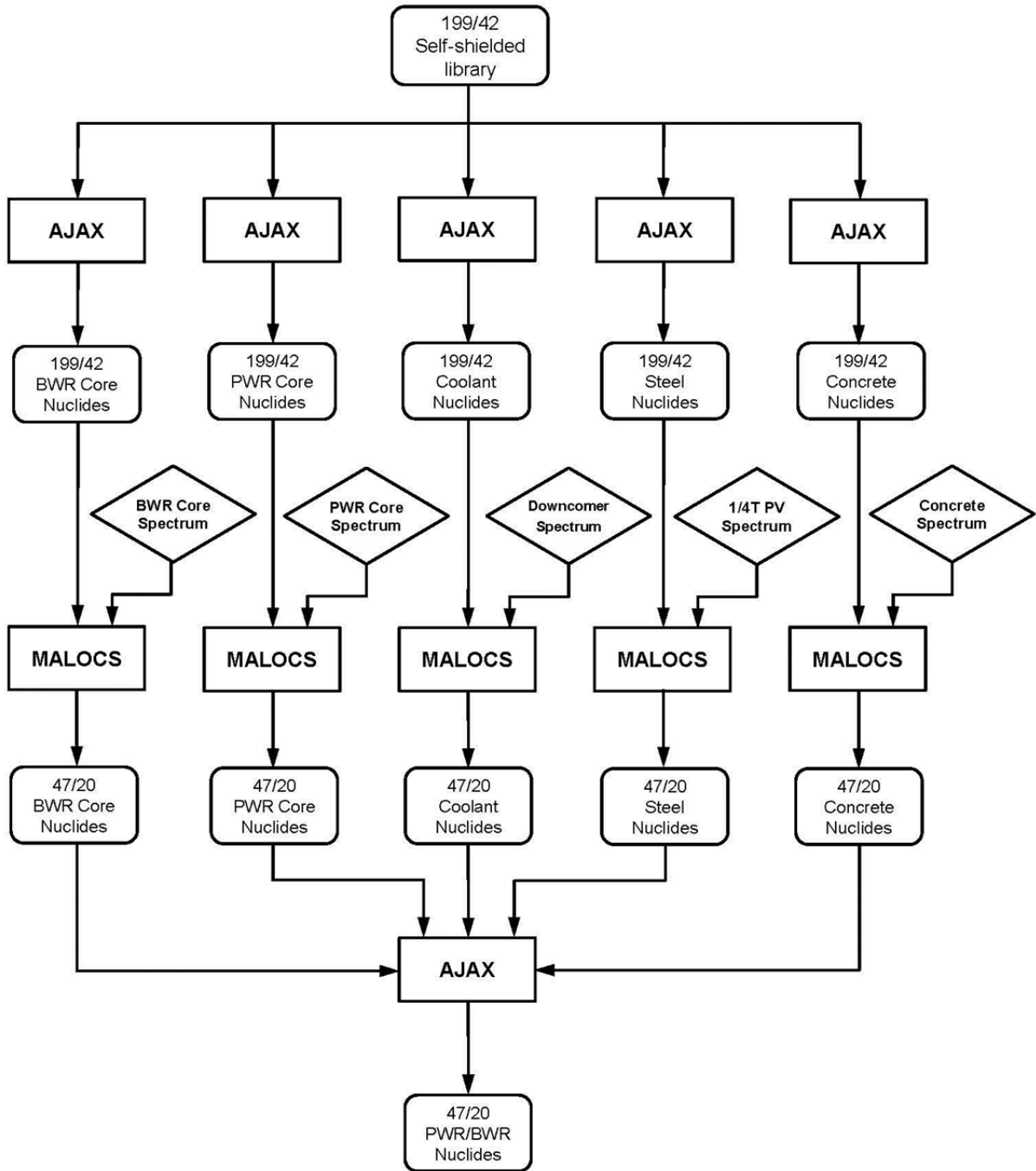
Figure 3.6. Procedure for collapsing self-shielded fine-group cross sections into the BUGLE-B7 library.

Figure 3.7. Procedure for generating infinitely dilute BUGLE-B7 data with the concrete weighting spectrum.

Table 3.13. Nuclides in BUGLE-B7 that are infinitely dilute and collapsed with the concrete weighting spectrum

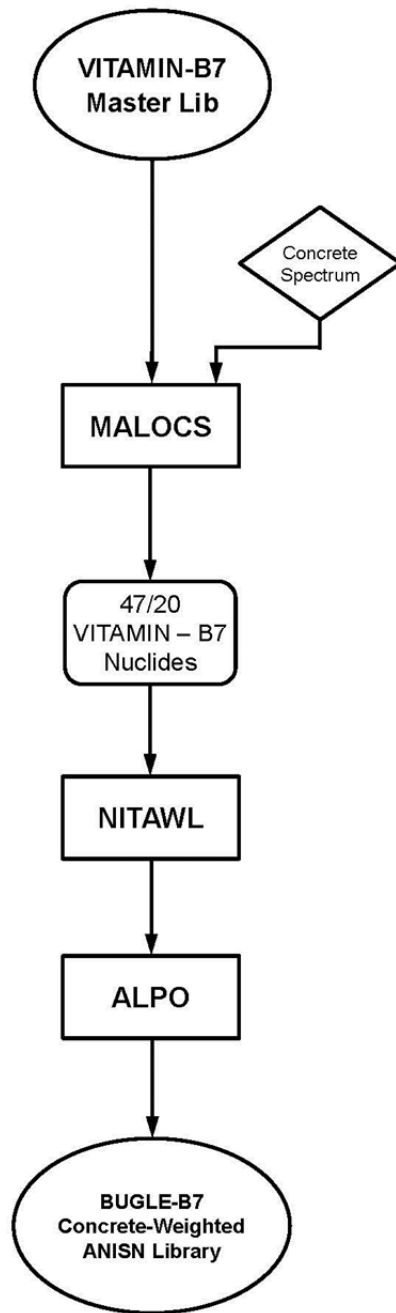| Nuclide	ANISN ID		Nuclide	ANISN ID		Nuclide	ANISN ID
Ag-107	1-6		Fe-54	275-282		Pa-233	567-572
Ag-109	7-12		Fe-56	283-290		Pb-206	573-578
Al-27	13-20		Fe-57	291-298		Pb-207	579-584
Am-241	21-26		Fe-58	299-306		Pb-208	585-590
Am-242	27-32		Ga	307-312		Pu-236	591-596
Am-242m	33-38		H-1 (H2O)	313-320		Pu-237	597-602
Am-243	39-44		H-1 (CH2)	321-328		Pu-238	603-608
Au-197	45-50		H-2 (D2O)	329-336		Pu-239	609-614
B-10	51-58		H-3	337-344		Pu-240	615-620
B-11	59-66		He-3	345-352		Pu-241	621-626
Ba-138	67-72		He-4	353-360		Pu-242	627-632
Be-9	73-80		Hf-174	361-366		Pu-243	633-638
Be-9 (Thermal)	81-88		Hf-176	367-372		Pu-244	639-644
Bi-209	89-94		Hf-177	373-378		Re-185	645-650
C	95-102		Hf-178	379-784		Re-187	651-656
C (Graphite)	103-110		Hf-179	385-390		S	657-664
Ca	111-118		Hf-180	391-396		S-32	665-672
Cd-Nat	119-124		In-Nat	397-402		Si	673-680
Cl-Nat	125-132		K	403-410		Sn-Nat	681-686
Cm-241	133-138		Li-6	411-418		Ta-181	687-692
Cm-242	139-144		Li-7	419-426		Ta-182	693-698
Cm-243	145-150		Mg	427-434		Th-230	699-704
Cm-244	151-156		Mn-55	435-442		Th-232	705-710
Cm-245	157-162		Mo	443-448		Ti	711-718
Cm-246	163-168		N-14	449-456		U-232	719-724
Cm-247	169-174		N-15	457-464		U-233	725-730
Cm-248	175-180		Na-23	465-472		U-234	731-736
Co-59	181-188		Nb-93	473-478		U-235	737-742
Cr-50	189-196		Ni-58	479-486		U-236	743-748
Cr-52	197-204		Ni-60	487-494		U-237	749-754
Cr-53	205-212		Ni-61	495-502		U-238	755-760
Cr-54	213-220		Ni-62	503-510		V	761-768
Cu-63	221-228		Ni-64	511-518		W-Nat	769-774
Cu-65	229-236		Np-237	519-524		W-182	775-780
Eu-151	237-242		Np-238	525-530		W-183	781-786
Eu-152	243-248		Np-239	531-536		W-184	787-792
Eu-153	249-254		O-16	537-544		W-186	793-798
Eu-154	255-260		O-17	545-552		Y-89	799-804
Eu-155	261-266		P-31	553-560		Zr	805-810
F-19	267-274		Pa-231	561-566		Zr (Zirc-2)	811-816

Table 3.14. Nuclides in BUGLE-B7 that are self-shielded and collapsed using specific BWR and PWR weighting spectra

Nuclide	ANISN ID	Description
B-10	1001-1008	PWR core coolant
Cr-50	1009-1016	PWR core clad
Cr-52	1017-1024	PWR core clad
Cr-53	1025-1032	PWR core clad
Cr-54	1033-1040	PWR core clad
Fe-54	1041-1048	PWR core clad
Fe-56	1049-1056	PWR core clad
Fe-57	1057-1064	PWR core clad
Fe-58	1065-1072	PWR core clad
H-1 (H2O)	1073-1080	PWR core coolant
Ni-58	1081-1088	PWR core clad
Ni-60	1089-1096	PWR core clad
Ni-61	1097-1104	PWR core clad
Ni-62	1105-1112	PWR core clad
Ni-64	1113-1120	PWR core clad
O-16	1121-1128	PWR core coolant
U-235	1129-1136	PWR core fuel
U-238	1137-1142	PWR core fuel
Zr	1149-1154	PWR core clad
H-1 (H2O)	2001-2008	PWR downcomer
O-16	2009-2016	PWR downcomer
C	2017-2024	PWR downcomer
Cr-50	2025-2032	PWR downcomer
Cr-52	2033-2040	PWR downcomer
Cr-53	2041-2048	PWR downcomer
Cr-54	2049-2056	PWR downcomer
Fe-54	2057-2064	PWR downcomer
Fe-56	2065-2072	PWR downcomer
Fe-57	2073-2080	PWR downcomer
Fe-58	2081-2088	PWR downcomer
Mn-55	2089-2096	PWR downcomer
Ni-58	2097-2104	PWR downcomer
Ni-60	2105-2112	PWR downcomer
Ni-61	2113-2120	PWR downcomer
Ni-62	2121-2128	PWR downcomer
Ni-64	2129-2136	PWR downcomer
C	3001-3008	PWR ¼ T in pressure vessel
Cr-50	3009-3016	PWR ¼ T in pressure vessel
Cr-52	3017-3024	PWR ¼ T in pressure vessel
Cr-53	3025-3032	PWR ¼ T in pressure vessel
Cr-54	3033-3040	PWR ¼ T in pressure vessel
Fe-54	3041-3048	PWR ¼ T in pressure vessel
Fe-56	3049-3056	PWR ¼ T in pressure vessel
Fe-57	3057-3064	PWR ¼ T in pressure vessel
Fe-58	3065-3072	PWR ¼ T in pressure vessel
Mn-55	3073-3080	PWR ¼ T in pressure vessel
Ni-58	3081-3088	PWR ¼ T in pressure vessel
Ni-60	3089-3096	PWR ¼ T in pressure vessel

Table 3.14. Nuclides in BUGLE-B7 that are self-shielded and collapsed using specific BWR and PWR weighting spectra

Nuclide	ANISN ID	Description
Ni-61	3097-3104	PWR ¼ T in pressure vessel
Ni-62	3105-3112	PWR ¼ T in pressure vessel
Ni-64	3113-3120	PWR ¼ T in pressure vessel
Al-27	4001-4008	Concrete type 04
C	4009-4016	Concrete type 04
Ca	4017-4024	Concrete type 04
Fe-54	4025-4032	Concrete type 04
Fe-56	4033-4040	Concrete type 04
Fe-57	4041-4048	Concrete type 04
Fe-58	4049-4056	Concrete type 04
H-1 (H2O)	4057-4064	Concrete type 04
K	4065-4072	Concrete type 04
Mg	4073-4080	Concrete type 04
Na-23	4081-4088	Concrete type 04
O-16	4089-4096	Concrete type 04
Si	4097-4104	Concrete type 04
C	5001-5008	Carbon steel
C	5009-5016	Stainless steel
Cr-50	5017-5024	Carbon steel
Cr-50	5025-5032	Stainless steel
Cr-52	5033-5040	Carbon steel
Cr-52	5041-5048	Stainless steel
Cr-53	5049-5056	Carbon steel
Cr-53	5057-5064	Stainless steel
Cr-54	5065-5072	Carbon steel
Cr-54	5073-5080	Stainless steel
Fe-54	5081-5088	Carbon steel
Fe-54	5089-5096	Stainless steel
Fe-56	5097-5104	Carbon steel
Fe-56	5105-5112	Stainless steel
Fe-57	5113-5120	Carbon steel
Fe-57	5121-5128	Stainless steel
Fe-58	5129-5136	Carbon steel
Fe-58	5137-5144	Stainless steel
Mn-55	5145-5152	Carbon steel
Mn-55	5153-5160	Stainless steel
Ni-58	5161-5168	Carbon steel
Ni-58	5169-5176	Stainless steel
Ni-60	5177-5185	Carbon steel
Ni-60	5186-5192	Stainless steel
Ni-61	5193-5200	Carbon steel
Ni-61	5201-5208	Stainless steel
Ni-62	5209-5216	Carbon steel
Ni-62	5217-5224	Stainless steel
Ni-64	5225-5232	Carbon steel
Ni-64	5233-5240	Stainless steel
Fe-54	6001-6008	BWR core clad
Fe-56	6009-6016	BWR core clad

**Table 3.14. Nuclides in BUGLE-B7 that are self-shielded and
collapsed using specific BWR and PWR weighting spectra**

Nuclide	ANISN ID	Description
Fe-57	6017-6024	BWR core clad
Fe-58	6025-6032	BWR core clad
H-1 (H2O)	6033-6040	BWR core coolant
O-16	6041-6048	BWR core coolant
O-16	6049-6056	BWR core fuel
U-235	6057-6062	BWR core fuel
U-238	6063-6068	BWR core fuel
Zr	6069-6074	BWR core clad

3.6   Response functions

The BUGLE-B7 ANISN libraries include response function data consistent with that in BUGLE-96. The following response functions are included:

1. Neutron cross sections for 43 reactions. These data are based primarily on ENDF/B-VII data. Some reaction data are based on the International Reactor Dosimetry File IRDF-2002 [17] and the SNLRML compendium of dosimetry data [18].
2. Fission spectra (χ) and neutrons per fission (ν) data for nine nuclides.
3. Silicon displacement kerma data from SNLRML.
4. Total kerma factors for neutrons and photons. Those factors were generated using the HEATR (neutron) and GAMINR (photon) modules in NJOY.
5. Several parameters related to the neutron group structure.
6. Multipliers for total neutron flux and for neutron flux with $E > 1.0$ MeV, $E > 0.1$ MeV, and $E < 0.414$ eV.

A list of the response functions is provided in Table 3.15. The broad-group responses were collapsed from fine-group data using two weighting spectra: a flat (uniform) spectrum and the fine-group spectrum calculated at the ¼-thickness location in the pressure vessel. The response functions are included in the library with the same structure as the cross-section data, that is, 67-by-70 cross-section matrices (or 67-by-74 for a library with upscatter groups). Within a matrix each row represents a different response function. The row positions of the response functions are listed in Table 3.15. The ANISN IDs of the response tables are 7001 and 7002 for the flat-weighted responses and 7003 and 7004 for the pressure-vessel-weighted responses.

Note that the In-115 and Rh-103 inelastic scattering cross sections (Rows 28 and 46, respectively) are actually the cross sections for the production of the metastable isomers for these two isotopes. In the ENDF/B data, inelastic scattering cross sections are provided to discrete levels (MT = 51–90) and to the continuum (MT = 91). For dosimetry purposes, the cross section of interest is the "inelastic to metastable" cross section, which incorporates the production of the metastable state based on the appropriate scattering levels and branching ratios for the decay of each excited state. In IRDF-2002, the "inelastic to metastable" pointwise cross-section data are found in File 10 rather than in File 3 (see page 12 of [19]).

The neutron and photon kerma factors are also provided in the format of cross-section tables with ANISN IDs of 8001–8004. The kerma factors were collapsed from the VITAMIN-B7 data using the concrete weighting spectra for neutrons and photons. The 8001 and 8002 sets

contain the neutron kerma factors for the 120 nuclides that were included in BUGLE-96. The 8003 and 8004 sets contain the photon kerma factors. Note that photon kermas are in many cases provided for multiple isotopes of a given element, even though photon kerma values are identical for all isotopes of a given element. This duplication is retained to provide consistent row ordering of the neutron and photon kerma data. The row positions for the kerma data are listed in Table 3.16 and Table 3.17.

Table 3.15. Neutron response functions included with the BUGLE-B7 ANISN-formatted library

Row	Response data	Source of data		Row	Response data	Source of data
Data sets 7001 (flat weighted) and 7003 (1/4-thickness pressure vessel weighted)
1	Group Upper Energy (MeV)	N/A		29	I-127 (n, 2n)	ENDF
2	U-235 fission spectrum (χ)	ENDF		30	Sc-45 (n, γ)	ENDF
3	Li-6 (n, x) He-4	SNLRML		31	Na-23 (n, γ)	ENDF
4	B-10 (n, α)	ENDF		32	Fe-58 (n, γ)	ENDF
5	Th-232 (n, f)	ENDF		33	Co-59 (n, γ)	ENDF
6	U-235 (n, f)	ENDF		34	Cu-63 (n, γ)	ENDF
7	U-238 (n, f)	ENDF		35	In-115 (n, γ)	ENDF
8	Np-237 (n, f)	ENDF		36	Au-197 (n, γ)	ENDF
9	Pu-239 (n, f)	ENDF		37	Th-232 (n, γ)	ENDF
10	Al-27 (n, p)	ENDF		38	U-238 (n, γ)	ENDF
11	Al-27 (n, α)	ENDF		39	Square root of E_{mid} (MeV$^{1/2}$)	N/A
12	S-32 (n, p)	SNLRML		40	Total neutron flux	N/A
13	Ti-46 (n, p)	ENDF		41	U-234 (n, f)	ENDF
14	Ti-47 (n, p)	ENDF		42	U-236 (n, f)	ENDF
15	Ti-47 (n, np)	ENDF		43	Pu-240 (n, f)	ENDF
16	Ti-48 (n, p)	ENDF		44	Pu-241 (n, f)	ENDF
17	Ti-48 (n, np)	ENDF		45	Pu-242 (n, f)	ENDF
18	Mn-55 (n, 2n)	ENDF		46	Rh-103 (n, n')	IRDF-2002
19	Fe-54 (n, p)	ENDF		47	Si displacement kerma (eV·b)	SNLRML
20	Fe-56 (n, p)	ENDF		48	U-238 fission spectrum (χ)	ENDF
21	Co-59 (n, 2n)	ENDF		49	Pu-239 fission spectrum (χ)	ENDF
22	Co-59 (n, α)	ENDF		50	Neutron flux with E > 1.0 MeV	N/A
23	Ni-58 (n, p)	ENDF		51	Neutron flux with E > 0.1 MeV	N/A
24	Ni-58 (n, 2n)	ENDF		52	Neutron flux with E < 0.414 eV	N/A
25	Ni-60 (n, p)	ENDF		53	Midpoint energy (MeV)	N/A
26	Cu-63 (n, α)	ENDF		54	Group energy width (MeV)	N/A
27	Cu-65 (n, 2n)	ENDF		55	Group lethargy width	N/A
28	In-115 (n, n')	IRDF-2002				
Data Sets 7002 (flat weighted) and 7004 (1/4-thickness pressure vessel weighted)
1	Pu-238 (n, f)	ENDF		9	Pu-241 neutrons/fission (ν)	ENDF
2	U-234 neutrons/fission (ν)	ENDF		10	Pu-242 neutrons/fission (ν)	ENDF
3	U-235 neutrons/fission (ν)	ENDF		11	U-234 fission spectrum (χ)	ENDF
4	U-236 neutrons/fission (ν)	ENDF		12	U-236 fission spectrum (χ)	ENDF
5	U-238 neutrons/fission (ν)	ENDF		13	Pu-238 fission spectrum (χ)	ENDF
6	Pu-238 neutrons/fission (ν)	ENDF		14	Pu-240 fission spectrum (χ)	ENDF
7	Pu-239 neutrons/fission (ν)	ENDF		15	Pu-241 fission spectrum (χ)	ENDF
8	Pu-240 neutrons/fission (ν)	ENDF		16	Pu-242 fission spectrum (χ)	ENDF

**Table 3.16. Row positions for neutron kerma factors with ANISN ID
8001 and gamma-ray kerma factors with ANISN ID 8003**

(All kerma values are in units of eV·b)

Row	Nuclide	Row	Nuclide	Row	Nuclide
1	Ag-107	21	Cm-242	41	Fe-54
2	Ag-109	22	Cm-243	42	Fe-56
3	Al-27	23	Cm-244	43	Fe-57
4	Am-241	24	Cm-245	44	Fe-58
5	Am-242	25	Cm-246	45	Ga
6	Am-242m	26	Cm-247	46	H-1 (H2O)
7	Am-243	27	Cm-248	47	H-1 (CH2)
8	Au-197	28	Co-59	48	H-2 (D2O)
9	B-10	29	Cr-50	49	H-3
10	B-11	30	Cr-52	50	He-3
11	Ba-138	31	Cr-53	51	He-4
12	Be-9	32	Cr-54	52	Hf-174
13	Be-9 (thermal)	33	Cu-63	53	Hf-176
14	Bi-209	34	Cu-65	54	Hf-177
15	C	35	Eu-151	55	Hf-178
16	C (graphite)	36	Eu-152	56	Hf-179
17	Ca	37	Eu-153	57	Hf-180
18	Cd	38	Eu-154	58	In
19	Cl	39	Eu-155	59	K
20	Cm-241	40	F-19	60	Li-6

**Table 3.17. Row positions for neutron kerma factors with ANISN ID
8002 and gamma-ray kerma factors with ANISN ID 8004**

(All kerma values are in units of eV·b)

Row	Nuclide	Row	Nuclide	Row	Nuclide
1	Li-7	21	Pa-233	41	Ta-182
2	Mg	22	Pb-206	42	Th-230
3	Mn-55	23	Pb-207	43	Th-232
4	Mo	24	Pb-208	44	Ti
5	N-14	25	Pu-236	45	U-232
6	N-15	26	Pu-237	46	U-233
7	Na-23	27	Pu-238	47	U-234
8	Nb-93	28	Pu-239	48	U-235
9	Ni-58	29	Pu-240	49	U-236
10	Ni-60	30	Pu-241	50	U-237
11	Ni-61	31	Pu-242	51	U-238
12	Ni-62	32	Pu-243	52	V
13	Ni-64	33	Pu-244	53	W-Nat
14	Np-237	34	Re-185	54	W-182
15	Np-238	35	Re-187	55	W-183
16	Np-239	36	S	56	W-184
17	O-16	37	S-32	57	W-186
18	O-17	38	Si	58	Y-89
19	P-31	39	Sn-Nat	59	Zr
20	Pa-231	40	Ta-181	60	Zr (Zirc-2)

4 LIBRARY VERIFICATION AND VALIDATION

The VITAMIN-B7 and BUGLE-B7 libraries were verified and validated using three levels of testing: (1) automatic diagnostic software routines to check for internal consistency of the data files, (2) "unit tests" of the processed cross sections for each element, and (3) computational evaluation of criticality and shielding benchmark problems.

Verification of the libraries was accomplished using the first two levels of testing. These steps were an important part of the processing methodology, as changes that are made to processing codes to resolve a problem may cause unexpected changes in other portions of the processed data files. This was particularly important for verification of the gamma yield matrices, as the formatting for the yield data has changed substantially for many newer evaluations, with data being moved from Files 12 and 13 to File 6. Details of the verification steps are provided in Sections 4.1 and 4.2.

The benchmark evaluations provide an additional level of verification of the processing of the data. In addition, the shielding benchmarks provide validation for the use of the libraries for LWR shielding applications. The benchmarks were analyzed using deterministic transport calculations, Monte Carlo calculations, and the hybrid MAVRIC sequence in SCALE. Details of the benchmark evaluations are provided in Sections 4.3 through 4.5.

4.1 Processing Methods

The first step in verifying the VITAMIN-B7 and BUGLE-B7 libraries made use of diagnostic checks in the AMPX code system. The RADE module was used to check all the AMPX-formatted libraries. RADE performs the tests listed below:

1. $\sigma_t = \sigma_a + \sigma_s$
2. $\sigma_{in} = \Sigma \, \sigma_{in}(\text{partial})$
3. $\sigma_a = \sigma_c + \sigma_f$
4. $\sigma_c = \sigma_{ng} + \sigma_{n\alpha} + \sigma_{np} + \sigma_{nd}$
5. $\sigma_{el}(g) = \Sigma_{g'}\sigma_{el,0}(g')$ (for all processes with a scattering matrix)
6. $\sigma_{0(g \rightarrow g')} > 0$
7. $\sigma_t, \sigma_a, \sigma_f, \sigma_{n\gamma}, \sigma_{np}, \ldots > 0$
8. $f_{l,min} \leq f_l(g \rightarrow g') \leq 1.0,$

    where $f(g \rightarrow g') = \dfrac{\sigma_l(g \rightarrow g')}{(2l+1)\sigma_0(g \rightarrow g')}$

and $f_{l,min} = -1.0$ for all odd l, and is given by the following values for even l:
   l = 2: −0.5
   l = 4: −0.433
   l = 6: −0.419
   l = 8: −0.414

4.2 Unit Tests

A significant difference between the VITAMIN-B6 and VITAMIN-B7 fine-group libraries is the processing techniques that were used to generate the libraries. When the VITAMIN-B6 library

was generated, the NJOY code system was the only cross-section processing code able to process ENDF/B-VI data. NJOY was thus used to generate the fine-group VITAMIN-B6 library, while the AMPX-77 code system was used to process VITAMIN-B6 into the broad-group BUGLE-96 library.

The current version of AMPX has the ability to process ENDF/B-VI and ENDF/B-VII data. As one means of verifying the processing of the ENDF evaluations by the various AMPX modules, a set of "unit tests" was performed for the fine-group data. The unit tests, which were performed for each element in the VITAMIN-B7 library, were used to compare neutron and photon fluxes calculated using XSDRNPM and the VITAMIN-B7 library with equivalent MCNP5 [20] calculations with continuous energy cross-section data based on ENDF/B-VII. These tests provided an assessment of the fine-group data based on the calculated fluxes and also confirmed that the AMPX processing of the fine-group library was consistent with the NJOY processing of the continuous energy MCNP data. This was particularly important for gamma yield matrices, as the formatting for the yield data has changed substantially for many newer evaluations, with data being moved from Files 12 and 13 to File 6.

4.3   Critical Benchmark Experiments

A set of criticality benchmark experiments was evaluated as the first step of validating the fine-group VITAMIN-B7 library. The benchmark critical configurations provide an important test of the cross-section processing methods and resulting libraries for fuel and moderator materials and some structural materials. The benchmarks, which are listed in Section 4.3.1, were selected from the International Handbook of Evaluated Criticality Safety Benchmark Experiments [21]. The selected benchmarks are also indicated by their CSEWG (Cross-Section Evaluation Working Group) identifiers.

Each of the benchmark experiments listed in Table 4.1 was modeled using the SCALE generalized geometry package and calculated using the KENO-VI Monte Carlo transport code in SCALE.

Table 4.1. Critical benchmark experiments used for validation of the VITAMIN-B7 library

	ICSBEP identifier	CSEWG identifier	Description
Thermal System Benchmarks	HEU-SOL-THERM-013, Cases 1-4	ORNL-1 through ORNL-4	Unreflected spheres of highly enriched uranium (93.2 wt % ^{235}U) as uranyl nitrate in H_2O. Some solutions were poisoned with boric acid. The $H/^{235}U$ ratios ranged from 972 to 1378. The spherical shell, which was constructed of aluminum, had a diameter of approximately 69.2 cm.
	HEU-SOL-THERM-032	ORNL-10	Unreflected sphere of highly enriched uranium (93.2 wt % ^{235}U) as uranyl nitrate in H_2O. The $H/^{235}U$ ratio was 1835. The spherical shell, which was constructed of aluminum, had a diameter of approximately 122 cm.
	PU-SOL-THERM-021, Cases 7,3,2, and 5	PNL-1, PNL-6, PNL-8, PNL-12	Unreflected and water-reflected spheres of plutonium (4.57 wt % ^{240}Pu) as plutonium nitrate in H_2O. The spherical shell, which was made of stainless steel, had a diameter of approximately 38.6 cm.
	PU-SOL-THERM-011, Cases 18-1, 18-6, and 16-5	PNL-3, PNL-4, PNL-5	Unreflected spheres of plutonium (4.17– 4.20 wt % ^{240}Pu) as plutonium nitrate in H_2O. The spherical shells, which were made of stainless steel, had diameters of approximately 40.6 and 45.7 cm.

Table 4.1. Critical benchmark experiments used for validation of the VITAMIN-B7 library

	ICSBEP identifier	CSEWG identifier	Description
	PU-SOL-THERM-004	PNL-7	Unreflected sphere of plutonium (0.54 wt % ^{240}Pu) as plutonium nitrate in H_2O. The spherical shell, which was made of stainless steel, had a diameter of approximately 35.6 cm.
Fast System Benchmarks	Jezebel	PU-MET-FAST-001	Unreflected 6.3849 cm sphere of Pu (98.98 wt %) and Ga (1.02 wt %). The atom percentages of ^{239}Pu, ^{240}Pu, and ^{241}Pu are 95.2, 4.5, and 0.3, respectively.
	Jezebel-Pu-240	PU-MET-FAST-002	Unreflected 6.6595 cm sphere of Pu (98.99 wt %) and Ga (1.01 wt %). The atom percentages of ^{239}Pu, ^{240}Pu, and ^{241}Pu are 76.4, 20.1, and 0.4, respectively.
	Jezebel-U-233	U233-MET-FAST-001	Unreflected 5.9838 cm sphere of U. The atom percentages of ^{233}U, ^{234}U, ^{235}U, and ^{238}U are 98.13, 1.24, 0.03, and 0.6, respectively.
	Godiva	HEU-MET-FAST-001, Case 1	Unreflected spherical geometry with six spherical shells of highly enriched uranium. The enrichment of each shell is slightly different, with weight percentages of ^{234}U, ^{235}U, and ^{238}U of approximately 1, 94, and 5, respectively. The outer shell radius is 8.7499 cm.
	Godiva	HEU-MET-FAST-001, Case 2	Unreflected sphere of highly enriched uranium. The weight percentages of ^{234}U, ^{235}U, and ^{238}U are 1.02, 93.71, and 5.27, respectively. The spherical radius is 8.7407 cm.
	FLATTOP-U-235	HEU-MET-FAST-028	A highly enriched uranium spherical core (6.1156-cm radius) with a large sphere (24.1242-cm radius) of natural uranium as a reflector.
	FLATTOP-PU	PU-MET-FAST-006	A spherical plutonium core (4.5532-cm radius) with weight percentages of 93.8, 4.8, 0.3, and 1.1 of ^{239}Pu, ^{240}Pu, ^{241}Pu, and Ga, respectively. The core is surrounded by a natural uranium reflector with an outer radius of 24.1242 cm.
	FLATTOP-U-233	U233-MET-FAST-005, Case 1	A 5.0444-cm uranium core surrounded by a beryllium reflector with an outer radius of 7.0891 cm. The weight percentages of ^{233}U, ^{234}U, and ^{238}U in the core were 98.2, 1.1, and 0.7, respectively.
	FLATTOP-U-233	U233-MET-FAST-005, Case 2	A 4.5999-cm uranium core surrounded by a beryllium reflector with an outer radius of 8.7960 cm. The weight percentages of ^{233}U, ^{234}U, and ^{238}U in the core were 98.2, 1.1, and 0.7, respectively.
	BIG TEN	IEU-MET-FAST-007	A reflected cylinder of uranium that is 10.0634 wt % ^{235}U. The cylindrical core is surrounded by inner and outer reflectors. The inner reflector consists of alternating plates of natural uranium and highly enriched uranium. The outer reflector is depleted uranium.
	ZPR-6-6A	IEU-COMP-FAST-001	A highly enriched uranium oxide plate fuel critical assembly with a depleted uranium reflector blanket and an outer reflector of structural materials.
	ZPR-6-7	MIX-COMP-FAST-001	A highly enriched critical assembly with a mixture of uranium oxide and plutonium oxide plates surrounded by a depleted uranium reflector blanket and an outer reflector of structural materials.

4.3.1 Results for the Criticality Benchmarks for Thermal Systems

The results of the validation tests for the thermal system benchmarks are summarized in Table 4.2. The eigenvalues calculated using VITAMIN-B7 are all within 2 sigma of the experimental k_{eff} values.

Table 4.2. Calculated eigenvalues for the thermal system critical benchmarks used for validation of the VITAMIN-B7 library

(All calculations were performed using KENO VI. Uncertainties are 1-sigma values)

ICSBEP identifier	CSEWG identifier	Experimental k_{eff}	Cross-section library used in KENO-VI		
			VITAMIN-B6	VITAMIN-B7	Continuous energy ENDF/B-VII
HEU-SOL-THERM-013, Case 1	ORNL-1	1.0012 ± 0.0026	0.9989 ± 0.0002	0.9987 ± 0.0002	0.9980 ± 0.0002
HEU-SOL-THERM-013, Case 2	ORNL-2	1.0007 ± 0.0036	0.9980 ± 0.0002	0.9978 ± 0.0002	0.9973 ± 0.0002
HEU-SOL-THERM-013, Case 3	ORNL-3	1.0009 ± 0.0036	0.9947 ± 0.0002	0.9944 ± 0.0002	0.9940 ± 0.0002
HEU-SOL-THERM-013, Case 4	ORNL-4	1.0003 ± 0.0036	0.9963 ± 0.0002	0.9961 ± 0.0002	0.9955 ± 0.0002
HEU-SOL-THERM-032	ORNL-10	1.0013 ± 0.0026	0.9989 ± 0.0002	1.0001 ± 0.0002	0.9992 ± 0.0002
PU-SOL-THERM-021, Case 7	PNL-1	1.0000 ± 0.0032	1.0077 ± 0.0002	1.0063 ± 0.0002	1.0044 ± 0.0002
PU-SOL-THERM-021, Case 3	PNL-6	1.0000 ± 0.0065	1.0035 ± 0.0002	1.0056 ± 0.0002	0.9982 ± 0.0002
PU-SOL-THERM-021, Case 2	PNL-8	1.0000 ± 0.0032	1.0068 ± 0.0002	1.0059 ± 0.0002	1.0035 ± 0.0002
PU-SOL-THERM-021, Case 5	PNL-12	1.0000 ± 0.0032	1.0044 ± 0.0002	1.0044 ± 0.0002	1.0033 ± 0.0002
PU-SOL-THERM-011, Case 18-1	PNL-3	1.0000 ± 0.0052	0.9960 ± 0.0002	0.9946 ± 0.0002	0.9936 ± 0.0002
PU-SOL-THERM-011, Case 18-6	PNL-4	1.0000 ± 0.0052	1.0019 ± 0.0002	1.0007 ± 0.0002	0.9990 ± 0.0002
PU-SOL-THERM-011, Case 16-5	PNL-5	1.0000 ± 0.0052	1.0071 ± 0.0002	1.0066 ± 0.0002	1.0037 ± 0.0002
PU-SOL-THERM-004	PNL-7	1.0000 ± 0.0047	1.0043 ± 0.0002	1.0044 ± 0.0002	1.0038 ± 0.0002

4.3.2 Results for the Criticality Benchmarks for Fast Systems

The results of the validation tests for the fast system benchmarks are summarized in Table 4.3. The eigenvalues calculated using VITAMIN-B7 are within 2 sigma of the experimental k_{eff} values for seven of the fast benchmarks but not for the FLATTOP-U233, BIG TEN, or ZPR benchmarks. The eigenvalues calculated using KENO-VI with continuous energy cross sections based on ENDF/B-VII were also outside the 2-sigma range for the same cases. Additional calculations were run using KENO-VI with continuous energy ENDF/B-VI cross sections and also using MCNP5 with ENDF/B-VI and ENDF/B-VII data. For the FLATTOP-U233, BIG TEN, and ZPR benchmarks, none of those calculations was within 2 sigma of the experimental values other than the second FLATTOP case using either KENO-VI or MCNP5 with ENDF/B-VI cross sections.

**Table 4.3. Calculated eigenvalues for the fast system critical benchmarks
used for validation of the VITAMIN-B7 library**

(All calculations were performed using KENO VI. Uncertainties are 1-sigma values)

ICSBEP identifier	CSEWG identifier	Experimental k_{eff}	Cross-section library used in KENO-VI		
			VITAMIN-B6	VITAMIN-B7	Continuous energy ENDF/B-VII
PU-MET-FAST-001	Jezebel	1.0000 ± 0.0020	0.9960 ± 0.0002	1.0003 ± 0.0002	0.9991 ± 0.0002
PU-MET-FAST-002	Jezebel-Pu-240	1.0000 ± 0.0020	0.9966 ± 0.0002	1.0005 ± 0.0002	0.9996 ± 0.0002
U233-MET-FAST-001	Jezebel-U-233	1.0000 ± 0.0010	0.9924 ± 0.0002	0.9994 ± 0.0002	0.9993 ± 0.0002
HEU-MET-FAST-001, Case 1	Godiva	1.0000 ± 0.0010	0.9951 ± 0.0002	1.0007 ± 0.0002	0.9999 ± 0.0002
HEU-MET-FAST-001, Case 2	Godiva	1.0000 ± 0.0010	0.9950 ± 0.0002	1.0005 ± 0.0002	0.9996 ± 0.0002
HEU-MET-FAST-028	FLATTOP-U-235	1.0000 ± 0.0030	1.0010 ± 0.0002	1.0055 ± 0.0002	1.0029 ± 0.0002
PU-MET-FAST-006	FLATTOP-PU	1.0000 ± 0.0030	1.0019 ± 0.0002	1.0028 ± 0.0002	1.0009 ± 0.0002
U233-MET-FAST-005, Case 1	FLATTOP-U-233	1.0000 ± 0.0030	0.9948 ± 0.0002	0.9931 ± 0.0002	0.9924 ± 0.0002
U233-MET-FAST-005, Case 2	FLATTOP-U-233	1.0000 ± 0.0030	0.9974 ± 0.0002	0.9907 ± 0.0002	0.9902 ± 0.0002
IEU-MET-FAST-007	BIG TEN	1.0062 ± 0.0003	1.0170 ± 0.0002	1.0097 ± 0.0002	1.0048 ± 0.0002
IEU-COMP-FAST-001	ZPR-6-6A	1.0017 ± 0.0009	1.0003 ± 0.0002	0.9986 ± 0.0002	0.9957 ± 0.0002
MIX-COMP-FAST-001	ZPR-6-7	1.0005 ± 0.0009	1.0000 ± 0.0002	0.9935 ± 0.0002	0.9891 ± 0.0002

4.4   SCALE Regression Tests

The next set of benchmark experiments are referred to as the "SCALE regression tests." They have been used to test the Monaco Monte Carlo transport code in SCALE and to verify the shielding multigroup libraries in SCALE: the 200-group neutron/47-group gamma ENDF/B-VI and ENDF/B-VII libraries, as well as the 27-group neutron/19-group gamma ENDF/B-VI and ENDF/B-VII libraries. These calculations were run using the configuration-controlled version of SCALE at ORNL, which will be released as SCALE 6.1.

An additional benchmark, the measurement of D-T neutrons through an iron sphere, was added to the SCALE regression tests. This experiment was added to provide a more rigorous test of the iron cross sections at high energies compared with the experiments using ^{252}Cf sources. One experiment from the original regression test set (doses in a three-section concrete labyrinth) was deleted. Simulations for the labyrinth experiment are very detailed and time-consuming and are not very relevant for testing an LWR cross-section library. A summary of the five problems that were modeled is provided in Table 4.4.

For the problems that could be modeled in one dimension, calculations were also run using XSDRNPM.

Table 4.4. Summary of the SCALE regression test problems used for verification and validation of the VITAMIN-B7 library

	Problem and description	Source	Materials (trace)	Geometry	Measured
1	^{252}Cf leakage spectrum through iron sphere	^{252}Cf n	Fe (C, S)	Sphere	n Flux
2	^{252}Cf leakage from different iron spheres (ALARM-CF-FE-SHIELD-001)	^{252}Cf n, γ	Fe (Mn, C, Cu)	Sphere	n Flux γ flux
3	D-T source transmission through iron sphere	D-T/D-D n	Fe (Mn, S, P, C)	Sphere	n Flux
4	^{252}Cf transmission through D_2O sphere	^{252}Cf n	D_2O (H_2O), B, concrete, polyethylene	Sphere with shields	n Flux
5	^{252}Cf through various shield types and thicknesses	^{252}Cf n	Paraffin, polyethylene, NS-4-FR, Resin-F, KRAFTON-HB, Type 304SS	Slab shields	n Dose equiv. rate

4.4.1 Neutron Transmission through an Iron Sphere

In the early 1990s, several experiments measuring the transmission of ^{252}Cf neutrons through a sphere of iron were performed to benchmark ENDF/B-VI cross-section data [22]. Two sets of measurements were made—one by the Czechoslovakian National Research Institute and the other by the Skoda Company.

The Monaco model consists of a point source and a spherical shell of iron. A region tally (for a thin spherical shell at radius =100 cm) was used to collect the flux information. For the source energy distribution $p(E)$, the Watt spectrum with constants *a* = 1.025 MeV and *b* = 2.926/MeV was used.

$$p(E) = ce^{-E/a}\sinh\left(\sqrt{bE}\right)$$

The measurements listed in [22] were normalized such that the total flux at the detector (at r=100 cm) without the iron shield would have been 1 n/cm^2/s. In Monaco, the source strength was set to a value of $4\pi(100)^2$ = 125664 n/s, which would yield exactly 1 n/cm^2/s at 100 cm for an unshielded source. No biasing was used, other than implicit capture. The Monaco results are shown in Figure 4.1.
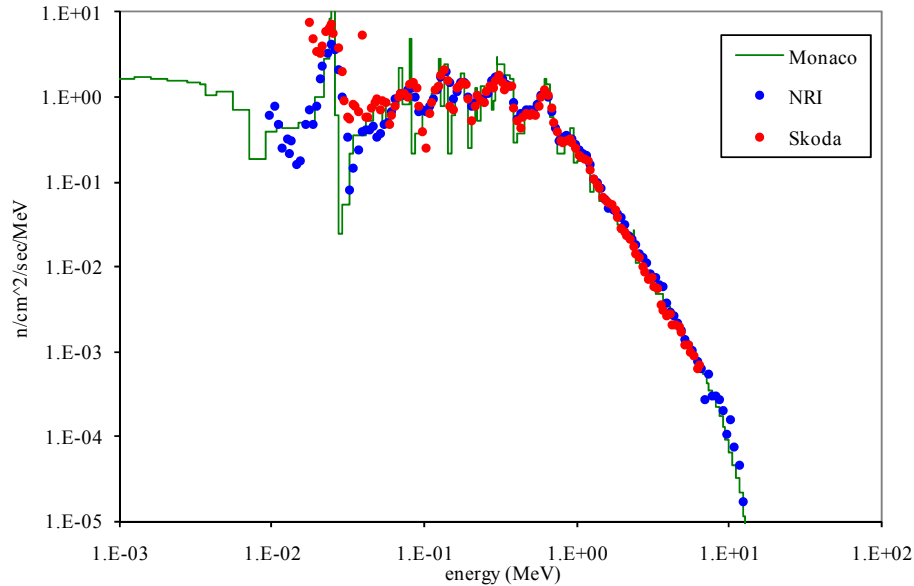
Figure 4.1. Comparison of the Monaco neutron calculation with two sets of experimental data for the iron sphere benchmark.

4.4.2 Neutron and Photon Leakage Spectra from a ^{252}Cf Source at the Centers of Six Iron Spheres of Different Diameters (ALARM-CF-FE-SHIELD-001)

Neutron and photon leakage spectra from a ^{252}Cf source surrounded by iron spheres of various diameters were measured in Russia during the 1980s. These data and instructions for benchmark calculations were presented in 2007 in an Organization for Economic Cooperation and Development report [23] with the identification number ALARM-CF-FE-SHIELD-001. Thirteen sets of experimental data are presented in the report—one for the bare source and one for each of six different diameters of iron shielding. Photon measurements are presented for the bare source and five different diameter spheres. Each measured data set was actually the difference of two measurements—one with and one without a solid conical shield between the source and detector. The conical shields, which were made of borated polyethylene for measurements of neutron spectra and lead for measurements of gamma spectra, were constructed to completely shadow the detector from radiation coming directly from each spherical geometry. The difference in the two sets of measurements effectively removed any detector response that was due to room return, and was used as the comparison basis for the calculations in [23] and in the present analysis.

The benchmark geometry consists of only the sphere without any room walls, as shown in Figure 4.2.
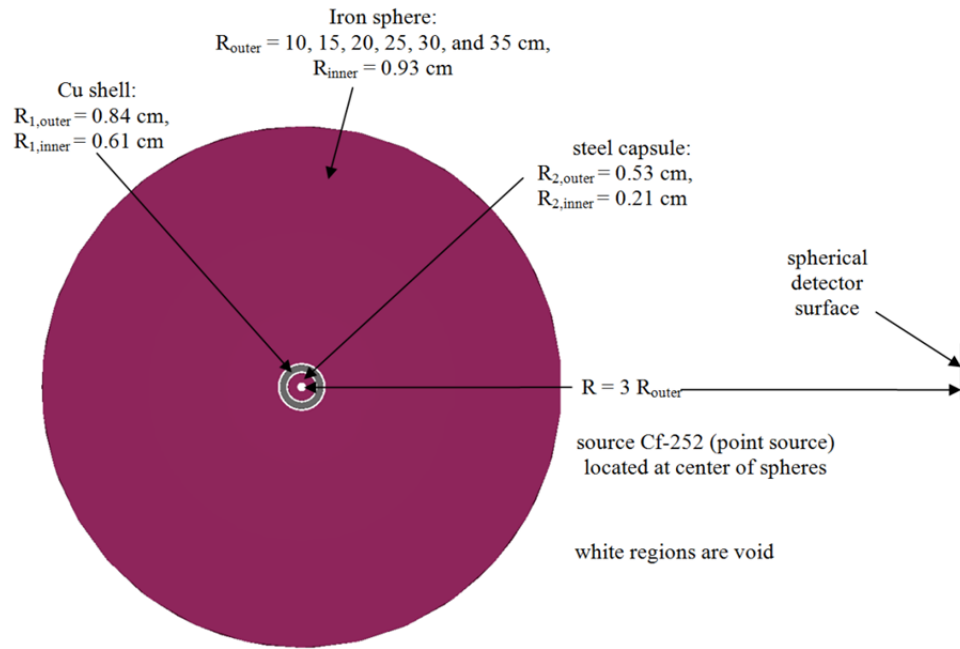
Figure 4.2. Benchmark geometry for the iron sphere leakage measurements.

Monaco was used with the VITAMIN-B7 library to compute the leakage spectra of both neutrons and photons according to the benchmark instructions. The benchmark model is one-dimensional and does not include the shield that was used to correct for room return.

The experimentally measured neutron flux spectrum of the bare source was used for the Monaco neutron source description. For the Monaco photon source, the experimentally measured photon flux spectrum of the bare source was used. Note that the "bare source" included copper and steel canisters, so a small fraction of the measured photon flux could have come from secondary gammas from neutrons interacting in the source capsule. The two strengths of the sources were set using the fact that for every neutron emitted from the ^{252}Cf source, 3.82 photons were emitted.

Benchmark results are listed in the reference document in terms of $4\pi R^2 \Phi(E)/Q$, where R is the radius of the detector (three times the radius of the shield, or 60 cm for the bare source) and Q is the neutron source strength. Experimental uncertainties ranged from 5% to 30%. The experimental values are shown on the following plots (Figure 4.3 through Figure 4.15) as two lines, representing the experimental values ± 1σ.

Since the Monaco source was created from the bare source measurements, the Monaco simulation for these should match the experiment well. This agreement is shown in Figure 4.3 and Figure 4.4. Comparisons of calculated and measured neutron transmission are shown in Figure 4.5 through Figure 4.10. Photon comparisons are shown in Figure 4.11 through Figure 4.15. For the 70-cm-diameter shield, MCNP simulations were also performed. The MCNP results are shown in Figure 4.10 and Figure 4.15.
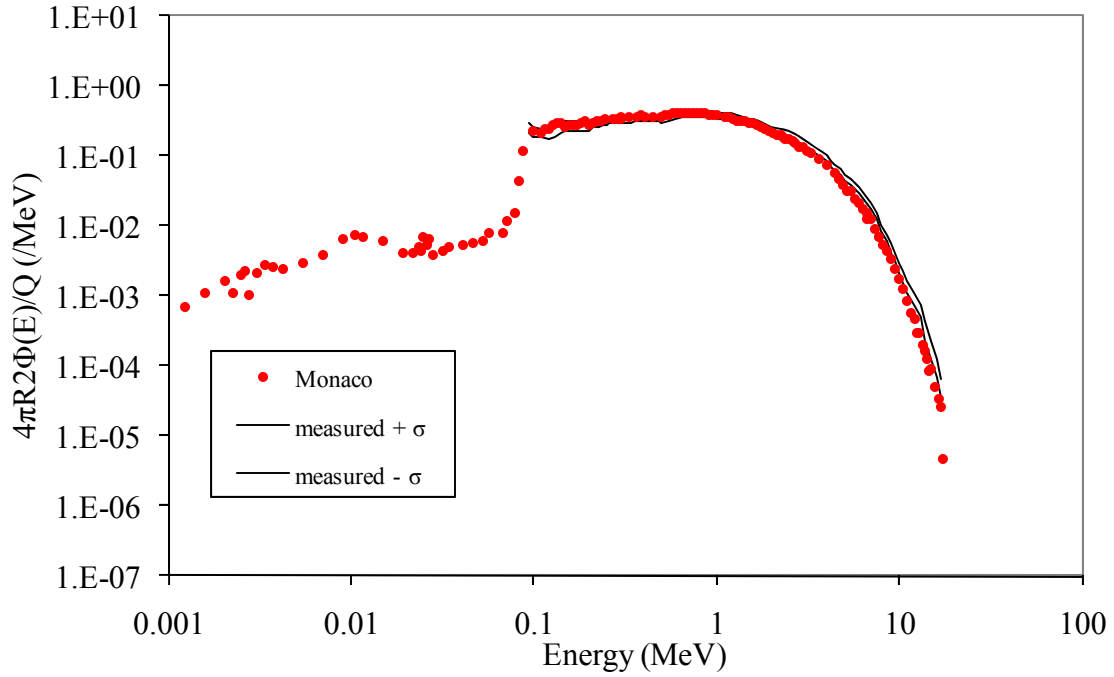
Figure 4.3. Comparison of the Monaco neutron spectrum with the measured spectrum from the bare source of the ALARM-CF-FE-SHIELD-001 experiment.
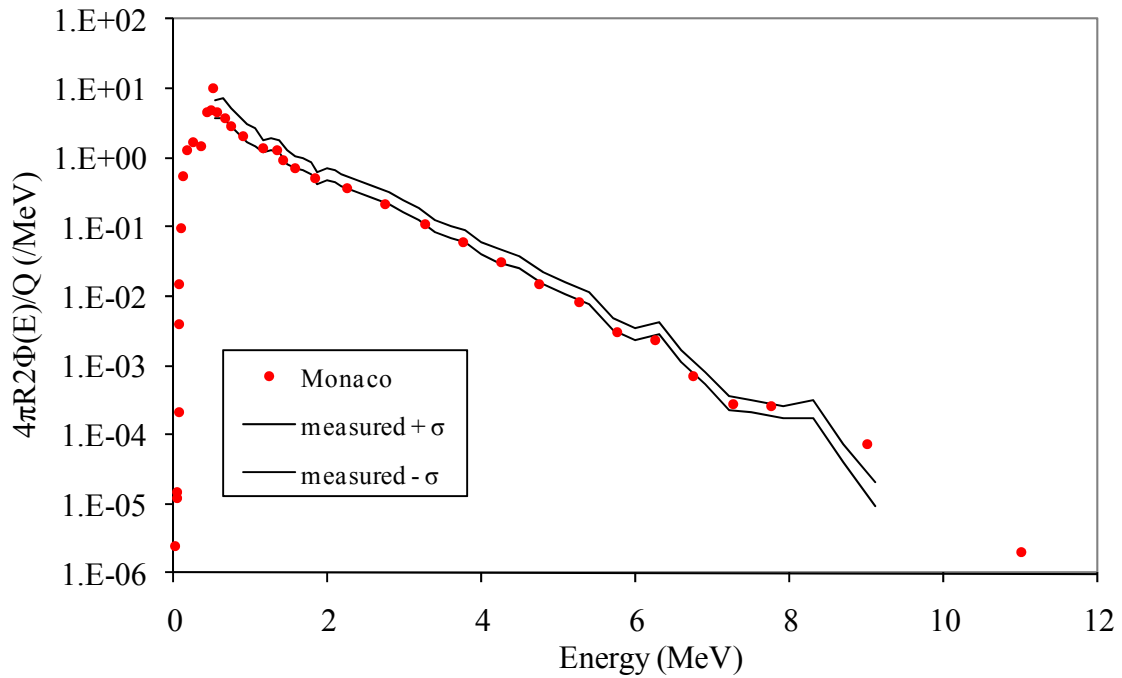
Figure 4.4. Comparison of the Monaco photon spectrum with the measured spectrum from the bare source of the ALARM-CF-FE-SHIELD-001 experiment.
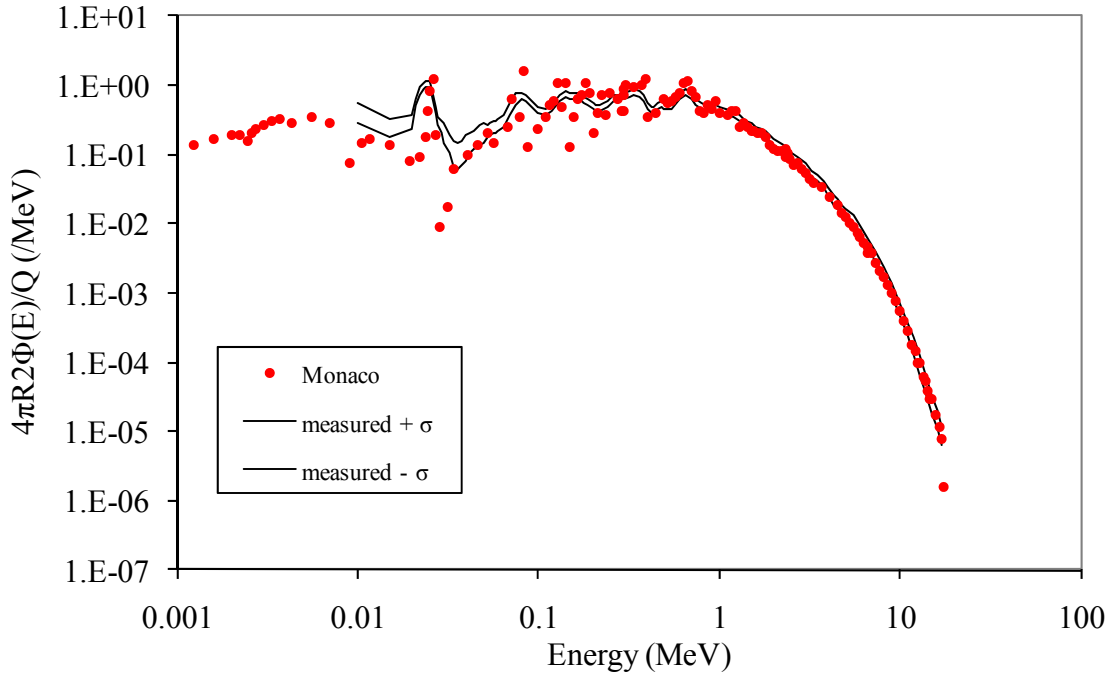
Figure 4.5. Comparison of the Monaco neutron spectrum with the measurement for the 20-cm-diameter shield from the ALARM-CF-FE-SHIELD-001 experiment.
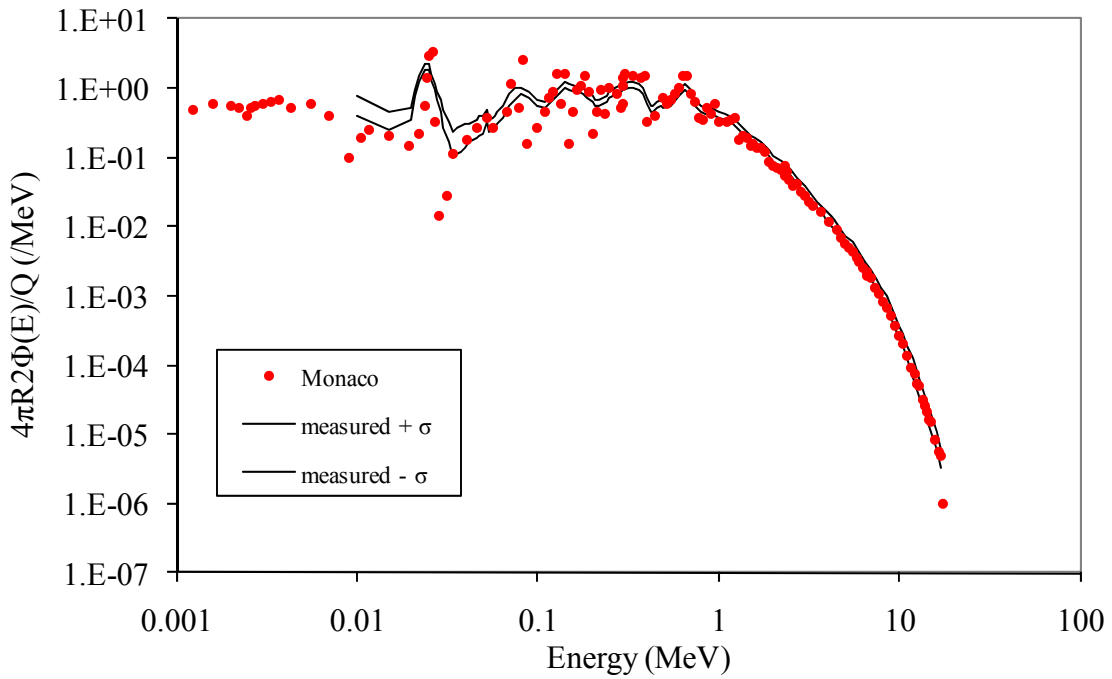
Figure 4.6. Comparison of the Monaco neutron spectrum with the measurement for the 30-cm-diameter shield from the ALARM-CF-FE-SHIELD-001 experiment.
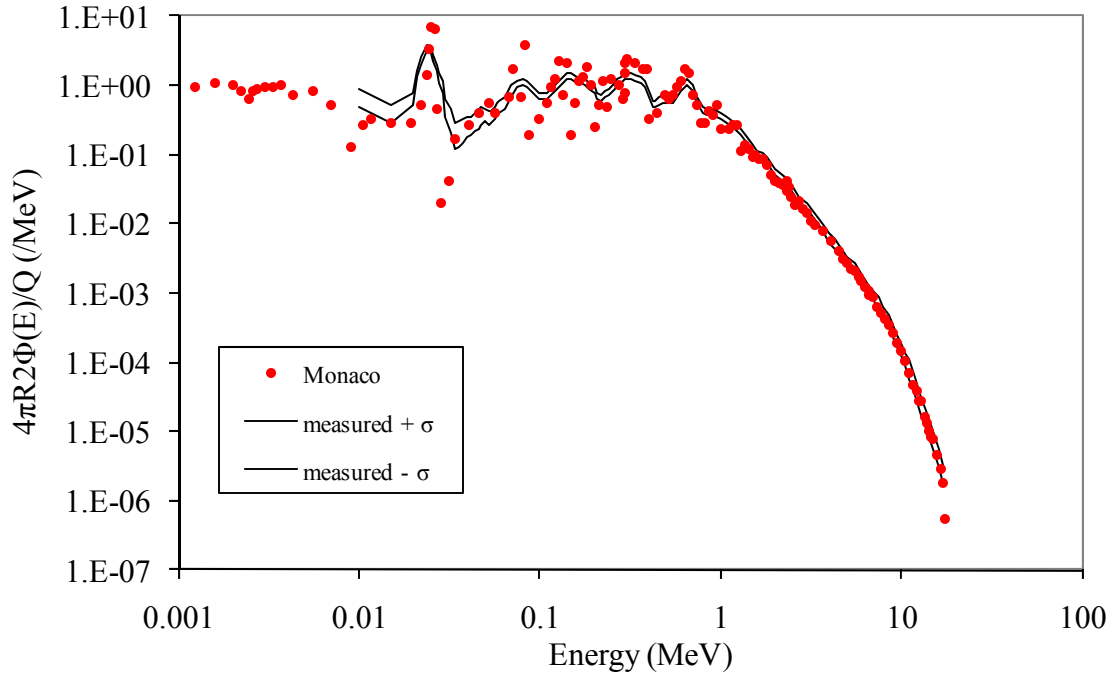
Figure 4.7. Comparison of the Monaco neutron spectrum with the measurement for the 40-cm-diameter shield from the ALARM-CF-FE-SHIELD-001 experiment.
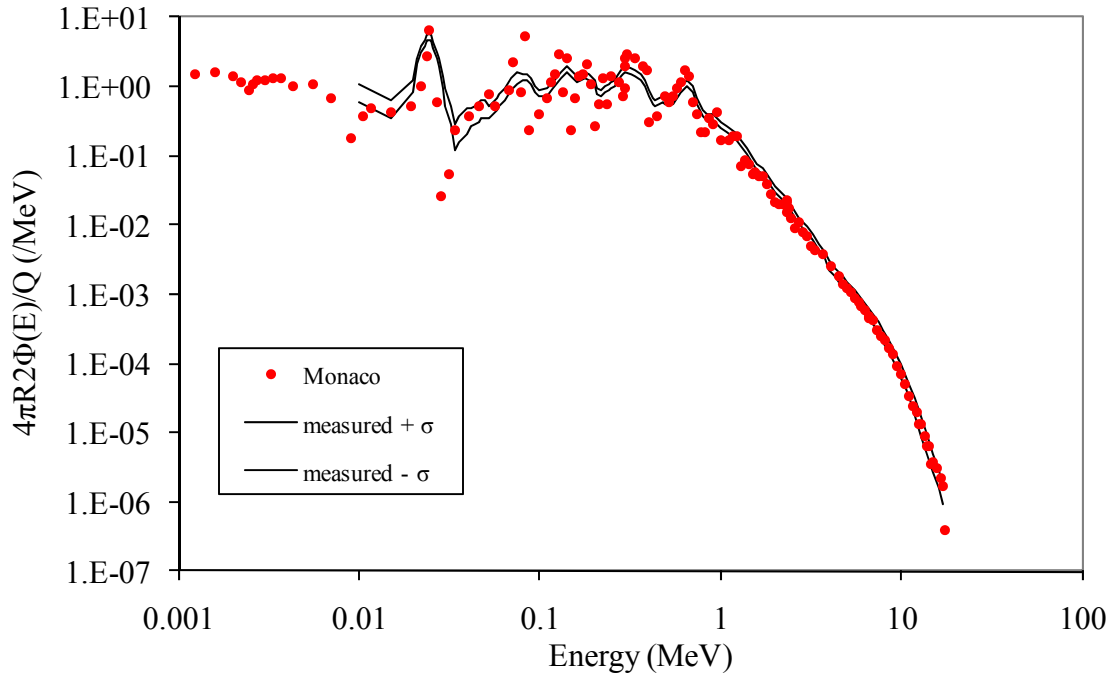
Figure 4.8. Comparison of the Monaco neutron spectrum with the measurement for the 50-cm-diameter shield from the ALARM-CF-FE-SHIELD-001 experiment.
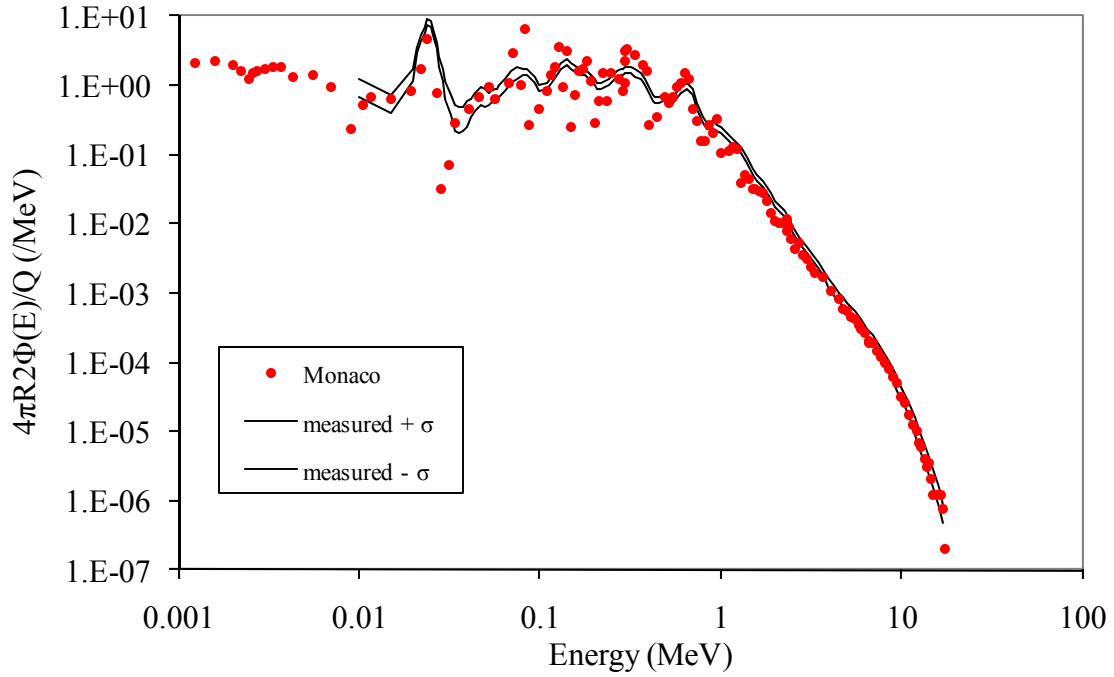
Figure 4.9. Comparison of the Monaco neutron spectrum with the measurement for the 60-cm-diameter shield from the ALARM-CF-FE-SHIELD-001 experiment.
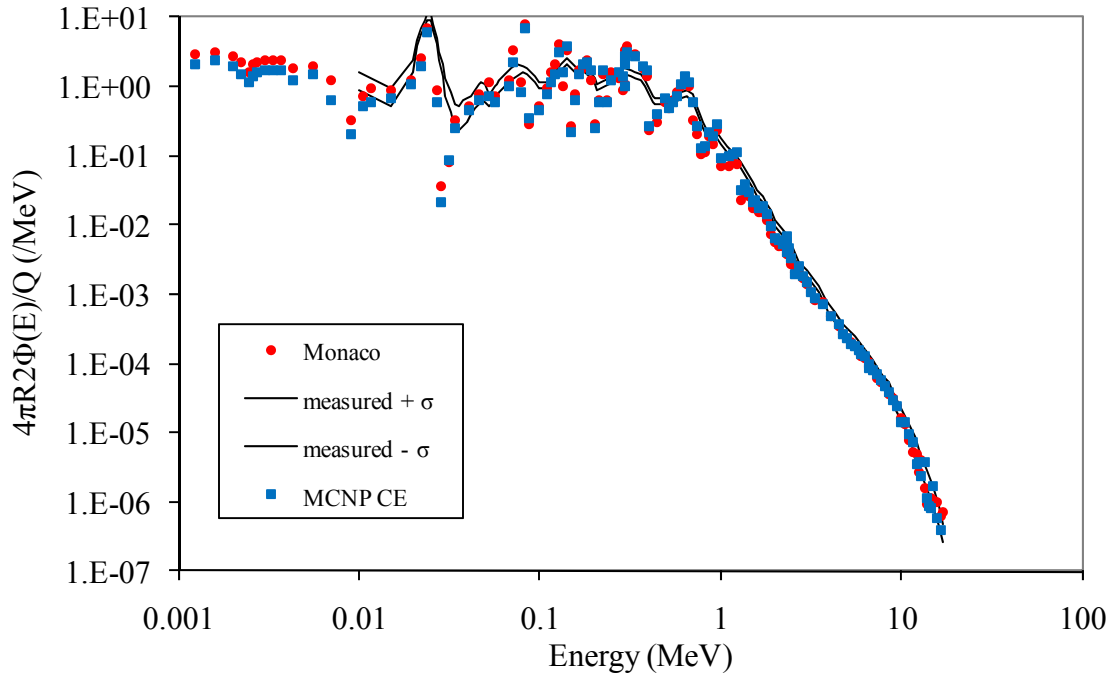
Figure 4.10. Comparison of the Monaco and MCNP neutron spectra with the measurement for the 70-cm-diameter shield from the ALARM-CF-FE-SHIELD-001 experiment.
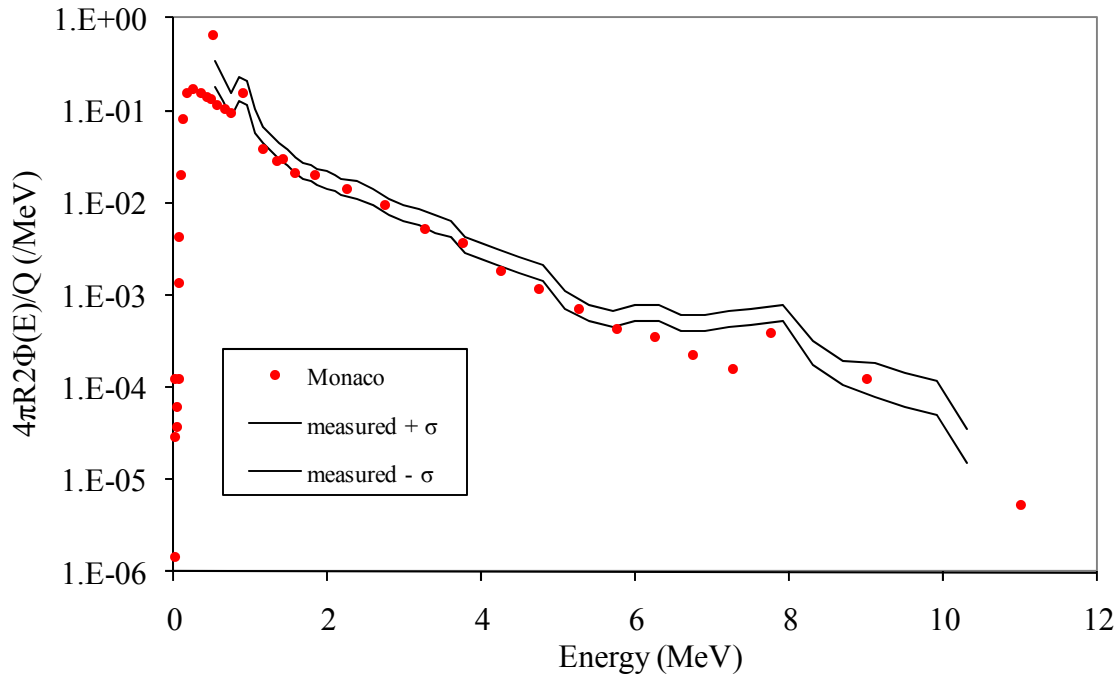
Figure 4.11. Comparison of the Monaco photon spectrum with the measurement for the 30-cm-diameter shield from the ALARM-CF-FE-SHIELD-001 experiment.
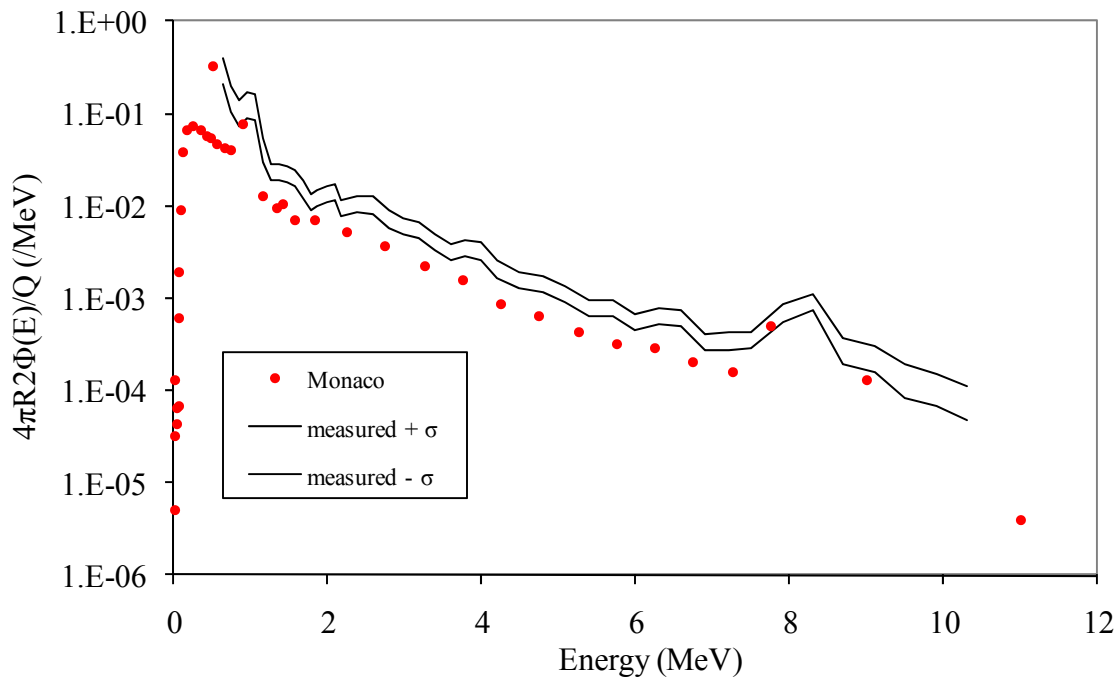
Figure 4.12. Comparison of the Monaco photon spectrum with the measurement for the 40-cm-diameter shield from the ALARM-CF-FE-SHIELD-001 experiment.
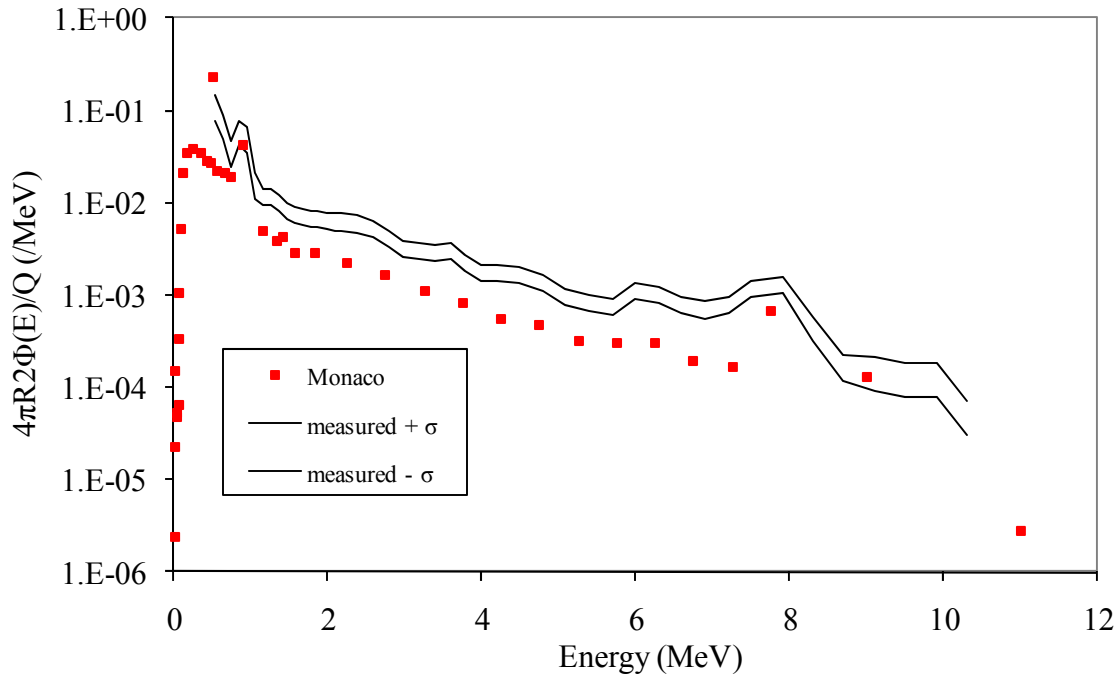
Figure 4.13. Comparison of the Monaco photon spectrum with the measurement for the 50-cm-diameter shield from the ALARM-CF-FE-SHIELD-001 experiment.
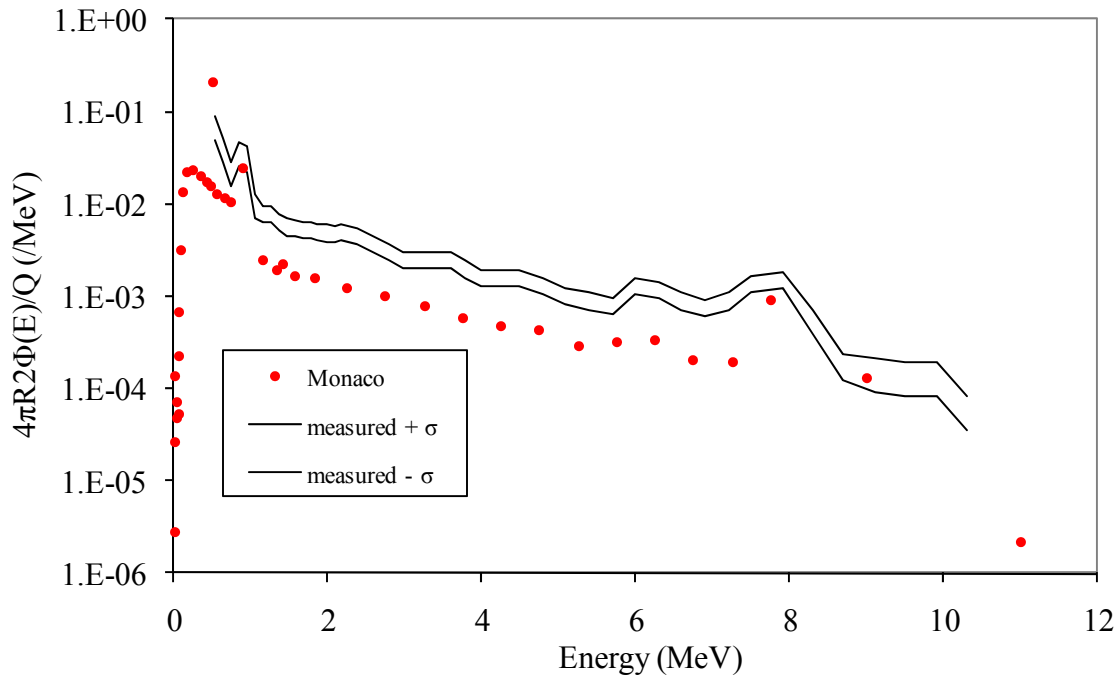
Figure 4.14. Comparison of the Monaco photon spectrum with the measurement for the 60-cm-diameter shield from the ALARM-CF-FE-SHIELD-001 experiment.
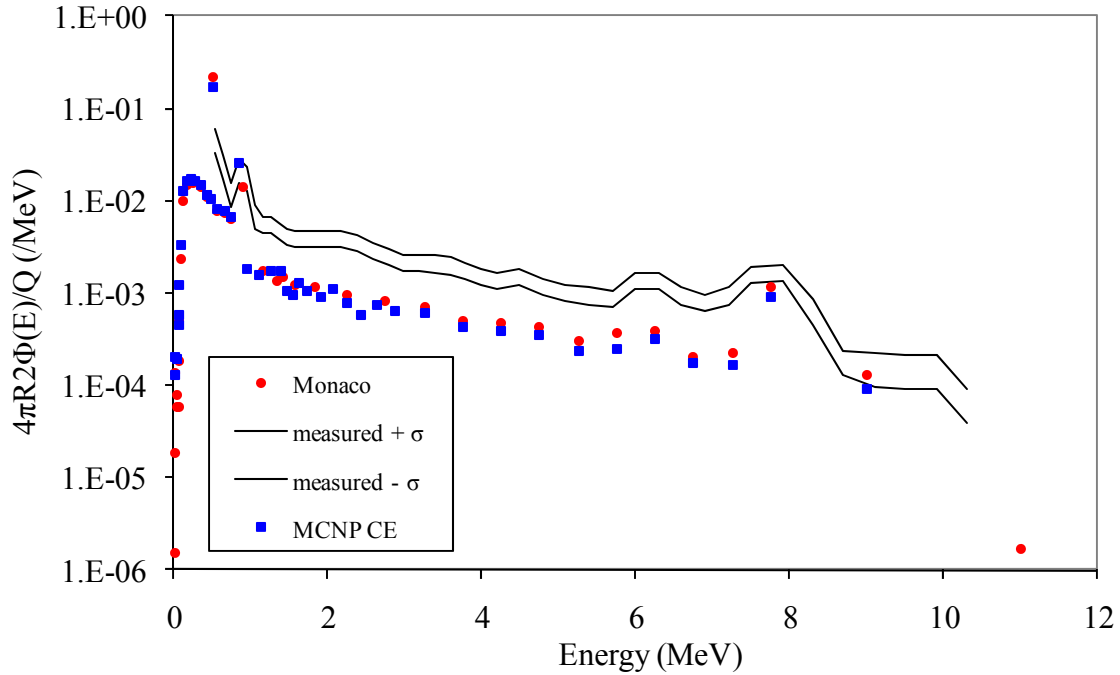
Figure 4.15. Comparison of the Monaco and MCNP photon spectra with the measurement for the 70-cm-diameter shield from the ALARM-CF-FE-SHIELD-001 experiment.

4.4.3 D-T Neutrons through an Iron Sphere

Integral measurements were made of the neutron flux from a D-T (with 5% D-D) neutron source transmitted through an iron spherical shell with a thickness of 30.45 cm [24]. This experiment at the University of Illinois in Urbana was also performed with a ^{252}Cf source and was included as a SINBAD benchmark experiment [25]. Some energy-dependent neutron flux data and computer simulation data were also presented in these references. The idealized problem geometry is shown in Figure 4.16.
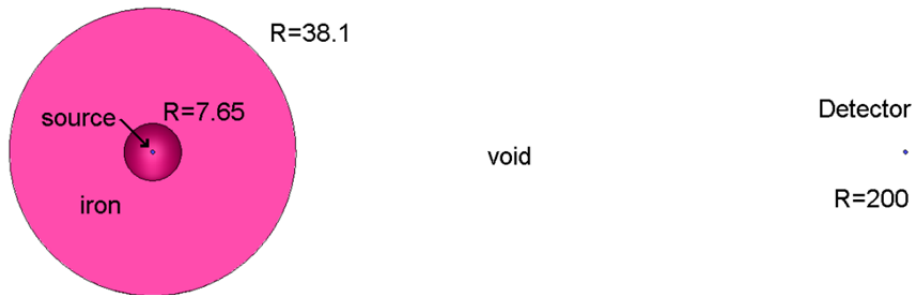
Figure 4.16. Geometry of the Urbana D-T transmission experiment.

The D-T (with 5% D-D) neutron source spectrum was given and used as a source in Monaco. The measurements reported in [22] were normalized such that the total flux at 200 cm without the iron sphere would have been 1 n/cm^2/s. The Monaco source strength was set to $4\pi(200)^2$ = 502654 n/s so that results at 200 cm would be 1 n/cm^2/s for an unshielded measurement. A region tally was used to collect flux information at 200 cm. No variance reduction, other than implicit capture, was used. The comparison with the measured values is shown in Figure 4.17. At high energies, calculation and the measurement agree well. At energies less than 10 MeV, the simulation underpredicts the measurement. This underprediction is consistent with the results of the simulations in the original references.
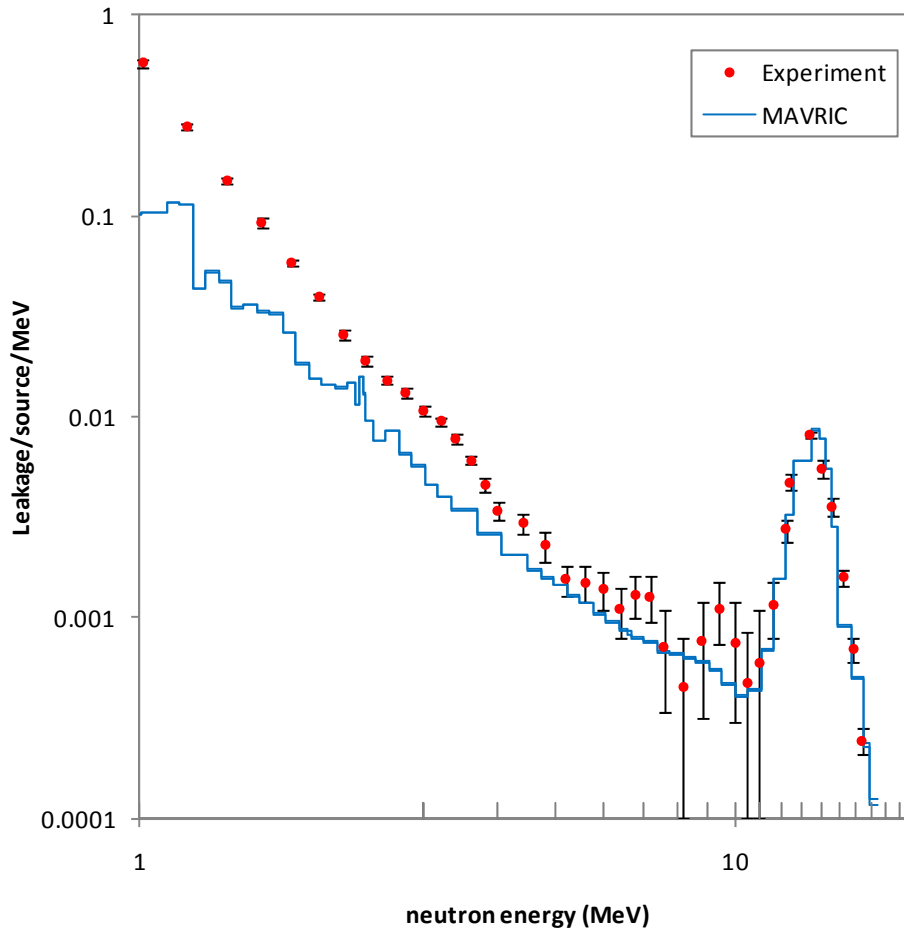
Figure 4.17. Comparison of the Monaco neutron spectrum at 200 cm with the measured data for the Urbana experiment.

4.4.4 Neutron Transmission through a Heavy Water Sphere

The transmission of ^{252}Cf neutrons through a sphere filled with heavy water was measured in Prague in the mid-1990s [26]. For each experiment, two measurements were made: one with an iron/polyethylene shield and one without the shield. The purpose of the shield was to block all direct particle transmission from the sphere to the detector. The difference in these two measurements accounts for scatter from the floor, walls, and ceiling (which is about a 5% effect for energies above 10 keV). A great amount of detail for the materials and geometry of the source holder, insertion tube, and detectors is provided in [26]. Two different assemblies holding the californium source were measured. The geometry, with the shield in place, is shown in Figure 4.18.
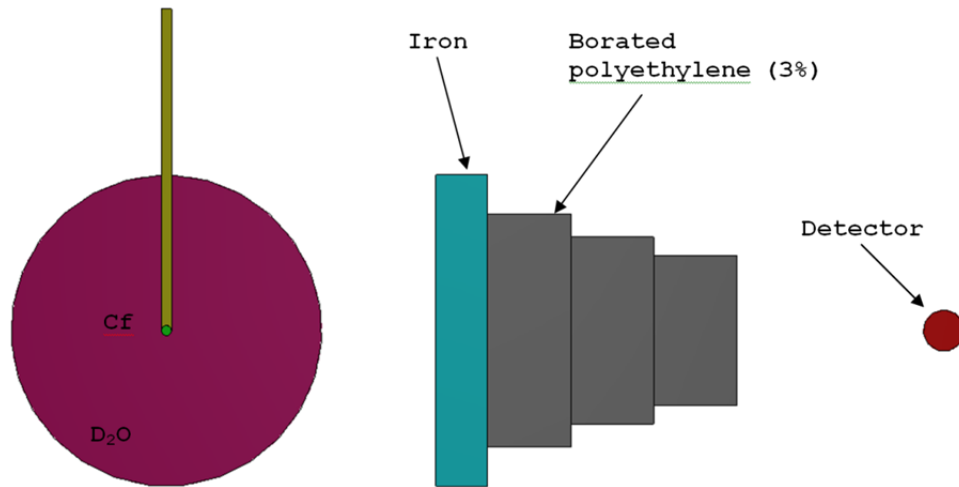
Figure 4.18. Geometry of the heavy water experiment.

The Monaco model for this benchmark consists of two nested spheres for the source and the heavy water. For the experiments where the iron/polyethylene shield is present, three borated polyethylene cylinders and one iron cylinder are placed between the sphere and the detector position at (75,0,0), where the origin of the coordinate system corresponds to the source at the center of the heavy water sphere. The experiment sat 2 m above the floor of an experimental hall that measured 10 × 13 × 25 m. Neither of the two source holder assemblies was modeled in any detail.

For the source energy distribution, the Watt spectrum with constants a =1.025 MeV and b =2.926/MeV was used.

$$p(E) = ce^{-E/a}\sinh\left(\sqrt{bE}\right)$$

The measurements listed in the paper were normalized such that the total flux at the detector (at r = 75 cm) without the D_2O sphere or the shields would have been 1 n/cm^2/s. In Monaco, the source strength was set to a strength of $4\pi(75)^2$ = 70686 n/s. No biasing was used, other than implicit capture.

A point detector tally at the detector location was used to calculate the energy-dependent neutron flux. Results are shown in Figure 4.19 for the Monaco simulation compared with the measurements using the two different source assemblies.
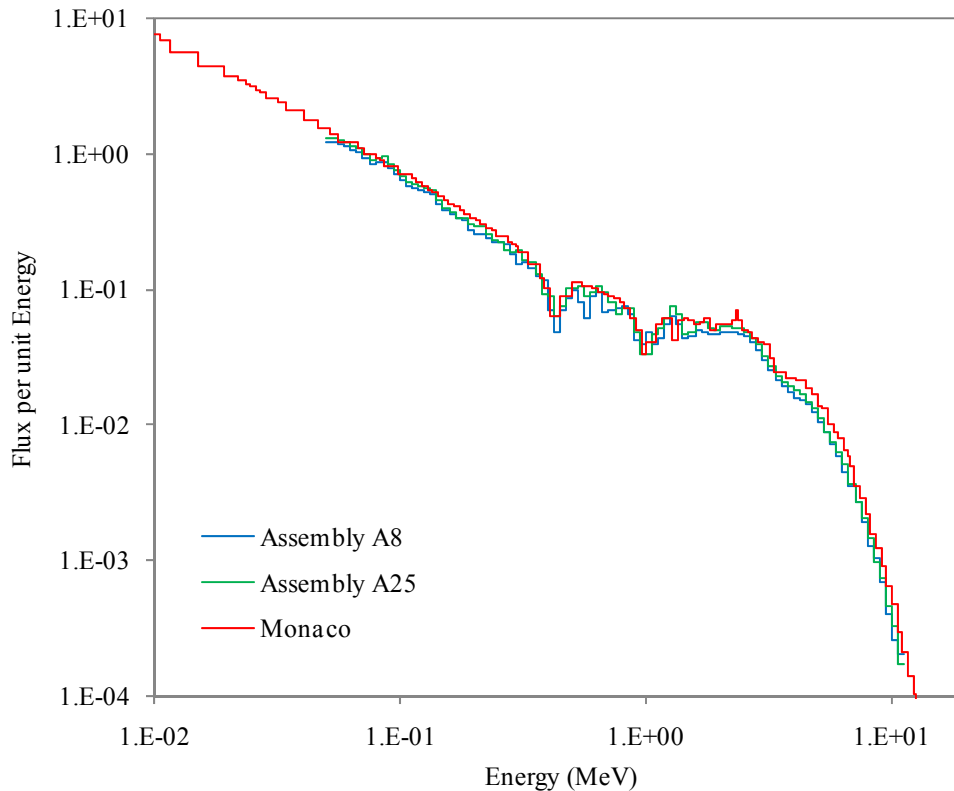
Figure 4.19. Comparison of the Monaco calculation and measured data for the heavy water transmission benchmark.

4.4.5 Ueki Shielding Measurements

K. Ueki et al. of the Nuclear Technology Division, Ship Research Division, in Japan performed a series of simple studies on a variety of shielding materials layered in different combinations [27]. These measurements used both neutron (^{252}Cf) and photon (^{60}Co) sources to investigate the shielding effectiveness of steel, graphite, and many hydrogenous materials as single shields or in combinations. The detector used was an Aloka moderator-type survey meter, made of polyethylene, which is supposed to mimic human dose response. The data were corrected for room scatter. Three types of experiments were performed: a single shield material (type 1), two-layer steel/polyethylene combinations (type 2), and three-layer steel/polyethylene combinations (type 3). The geometry for a type 3 experiment is shown in Figure 4.20.

MAVRIC was used to simulate the experiments that used the neutron source. For penetration through thick shields, the MAVRIC sequence and the CADIS methodology [28] can be used to calculate results with low relative uncertainties in short times. For each of the 46 shield configurations that Ueki measured, an input file was constructed that utilized the advanced variance reduction. For these simulations, an adjoint calculation using Denovo was performed using a broad-group version of the VITAMIN-B7 library. An importance map and a biased

source distribution were then calculated by MAVRIC from the adjoint fluxes. The Monaco simulation used the VITAMIN-B7 fine-group shielding library, the broad-group importance map, and a biased source distribution (constructed from a combination of the fine-group representation of the original source and the broad-group importances).
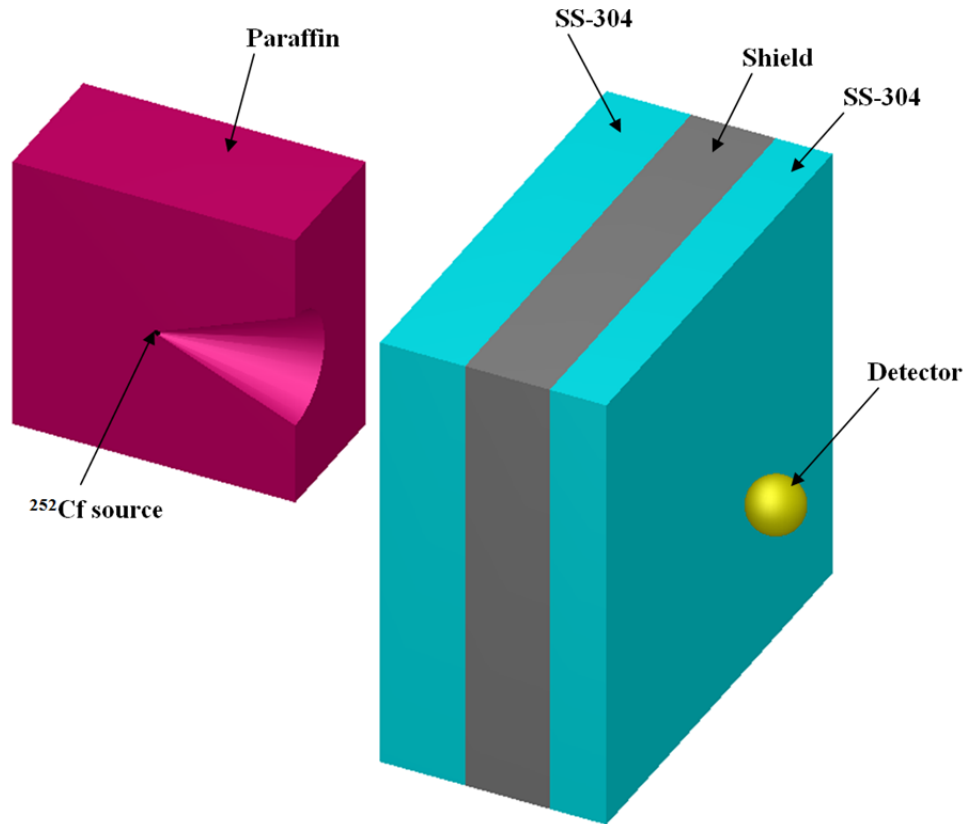
Figure 4.20. Geometry of a type 3 configuration from the neutron shielding experiments of Ueki et al. Half of the paraffin block surrounding the source has been removed from the model to show the source and the conical cutout.

The MAVRIC calculations for the type 1 experiments (single shield) are summarized in Table 4.5, and the ratios of the calculated to measured values are shown in Figure 4.21. All of the calculated values are within ±20% of the measured data, with the exception of polyethylene. Reported results with MCNP also show good agreement with the findings of Ueki et al. for all materials except polyethylene. It is not clear if this mismatch is related to thermal scattering cross sections common to both MAVRIC and MCNP or if may be related to the way in which Ueki processed his experimental results.

Comparisons of the MAVRIC calculations and measured data for the type 2 and type 3 experiments are shown in Figure 4.22, Figure 4.23, and Figure 4.24. The poor agreement is probably due to the polyethylene component that MAVRIC could not match in the type 1 experiments.

Table 4.5. Summary of MAVRIC results for the Ueki type 1 experiments with a ^{252}Cf neutron source

| shield | | Ueki | Runtime (min) | | MAVRIC Neutron Dose-Equivalent (µSv/h) | | |
mat	cm	(µSv/h)	Adj. Sn	MC	value	rel unc	C/E
none	0	6.90E+02	1.3	10.3	6.19E+02	0.09%	0.90
Polyethylene	5	2.98E+02	13.0	42.0	3.01E+02	0.59%	1.01
	10	1.12E+02	11.3	62.1	1.27E+02	0.99%	1.14
	15	4.38E+01	12.6	91.9	5.48E+01	1.14%	1.25
	20	1.81E+01	38.9	181.3	2.37E+01	0.99%	1.31
	25	7.98E+00	39.0	241.4	1.11E+01	0.99%	1.40
	30	3.46E+00	38.3	241.2	5.32E+00	1.12%	1.54
NS-4-FR	5	3.43E+02	1.2	10.1	3.14E+02	0.40%	0.91
	10	1.42E+02	1.3	10.6	1.40E+02	0.58%	0.98
	15	6.09E+01	1.3	10.7	6.20E+01	0.67%	1.02
	20	2.79E+01	1.3	10.7	2.83E+01	0.71%	1.02
	25	1.27E+01	1.2	10.2	1.28E+01	0.74%	1.00
	30		1.2	10.8	6.13E+00	0.74%	
Resin-F	5	3.43E+02	1.1	10.2	3.32E+02	0.38%	0.97
	10	1.51E+02	1.2	10.3	1.54E+02	0.56%	1.02
	15	6.65E+01	1.3	10.7	7.22E+01	0.66%	1.09
	20	3.04E+01	1.3	10.6	3.42E+01	0.71%	1.12
	25	1.38E+01	1.3	10.8	1.63E+01	0.72%	1.18
	30	6.89E+00	1.3	10.4	7.94E+00	0.74%	1.15
KRAFTON-HB	5.3	3.04E+02	1.2	10.4	2.96E+02	0.44%	0.97
	11	1.27E+02	1.2	10.2	1.26E+02	0.64%	0.99
	16	5.58E+01	1.2	10.4	5.35E+01	0.84%	0.96
	21	2.55E+01	1.2	10.3	2.38E+01	0.87%	0.93
	27	1.22E+01	1.3	10.2	1.05E+01	0.86%	0.86
	32	6.09E+00	1.3	10.8	5.04E+00	0.85%	0.83
SS-304	5	4.87E+02	1.4	10.4	4.73E+02	0.33%	0.97
	10	3.62E+02	1.5	10.5	3.49E+02	0.57%	0.96
	15	2.67E+02	1.6	10.2	2.52E+02	0.76%	0.95
	20	1.95E+02	1.7	10.1	1.77E+02	0.89%	0.91
	25	1.42E+02	1.8	10.1	1.22E+02	0.98%	0.86
	30	1.03E+02	2.0	15.4	8.47E+01	0.86%	0.82
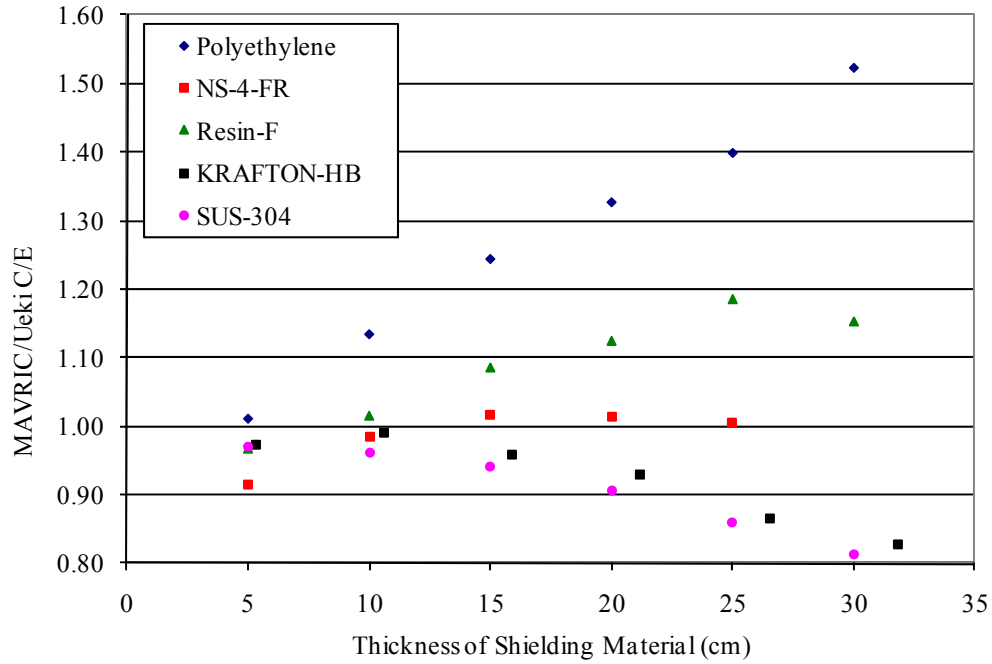
Figure 4.21. MAVRIC C/E ratios for the neutron dose rates from the Ueki type 1 experiments for single material shields of a given thickness.
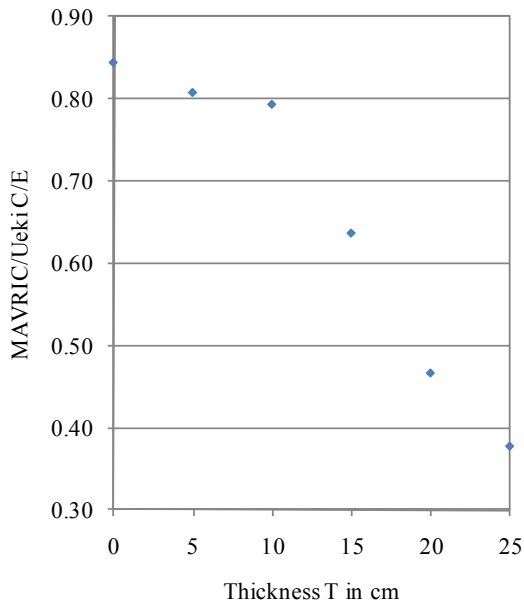
Figure 4.22. MAVRIC C/E ratios for the neutron dose rates from the type 2a experiments, which consist of 25 cm of SS-304 followed by *T* cm of polyethylene.
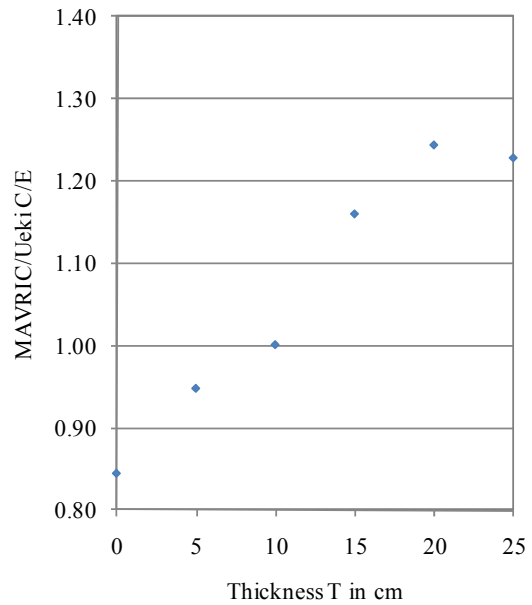
Figure 4.23. MAVRIC C/E ratios for the neutron dose rates from the type 2b experiments, which consist of *T* cm of polyethylene followed by 25 cm of SS-304.
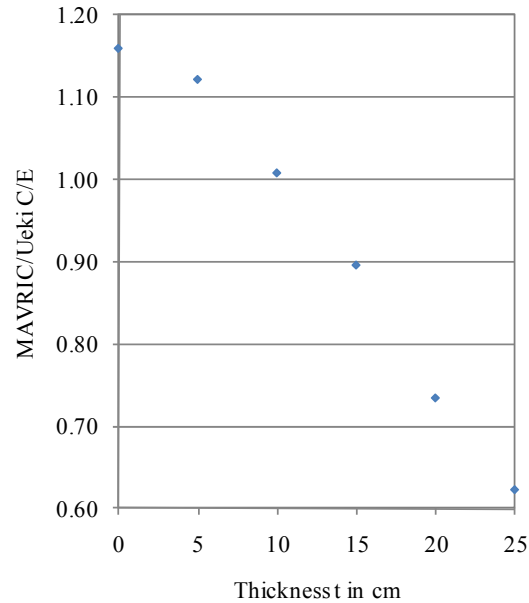
Figure 4.24. MAVRIC C/E ratios for the neutron dose rates from the type 3 experiments, which consist of *t* cm of SS-304, 15 cm ofpolyethylene, and (25-*t*) cm of SS-304.

4.4.6 XSDRN Results

The SCALE regression tests described in Sections 4.4.1 through 4.4.3 are essentially one dimensional. XSDRN inputs were constructed for these experiments and compared with the 3D MAVRIC results. In general, the results from the XSDRN calculations were essentially identical to the MAVRIC results.

4.4.7 Summary of SCALE Regression Tests

The VITAMIN-B7 library performed well for nearly all the XSDRN and MAVRIC simulations of the various experiments. The only exceptions were for the calculated photon spectra for several of the iron spheres from the ALARM-CF-FE-SHIELD-001 benchmark and the Ueki experiments that contained polyethylene in the shields.

4.5 Light Water Reactor Pressure Vessel Dosimetry Benchmarks

4.5.1 H.B. Robinson Unit 2 Pressure Vessel Benchmark

H. B. Robinson Unit 2 (HBR-2) is a 2300 MWt PWR designed by Westinghouse and placed into operation in March 1971. The HBR-2 core consists of 157 fuel elements with a 15 × 15 lattice. The core is enclosed by a core baffle, core barrel, thermal shield, pressure vessel, and biological shield.

In [29] dosimetry activities were calculated for a thermal shield surveillance capsule at an azimuthal angle of 20º and a reactor cavity location at 0º based on power distribution data for fuel cycle 9. The DORT discrete-ordinates radiation transport code was used to calculate one-dimensional (1D) and two-dimensional (2D) neutron flux distributions. A flux synthesis method was used to construct a three-dimensional (3D) flux distribution from the 1D and 2D transport solutions [30]. The synthesized flux was used with dosimetry cross sections from the CROSS-95 dosimetry library [31] to calculate reaction rates for the following dosimetry reactions: ^{237}Np(n,f)^{137}Cs, ^{238}U(n,f)^{137}Cs, ^{58}Ni(n,p)^{58}Co, ^{54}Fe(n,p)^{54}Mn, ^{46}Ti(n,p)^{46}Sc, and ^{63}Cu(n,α)^{60}Co. Details of the analysis are provided in [29].

For this benchmark comparison, the calculations described in [29] were updated using the BUGLE-B7 library. The calculated activities increased by approximately 2.5% to 4.5% for the threshold [(n,p) and n,α)] reactions. The activities for the fission reactions increased slightly at the capsule location and were essentially unchanged at the reactor cavity location. In all cases, the increases provide improved agreement with the measured data. The calculated-to-experiment (C/E) values for calculations using the BUGLE-96 and BUGLE-B7 libraries are presented in Table 4.6.

Table 4.6. Calculated-to-experiment ratios (C/E) for dosimetry activities from H. B. Robinson Unit 2, Cycle 9

Dosimetry location and cross-section library	Dosimetry reaction						Average[a]
	^{237}Np(n,f) ^{137}Cs	^{238}U(n,f) ^{137}Cs	^{58}Ni(n,p) ^{58}Co	^{54}Fe(n,p) ^{54}Mn	^{46}Ti(n,p) ^{46}Sc	^{63}Cu(n,α) ^{60}Co	
Capsule							
BUGLE-96	0.90 (0.92)[b]	0.85 (0.89)	0.96	0.93	0.85	0.90 (0.93)	0.90 ± 0.04 (0.91 ± 0.04)
BUGLE-B7	0.91 (0.93)	0.86 (0.91)	0.98	0.96	0.88	0.94 (0.96)	0.92 ± 0.05 (0.94 ± 0.04)
Cavity							
BUGLE-96	0.58 (0.61)	0.74 (0.82)	0.97	0.96	0.90	0.93 (0.96)	0.90 ± 0.09 (0.92 ± 0.06)
BUGLE-B7	0.58 (0.61)	0.74 (0.83)	1.00	0.99	0.94	0.97 (1.00)	0.93 ± 0.11 (0.95 ± 0.07)

[a] The average C/M and standard deviation values exclude the ^{237}Np reaction at the cavity location, which is suspected of having an inaccurate measurement. This exclusion is consistent with the data reduction performed in [29].

[b] The ratio values in parentheses for the ^{237}Np, ^{238}U, and ^{63}Cu reactions include the effect of adjustments to the measured data. These adjustments, described on page 11 of [29], are intended to compensate for photofission in the ^{237}Np and ^{238}U dosimeters and for Co impurities in the ^{63}Cu dosimeter. The measured ^{137}Cs activities in the ^{237}Np dosimeters were reduced by 2.5% and 5% at the capsule and cavity locations, respectively. The corresponding reduction factors for the ^{238}U dosimeters were 5% and 10%. The measured ^{60}Co activities in the ^{63}Cu dosimeters were reduced by 2.5% at both locations.

4.5.2 Oak Ridge National Laboratory Pool Critical Assembly (PCA)

The ORNL Pool Critical Assembly (ORNL PCA) pressure vessel wall benchmark facility (PVWBF) is one of the most widely used benchmarks for the qualification of radiation transport methods for LWR applications. The purpose of this benchmark was to validate the capabilities of calculational methods to predict the reaction rates in the region outside a reactor core when the neutron source, material compositions, and geometry are well defined. Analysis of the PCA benchmark can be used for partial fulfillment of the requirements for the qualification of the methodology for pressure vessel neutron fluence calculations, as required by Regulatory Guide 1.190. Details of the benchmark can be found in [32] and will not be repeated here except to point out differences with previous models and benchmarks.

The PCA is a small critical assembly composed of material test reactor (MTR) fuel elements (approximately 3" by 3" plates) in a water pool. The benchmark experiment consisted of the PCA reactor core (nominally 10 kW) and the components used to mock up the core-to-cavity region in LWRs. These components were the thermal shield, the pressure vessel simulator, and the void box, which simulated the reactor cavity. An overall view of the PCA core as modeled in KENO-VI geometry is shown in Figure 4.25, while an overall view of the entire PVWBF in KENO-VI geometry is shown in Figure 4.26. An aluminum plate, referred to as the reactor window simulator, was added to the facility for operational reasons. The thickness of the water gaps between the aluminum window and thermal shield and that between the thermal shield and the pressure vessel steel block was varied by the experimental run.

The set of measurements analyzed in this evaluation is the 12/13 (12 cm between the aluminum window and the thermal shield and 13 cm between the thermal shield and the pressure vessel steel block). The PCA 12/13 configuration is geometrically similar to the thermal shield–downcomer–pressure vessel design that is typical of many PWRs. In particular, the 12-cm water gap on the core side of the thermal shield, the 13-cm water gap between the thermal shield and the pressure vessel simulator, the 6-cm-thick stainless steel thermal shield, the 22.5-cm-thick low-alloy-steel pressure vessel, and the simulated reactor cavity (void box) positioned behind the pressure vessel mockup retain the characteristics of a PWR.

The PCA source was composed of 25 MTR new fuel elements with 93% ^{235}U enrichment. The power distribution of the fuel elements was obtained from fission chamber measurements and calculations and was provided as a two-dimensional distribution function as a part of the benchmark specification. These source data values were not utilized in the present analysis, because the computational sequence described below is capable of generating the critical reactor source term.

During the PCA experiments, measurements were taken at several locations within the mockup via vertically oriented experimental access tubes. The tube locations, which are described in detail in [32], provide transverse data extending from the reactor core outward through the pressure vessel simulator and into the void box. All of the foil measurements were conducted at locations in the experiment tubes at the core midplane elevation.

The measurements provide sufficient data to generate comparisons of measurements to calculations throughout the entire 12/13 configuration. Data from experiment tube locations A4, A5, and A6 establish the means for verification of calculated flux gradients within the pressure vessel wall itself. Since measurements at operating reactors can provide data only in the downcomer region internal to the pressure vessel or in the reactor cavity external to the vessel wall, the PCA data points located inside the thick-walled vessel establish a key set of comparisons to aid in the accurate determination of flux gradients within the pressure vessel wall.

Figure 4.25 shows a view of the MTR fuel assemblies used in the PCA core, with the safety and regulation rods fully inserted. The standard elements (shown in blue) consist of 18 MTR fuel plates. The elements shown in green contain 19 fuel plates, which was the standard fuel element design in the Oak Ridge Research Reactor. Note that the individual plates with the fuel meat interior region are modeled. This eliminates the need for using homogenized assemblies as were used in previous benchmark studies.

Figure 4.26 shows the complete SCALE Generalized Geometry Package (SGGP) model used in the KENO-VI criticality source calculations and the MAVRIC/Monaco shielding calculations. The pool water has been omitted from the picture for illustration purposes. The vertical experiment tubes centered along the midpoint of the PCA core are numbered A1–A8, with A1 being the tube closest to the core and A8 designating the largest tube, which is outside the void box. These tubes contained the foils and fission detectors used to experimentally measure the fluxes at the A1–A7 locations as given in Table 1.6 of [32].

The procedure for calculating the fluxes and reaction rates in this evaluation was as follows:

1. An initial KENO-VI calculation was run to determine the critical rod positions.
2. The KENO-VI calculation was rerun specifying a mesh to tally the spatial- and energy-dependent source particle distributions for subsequent transport using the Monaco code in the MAVRIC sequence. This calculation used a much larger number of particles than a standard k_{eff} calculation, because the objective was to obtain a well-converged source distribution to use in subsequent MONACO/Mavric calculations.
3. The MAVRIC sequence was run using the source mesh file for the source particles in conjunction with an importance map and biased source generated with adjoint fluxes calculated by the Denovo discrete-ordinates code. This automated variance reduction process provides consistent weight windows and biased source distributions for transport of the core neutrons to the desired locations (experimental tubes A1–A7). Calculation of the reaction rates of interest is discussed in Section 4.5.2.1.

4.5.2.1 Comparison of Calculated Reaction Rates with Experimental Results

A number of activation foils were used in the PVWBF experiments to calculate the flux. To minimize potential errors and provide a common basis for the benchmark exercises, the measured reaction rates were converted to equivalent fission fluxes, which are defined as

$$\phi_{fe} = \frac{\int \sigma_i(E)\phi(E)dE}{\int \sigma_i(E)\chi^{235}(E)dE}$$

where $\sigma_i(E)$ = the dosimetry cross section for the reaction being considered,
       $\phi(E)$ = the neutron flux at the dosimetry location, and
       $\chi^{235}(E)$ = the ^{235}U fission spectrum

The benchmark evaluation lists the foils that were used for radiometric measurements of equivalent fission fluxes. The reactions are $^{237}Np(n,f)^{137}Cs$, $^{238}U(n,f)^{137}Cs$, $^{103}Rh(n,n')^{103m}Rh$, $^{115}In(n,n')^{115m}In$, $^{58}Ni(n,p)^{58}Co$, and $^{27}Al(n,\alpha)^{24}Na$. For the ^{103}Rh and ^{115}In reactions, the reaction rates in the numerator were calculated using dosimetry cross sections from [17] for the response function in the MAVRIC sequence. Note that for those two inelastic scattering reactions, there is no single ENDF reaction type (MT value) which can be used to compute the production rate of the metastable isomer. For the other four reactions, the appropriate reaction cross sections from the transport library (either VITAMIN-B6 or VITAMIN-B7) were used as the reponse functions. The fission-spectrum-averaged cross sections in the denominator were

taken from Table 1.6 of [32]. These values were also calculated using the reaction cross sections used in the numerator and the [235]U fission spectra from the VITAMIN-B6 and VITAMIN-B7 libraries, and shown to be in very good agreement with the values listed in [32].

The measured and calculated fission equivalent fluxes for the six reactions listed above are provided in Table 4.7 through Table 4.12. The calculated values have relative uncertainties of less than ~1% at the 1σ level for the fission and inelastic scattering reactions, and less than ~2% for the [58]Ni and [27]Al reactions.
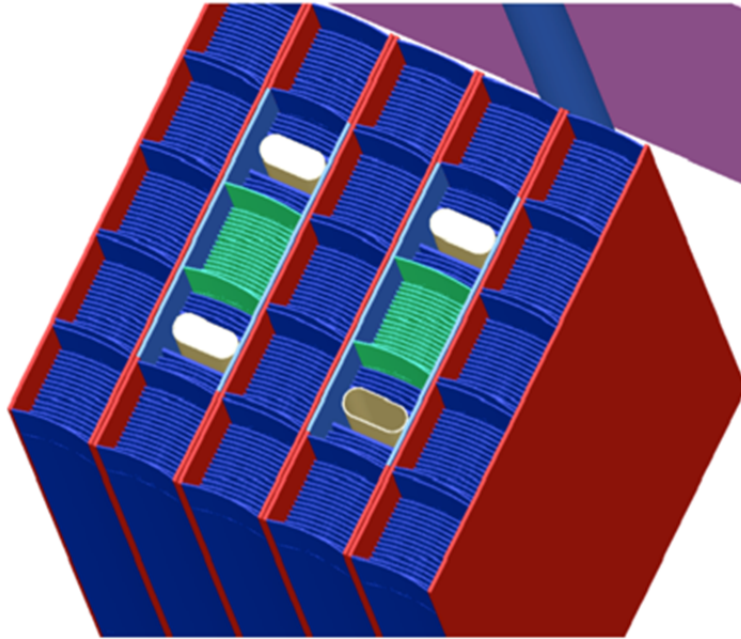
Figure 4.25. Close-up of the SCALE model of the PCA core.
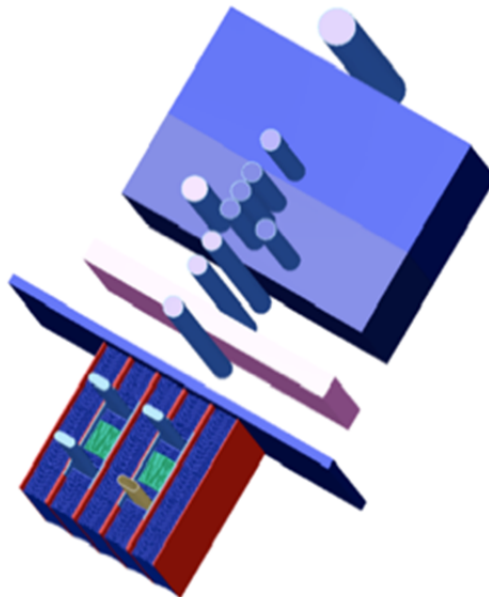
Figure 4.26. SCALE model of the pressure vessel wall benchmark facility (water omitted).

Table 4.7. ^{237}Np(n,f)^{137}Cs results for the PVWBF benchmark analysis

Experiment tube position	Distance from core (cm)	Experimental fission equivalent flux	Monaco/MAVRIC fission equivalent flux using VITAMIN-B6 Library	VITAMIN-B6 C/E ratio	Monaco/MAVRIC fission equivalent flux using VITAMIN-B7 Library	VITAMIN-B7 C/E ratio
A1	12.0	6.64E-06	6.55E-06	0.99	6.92E-06	1.04
A3	29.7	2.27E-07	2.51E-07	1.11	2.66E-07	1.17
A4	39.5	9.27E-08	9.04E-08	0.98	9.69E-08	1.05
A5	44.7	5.18E-08	5.04E-08	0.97	5.37E-08	1.04
A6	50.1	2.70E-08	2.59E-08	0.96	2.78E-08	1.03
A7	59.1	7.25E-09	7.51E-09	1.04	8.12E-09	1.12

Table 4.8. ^{238}U(n,f)^{137}Cs results for the PVWBF benchmark analysis

Experiment tube no.	Distance from core (cm)	Experimental fission equivalent flux	Monaco/MAVRIC fission equivalent flux using VITAMIN-B6 library	VITAMIN-B6 C/E ratio	Monaco/MAVRIC fission equivalent flux using VITAMIN-B7 library	VITAMIN-B7 C/E ratio
A4	39.5	6.11E-08	5.88E-08	0.96	6.07E-08	0.99
A5	44.7	2.74E-08	2.60E-08	0.95	2.64E-08	0.96
A6	50.1	1.12E-08	1.06E-08	0.95	1.07E-08	0.96

Table 4.9. ^{103}Rh(n,n')^{103m}Rh results for the PVWBF benchmark analysis

Experiment tube position	Distance from core (cm)	Experimental fission equivalent flux	Monaco/MAVRIC fission equivalent flux using VITAMIN-B6 library	VITAMIN-B6 C/E ratio	Monaco/MAVRIC fission equivalent flux using VITAMIN-B7 library	VITAMIN-B7 C/E ratio
A1	12.0	5.54E-06	5.91E-06	1.07	6.01E-06	1.09
A4	39.5	7.74E-08	8.34E-08	1.08	8.58E-08	1.11
A5	44.7	4.35E-08	4.54E-08	1.04	4.63E-08	1.06
A6	50.1	2.19E-08	2.29E-08	1.05	2.35E-08	1.07

Table 4.10. ^{115}In(n,n')^{115m}In results for the PVWBF benchmark analysis

Experiment tube position	Distance from core (cm)	Experimental fission equivalent flux	Monaco/MAVRIC fission equivalent flux using VITAMIN-B6 library	VITAMIN-B6 C/E ratio	Monaco/MAVRIC fission equivalent flux using VITAMIN-B7 library	VITAMIN-B7 C/E ratio
A1	12.0	5.61E-06	5.80E-06	1.03	5.92E-06	1.06
A2	23.8	6.06E-07	6.43E-07	1.06	6.49E-07	1.07
A3	29.7	1.99E-07	2.22E-07	1.11	2.26E-07	1.14
A4	39.5	5.87E-08	6.48E-08	1.10	6.63E-08	1.13
A5	44.7	2.76E-08	3.03E-08	1.10	3.08E-08	1.12
A6	50.1	1.17E-08	1.33E-08	1.13	1.34E-08	1.15

Table 4.11. ^{58}Ni(n,p)^{58}Co results for the PVWBF benchmark analysis

Experiment tube position	Distance from core (cm)	Experimental fission equivalent flux	Monaco/MAVRIC fission equivalent flux using VITAMIN-B6 library	VITAMIN-B6 C/E ratio	Monaco/MAVRIC fission equivalent flux using VITAMIN-B7 library	VITAMIN-B7 C/E ratio
A1	12.0	5.83E-06	5.78E-06	0.99	5.89E-06	1.01
A2	23.8	6.18E-07	6.31E-07	1.02	6.39E-07	1.03
A3	29.7	2.31E-07	2.48E-07	1.07	2.53E-07	1.10
A4	39.5	5.30E-08	5.34E-08	1.01	5.50E-08	1.04
A5	44.7	2.09E-08	2.15E-08	1.03	2.19E-08	1.05
A6	50.1	7.43E-09	8.22E-09	1.11	8.26E-09	1.11

Table 4.12. ^{27}Al(n,α)^{23}Na results for the PVWBF benchmark analysis

Experiment tube position	Distance from core (cm)	Experimental fission equivalent flux	Monaco/MAVRIC fission equivalent flux using VITAMIN-B6 library	VITAMIN-B6 C/E ratio	Monaco/MAVRIC fission equivalent flux using VITAMIN-B7 library	VITAMIN-B7 C/E ratio
A1	12.0	7.87E-06	7.73E-06	0.98	7.74E-06	0.98
A2	23.8	1.02E-06	1.00E-06	0.98	1.03E-06	1.01
A3	29.7	4.48E-07	4.56E-07	1.02	4.60E-07	1.03
A4	39.5	1.02E-07	9.97E-08	0.98	1.01E-07	0.99
A5	44.7	4.10E-08	4.08E-08	0.99	4.19E-08	1.02
A6	50.1	1.54E-08	1.61E-08	1.05	1.65E-08	1.07

4.5.3   CEN/SK Laboratory VENUS-3 Benchmark

The VENUS Critical Facility is a low power (approximately 650 W) reactor located at SCK/CEN in Belgium. The VENUS-3 benchmark experiment [33 and 34] was a joint effort between ORNL, under the direction of the NRC, and the Belgian regulatory authority. The objective was to study the applicability of 1D and 2D flux synthesis methods for configurations in which partial length shield assemblies (PLSAs) are used in a reactor. In the VENUS-3 PLSAs, some of the UO$_2$ fuel was replaced with stainless steel in fuel rods near the periphery of the core to reduce the neutron fluence at the pressure vessel.

The VENUS-3 benchmark used fuel assemblies with 4% and 3.3% enriched ^{235}U UO$_2$ fuel rods, with some of the 3.3% enriched fuel replaced by PLSAs. The standard fuel rods had a fuel length of 50 cm. In the PLSAs, the lower 25 cm of fuel was replaced by 25 cm of stainless steel. The fuel rods were spaced with a 1.26 cm pitch, which is typical of commonly used 17 × 17 PWR fuel assemblies.

In the southwest quadrant of the VENUS-3 experiment, a mockup of the internal structure of a reactor vessel was placed next to the VENUS reactor. The mockup structure, which started at the fuel assemblies and extended outward toward the pressure vessel, consisted of an outer core baffle, core barrel, water gap, neutron pad, jacket, and pressure vessel. A picture of the southwest quadrant of the VENUS benchmark geometry, as constructed with the SGGP, is shown in Figure 4.27. (All water has been omitted from the figure for clarity.) In Figure 4.27, the PLSAs are the rods where the fuel in the upper half of the rods is colored bright green and the stainless steel in the lower half of the rods is colored blue. To the right of the PLSAs in Figure 4.27 are the outer core baffle (dark blue), the core barrel (white), the neutron pad (red), and the jacket and pressure vessel (magenta).

During the VENUS-3 benchmark, reaction rates were measured at 30 different radial locations. At each of these radial locations there were up to 14 different measurements in the axial direction. At each of these axial positions up to 3 activation reactions were measured. These activation reactions were measured inside the inner baffle, outer baffle, core barrel, water gap, PLSA rods, and 3.3% enriched fuel rods in the southwest quadrant of the reactor. The activation reactions that were measured are:

1. ^{58}Ni(n,p)^{58}Co
2. ^{115}In(n,n')^{115m}In
3. ^{27}Al(n,α)^{24}Na

The benchmark consists of 38 ^{27}Al(n,α)^{24}Na measurements, 104 ^{115}In(n,n')^{115m}In measurements, and 242 ^{58}Ni(n,p)^{58}Co measurements. The measured reaction rates were not reported in the benchmark. Instead the equivalent fission fluxes (see Section 4.5.2.1) were reported.

For the present evaluation, the TORT [35] discrete ordinates radiation transport code was used to model the VENUS-3 benchmark. Calculations were run using the BUGLE-96 and BUGLE-B7 libraries. For each dosimetry reaction, equivalent fission fluxes were calculated using the flat-weighted response function data in the BUGLE libraries. The fission-spectrum-averaged cross sections were taken from [34].
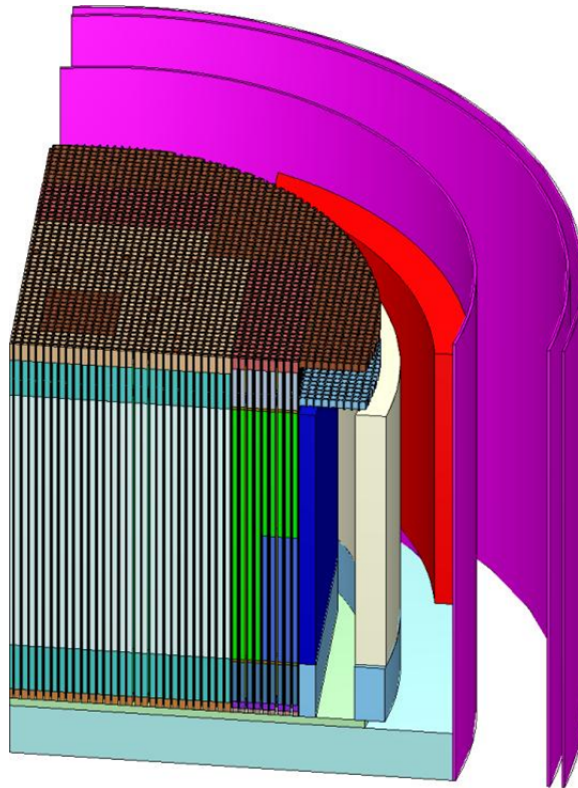
Figure 4.27. Southwest quadrant of the VENUS-3 benchmark geometry as modeled in the SGGP (water omitted).

Table 4.13. Calculated-to-Measured (C/M) Ratios for the VENUS-3 Benchmark Experiment
^{58}Ni(n,p)^{58}Co Equivalent Fission Fluxes using TORT with BUGLE-96 and BUGLE-B7 Cross-Sections

Measurement Zone	Position (cm)				Measured Equivalent Fission Flux**	TORT with BUGLE-96			TORT with BUGLE-B7	
	X	Y	Z*			Equivalent Fission Flux	C/M		Equivalent Fission Flux	C/M
3.3% Fuel	-29.61	-0.63	106.05		9.316E+08	8.82E+08	0.95		8.85E+08	0.95
			110.15		1.282E+09	1.28E+09	1.00		1.29E+09	1.00
			114.25		1.644E+09	1.56E+09	0.95		1.57E+09	0.95
			118.35		1.986E+09	1.88E+09	0.95		1.89E+09	0.95
			122.45		2.276E+09	2.27E+09	1.00		2.27E+09	1.00
			125.55		2.494E+09	2.45E+09	0.98		2.46E+09	0.99
			128.65		2.683E+09	2.68E+09	1.00		2.69E+09	1.00
			131.75		2.860E+09	2.81E+09	0.98		2.82E+09	0.99
			134.85		2.925E+09	2.87E+09	0.98		2.87E+09	0.98
			137.95		2.855E+09	2.82E+09	0.99		2.83E+09	0.99
			141.05		2.744E+09	2.69E+09	0.98		2.69E+09	0.98
			145.15		2.406E+09	2.38E+09	0.99		2.38E+09	0.99
			149.25		1.967E+09	1.95E+09	0.99		1.95E+09	0.99
			153.35		1.473E+09	1.57E+09	1.06		1.57E+09	1.07
3.3% Fuel	-27.09	0.63	106.05		1.141E+09	1.09E+09	0.96		1.10E+09	0.96
			110.15		1.589E+09	1.60E+09	1.01		1.60E+09	1.01
			114.25		2.014E+09	1.93E+09	0.96		1.94E+09	0.96
			118.35		2.424E+09	2.33E+09	0.96		2.34E+09	0.97
			122.45		2.774E+09	2.77E+09	1.00		2.78E+09	1.00
			125.55		2.988E+09	2.97E+09	1.00		2.99E+09	1.00
			128.65		3.160E+09	3.17E+09	1.00		3.19E+09	1.01
			131.75		3.267E+09	3.25E+09	1.00		3.27E+09	1.00
			134.85		3.295E+09	3.28E+09	0.99		3.29E+09	1.00
			137.95		3.218E+09	3.21E+09	1.00		3.22E+09	1.00
			141.05		3.046E+09	3.03E+09	1.00		3.04E+09	1.00
			145.15		2.679E+09	2.66E+09	0.99		2.67E+09	1.00
			149.25		2.195E+09	2.18E+09	0.99		2.19E+09	1.00
			153.35		1.651E+09	1.75E+09	1.06		1.76E+09	1.07
3.3% Fuel	-30.87	-3.15	106.05		7.661E+08	7.21E+08	0.94		7.25E+08	0.95
			110.15		1.057E+09	1.04E+09	0.98		1.04E+09	0.99
			114.25		1.350E+09	1.27E+09	0.94		1.27E+09	0.94
			118.35		1.620E+09	1.53E+09	0.95		1.54E+09	0.95
			122.45		1.876E+09	1.84E+09	0.98		1.85E+09	0.99
			125.55		2.067E+09	2.03E+09	0.98		2.03E+09	0.98
			128.65		2.280E+09	2.30E+09	1.01		2.31E+09	1.01
			131.75		2.527E+09	2.51E+09	0.99		2.51E+09	0.99
			134.85		2.628E+09	2.60E+09	0.99		2.61E+09	0.99
			137.95		2.622E+09	2.58E+09	0.99		2.59E+09	0.99
			141.05		2.495E+09	2.46E+09	0.99		2.47E+09	0.99
			145.15		2.209E+09	2.19E+09	0.99		2.19E+09	0.99
			149.25		1.829E+09	1.79E+09	0.98		1.79E+09	0.98
			153.35		1.376E+09	1.44E+09	1.05		1.45E+09	1.05

Table 4.13. Calculated-to-Measured (C/M) Ratios for the VENUS-3 Benchmark Experiment
^{58}Ni(n,p)^{58}Co Equivalent Fission Fluxes using TORT with BUGLE-96 and BUGLE-B7 Cross-Sections

| Measurement | Position (cm) | | | | Measured Equivalent Fission Flux** | | TORT with BUGLE-96 | | | TORT with BUGLE-B7 | |
Zone	X	Y	Z*				Equivalent Fission Flux	C/M		Equivalent Fission Flux	C/M
3.3% Fuel	-0.63	-32.13	106.05		1.285E+09		1.25E+09	0.97		1.25E+09	0.97
			110.15		1.768E+09		1.80E+09	1.02		1.80E+09	1.02
			114.25		2.210E+09		2.16E+09	0.98		2.17E+09	0.98
			118.35		2.606E+09		2.56E+09	0.98		2.56E+09	0.98
			122.45		2.898E+09		2.94E+09	1.02		2.94E+09	1.02
			125.55		3.045E+09		3.09E+09	1.02		3.10E+09	1.02
			128.65		3.120E+09		3.15E+09	1.01		3.16E+09	1.01
			131.75		3.118E+09		3.14E+09	1.01		3.15E+09	1.01
			134.85		3.047E+09		3.08E+09	1.01		3.08E+09	1.01
			137.95		2.894E+09		2.95E+09	1.02		2.95E+09	1.02
			141.05		2.706E+09		2.74E+09	1.01		2.74E+09	1.01
			145.15		2.333E+09		2.38E+09	1.02		2.38E+09	1.02
			149.25		1.888E+09		1.92E+09	1.02		1.92E+09	1.02
			153.35		1.403E+09		1.57E+09	1.12		1.58E+09	1.12
PLSA	-32.13	-0.63	131.05		2.280E+09		2.23E+09	0.98		2.23E+09	0.98
			134.15		2.426E+09		2.40E+09	0.99		2.40E+09	0.99
			137.25		2.443E+09		2.41E+09	0.99		2.41E+09	0.99
			141.35		2.309E+09		2.28E+09	0.99		2.28E+09	0.99
			145.45		2.030E+09		2.01E+09	0.99		2.01E+09	0.99
			149.55		1.656E+09		1.65E+09	1.00		1.66E+09	1.00
			153.65		1.250E+09		1.04E+09	0.83		1.04E+09	0.83
PLSA	-32.13	0.63	106.5		5.115E+08		5.17E+08	1.01		5.20E+08	1.02
			110.5		7.161E+08		7.55E+08	1.05		7.59E+08	1.06
			114.5		9.113E+08		9.48E+08	1.04		9.53E+08	1.05
			118.5		1.094E+09		1.13E+09	1.04		1.14E+09	1.04
			122.5		1.264E+09		1.31E+09	1.04		1.32E+09	1.04
			125.5		1.400E+09		1.45E+09	1.03		1.45E+09	1.04
			128.5		1.624E+09		1.65E+09	1.01		1.65E+09	1.02
PLSA	-34.65	0.63	106.5		2.713E+08		2.72E+08	1.00		2.74E+08	1.01
			110.5		3.843E+08		4.02E+08	1.05		4.06E+08	1.06
			114.5		4.896E+08		5.03E+08	1.03		5.07E+08	1.04
			118.5		5.899E+08		6.02E+08	1.02		6.07E+08	1.03
			122.5		6.947E+08		7.16E+08	1.03		7.21E+08	1.04
			125.5		7.980E+08		8.20E+08	1.03		8.26E+08	1.03
			128.5		1.025E+09		1.04E+09	1.02		1.05E+09	1.02
			131.05		1.617E+09		1.62E+09	1.00		1.63E+09	1.01
			134.15		1.846E+09		1.85E+09	1.00		1.85E+09	1.00
			137.25		1.897E+09		1.88E+09	0.99		1.88E+09	0.99
			141.35		1.846E+09		1.80E+09	0.97		1.80E+09	0.97
			145.45		1.628E+09		1.59E+09	0.98		1.60E+09	0.98
			149.55		1.354E+09		1.31E+09	0.97		1.31E+09	0.97
			153.65		1.033E+09		8.31E+08	0.80		8.32E+08	0.81

Table 4.13. Calculated-to-Measured (C/M) Ratios for the VENUS-3 Benchmark Experiment
^{58}Ni(n,p)^{58}Co Equivalent Fission Fluxes using TORT with BUGLE-96 and BUGLE-B7 Cross-Sections

Measurement Zone	Position (cm)				Measured Equivalent Fission Flux**		TORT with BUGLE-96			TORT with BUGLE-B7	
	X	Y	Z*				Equivalent Fission Flux	C/M		Equivalent Fission Flux	C/M
PLSA	-37.17	-0.63	131.05		1.084E+09		1.05E+09	0.97		1.05E+09	0.97
			134.15		1.234E+09		1.21E+09	0.98		1.21E+09	0.98
			137.25		1.280E+09		1.25E+09	0.98		1.25E+09	0.98
			141.35		1.227E+09		1.19E+09	0.97		1.19E+09	0.97
			145.45		1.108E+09		1.07E+09	0.96		1.07E+09	0.96
			149.55		9.125E+08		8.83E+08	0.97		8.85E+08	0.97
			153.65		7.026E+08		5.66E+08	0.81		5.67E+08	0.81
PLSA	-37.17	0.63	106.5		1.648E+08		1.68E+08	1.02		1.70E+08	1.03
			110.5		2.296E+08		2.48E+08	1.08		2.51E+08	1.09
			114.5		2.947E+08		3.14E+08	1.06		3.17E+08	1.08
			118.5		3.548E+08		3.83E+08	1.08		3.87E+08	1.09
			122.5		4.275E+08		4.56E+08	1.07		4.60E+08	1.08
			125.5		5.062E+08		5.37E+08	1.06		5.41E+08	1.07
			128.5		6.752E+08		6.92E+08	1.03		6.96E+08	1.03
PLSA	-37.17	-14.49	106.5		1.141E+08		1.17E+08	1.03		1.19E+08	1.04
			110.5		1.480E+08		1.72E+08	1.16		1.74E+08	1.17
			114.5		1.793E+08		2.17E+08	1.21		2.20E+08	1.23
			118.5		2.212E+08		2.64E+08	1.19		2.67E+08	1.21
			122.5		2.646E+08		3.12E+08	1.18		3.15E+08	1.19
			125.5		3.204E+08		3.63E+08	1.13		3.66E+08	1.14
			128.5		4.479E+08		4.62E+08	1.03		4.65E+08	1.04
Inner Baffle	-4.41	-4.41	114.5		1.474E+09		1.51E+09	1.02		1.52E+09	1.03
			131.5		2.091E+09		2.12E+09	1.01		2.14E+09	1.02
			145.5		1.523E+09		1.57E+09	1.03		1.59E+09	1.04
Inner Baffle	-4.41	-0.63	114.5		1.233E+09		1.25E+09	1.01		1.26E+09	1.02
			131.5		1.752E+09		1.76E+09	1.00		1.78E+09	1.01
			145.5		1.248E+09		1.31E+09	1.05		1.32E+09	1.06
Outer Baffle	-39.69	-18.27	114.5		9.002E+07		1.00E+08	1.11		1.01E+08	1.13
			131.5		2.211E+08		2.29E+08	1.04		2.31E+08	1.04
			145.5		2.167E+08		2.21E+08	1.02		2.22E+08	1.02
Outer Baffle	-39.69	-11.97	114.5		1.362E+08		1.50E+08	1.10		1.52E+08	1.11
			131.5		3.803E+08		3.88E+08	1.02		3.90E+08	1.02
			145.5		3.778E+08		3.84E+08	1.02		3.85E+08	1.02
Outer Baffle	-39.69	-5.67	114.5		1.636E+08		1.82E+08	1.11		1.83E+08	1.12
			131.5		4.639E+08		4.79E+08	1.03		4.81E+08	1.04
			145.5		4.638E+08		4.77E+08	1.03		4.78E+08	1.03

Table 4.13. Calculated-to-Measured (C/M) Ratios for the VENUS-3 Benchmark Experiment
^{58}Ni(n,p)^{58}Co Equivalent Fission Fluxes using TORT with BUGLE-96 and BUGLE-B7 Cross-Sections

Measurement Zone	Position (cm)				Measured Equivalent Fission Flux**		TORT with BUGLE-96			TORT with BUGLE-B7	
	X	Y	Z*				Equivalent Fission Flux	C/M		Equivalent Fission Flux	C/M
Outer Baffle	-39.69	-0.63	106.5		9.802E+07		1.03E+08	1.05		1.04E+08	1.07
			110.5		1.360E+08		1.52E+08	1.12		1.53E+08	1.13
			114.5		1.750E+08		1.90E+08	1.09		1.92E+08	1.10
			118.5		2.106E+08		2.32E+08	1.10		2.34E+08	1.11
			122.5		2.576E+08		2.79E+08	1.08		2.81E+08	1.09
			125.5		3.085E+08		3.29E+08	1.07		3.31E+08	1.07
			128.5		3.880E+08		4.12E+08	1.06		4.14E+08	1.07
			131.5		5.003E+08		5.06E+08	1.01		5.08E+08	1.01
			134.5		5.571E+08		5.68E+08	1.02		5.69E+08	1.02
			137.5		5.731E+08		5.88E+08	1.03		5.89E+08	1.03
			141.5		5.544E+08		5.65E+08	1.02		5.66E+08	1.02
			145.5		4.945E+08		5.05E+08	1.02		5.06E+08	1.02
			149.5		4.052E+08		4.20E+08	1.04		4.21E+08	1.04
			153.5		2.912E+08		2.89E+08	0.99		2.89E+08	0.99
Outer Baffle	-37.17	-20.79	114.5		1.059E+08		1.15E+08	1.09		1.16E+08	1.10
			131.5		2.395E+08		2.44E+08	1.02		2.45E+08	1.02
			145.5		2.220E+08		2.29E+08	1.03		2.30E+08	1.04
Outer Baffle	-30.87	-20.79	114.5		3.080E+08		3.11E+08	1.01		3.13E+08	1.02
			131.5		5.194E+08		5.33E+08	1.03		5.36E+08	1.03
			145.5		4.341E+08		4.52E+08	1.04		4.55E+08	1.05
Outer Baffle	-24.57	-20.79	114.5		6.242E+08		6.39E+08	1.02		6.44E+08	1.03
			131.5		9.238E+08		9.44E+08	1.02		9.51E+08	1.03
			145.5		7.106E+08		7.34E+08	1.03		7.39E+08	1.04
Outer Baffle	-44.73	-0.63	106.5		3.736E+07		3.77E+07	1.01		3.86E+07	1.03
			110.5		5.027E+07		5.23E+07	1.04		5.34E+07	1.06
			114.5		6.366E+07		6.62E+07	1.04		6.75E+07	1.06
			118.5		7.684E+07		8.14E+07	1.06		8.30E+07	1.08
			122.5		9.566E+07		1.01E+08	1.05		1.02E+08	1.07
			125.5		1.124E+08		1.14E+08	1.01		1.16E+08	1.03
			128.5		1.330E+08		1.36E+08	1.02		1.38E+08	1.04
			131.5		1.509E+08		1.49E+08	0.99		1.51E+08	1.00
			134.5		1.646E+08		1.67E+08	1.01		1.69E+08	1.03
			137.5		1.680E+08		1.70E+08	1.01		1.72E+08	1.02
			141.5		1.636E+08		1.66E+08	1.01		1.68E+08	1.03
			145.5		1.448E+08		1.49E+08	1.03		1.51E+08	1.04
			149.5		1.207E+08		1.26E+08	1.04		1.27E+08	1.05
			153.5		8.650E+07		8.71E+07	1.01		8.83E+07	1.02
Core Barrel	-49.77	-9.45	114.5		2.486E+07		2.73E+07	1.10		2.79E+07	1.12
			131.5		5.210E+07		5.41E+07	1.04		5.49E+07	1.05
			145.5		5.039E+07		5.24E+07	1.04		5.31E+07	1.05

Table 4.13. Calculated-to-Measured (C/M) Ratios for the VENUS-3 Benchmark Experiment
^{58}Ni(n,p)^{58}Co Equivalent Fission Fluxes using TORT with BUGLE-96 and BUGLE-B7 Cross-Sections

Measurement Zone	Position (cm)				Measured Equivalent Fission Flux**		TORT with BUGLE-96			TORT with BUGLE-B7	
	X	Y	Z*				Equivalent Fission Flux	C/M		Equivalent Fission Flux	C/M
Core Barrel	-49.77	-0.63	106.5		1.694E+07		1.80E+07	1.06		1.84E+07	1.08
			110.5		2.221E+07		2.47E+07	1.11		2.52E+07	1.13
			114.5		2.824E+07		3.18E+07	1.13		3.24E+07	1.15
			118.5		3.597E+07		3.88E+07	1.08		3.95E+07	1.10
			122.5		4.388E+07		4.58E+07	1.04		4.66E+07	1.06
			125.5		4.936E+07		5.25E+07	1.06		5.34E+07	1.08
			128.5		5.539E+07		5.99E+07	1.08		6.09E+07	1.10
			131.5		6.090E+07		6.35E+07	1.04		6.45E+07	1.06
			134.5		6.453E+07		6.91E+07	1.07		7.01E+07	1.09
			137.5		6.676E+07		7.00E+07	1.05		7.10E+07	1.06
			141.5		6.438E+07		6.80E+07	1.06		6.90E+07	1.07
			145.5		5.873E+07		6.18E+07	1.05		6.27E+07	1.07
			149.5		4.932E+07		5.27E+07	1.07		5.35E+07	1.08
			153.5		3.757E+07		3.87E+07	1.03		3.93E+07	1.05
Core Barrel	-47.25	-18.27	106.5		1.415E+07		1.54E+07	1.09		1.57E+07	1.11
			110.5		1.923E+07		2.10E+07	1.09		2.14E+07	1.11
			114.5		2.383E+07		2.69E+07	1.13		2.73E+07	1.15
			118.5		2.960E+07		3.25E+07	1.10		3.30E+07	1.12
			122.5		3.559E+07		3.87E+07	1.09		3.93E+07	1.10
			125.5		4.042E+07		4.35E+07	1.08		4.41E+07	1.09
			128.5		4.540E+07		4.92E+07	1.08		4.99E+07	1.10
			131.5		5.030E+07		5.27E+07	1.05		5.34E+07	1.06
			134.5		5.411E+07		5.69E+07	1.05		5.76E+07	1.06
			137.5		5.520E+07		5.74E+07	1.04		5.81E+07	1.05
			141.5		5.348E+07		5.56E+07	1.04		5.62E+07	1.05
			145.5		4.780E+07		5.02E+07	1.05		5.08E+07	1.06
			149.5		4.042E+07		4.23E+07	1.05		4.28E+07	1.06
			153.5		3.071E+07		3.06E+07	1.00		3.11E+07	1.01
Core Barrel	-45.99	-22.05	114.5		2.187E+07		2.45E+07	1.12		2.50E+07	1.14
			131.5		4.348E+07		4.57E+07	1.05		4.63E+07	1.07
			145.5		4.092E+07		4.27E+07	1.04		4.31E+07	1.05
Core Barrel	-44.73	-24.57	114.5		2.108E+07		2.32E+07	1.10		2.36E+07	1.12
			131.5		3.942E+07		4.14E+07	1.05		4.20E+07	1.07
			145.5		3.673E+07		3.81E+07	1.04		3.86E+07	1.05
Core Barrel	-42.21	-28.35	114.5		2.880E+07		2.58E+07	0.89		2.63E+07	0.91
			131.5		4.480E+07		4.14E+07	0.92		4.21E+07	0.94
			145.5		3.927E+07		3.60E+07	0.92		3.66E+07	0.93
Core Barrel	-38.43	-33.39	114.5		2.534E+07		2.59E+07	1.02		2.65E+07	1.05
			131.5		3.764E+07		3.83E+07	1.02		3.92E+07	1.04
			145.5		3.059E+07		3.24E+07	1.06		3.31E+07	1.08

Table 4.13. Calculated-to-Measured (C/M) Ratios for the VENUS-3 Benchmark Experiment
^{58}Ni(n,p)^{58}Co Equivalent Fission Fluxes using TORT with BUGLE-96 and BUGLE-B7 Cross-Sections

Measurement Zone	Position (cm)				Measured Equivalent Fission Flux**		TORT with BUGLE-96			TORT with BUGLE-B7	
	X	Y	Z*				Equivalent Fission Flux	C/M		Equivalent Fission Flux	C/M
Core Barrel	-35.91	-35.91	106.5		1.749E+07		1.77E+07	1.01		1.82E+07	1.04
			110.5		2.249E+07		2.33E+07	1.04		2.38E+07	1.06
			114.5		2.743E+07		2.91E+07	1.06		2.98E+07	1.09
			118.5		3.162E+07		3.30E+07	1.04		3.38E+07	1.07
			122.5		3.529E+07		3.66E+07	1.04		3.75E+07	1.06
			125.5		3.743E+07		3.88E+07	1.04		3.97E+07	1.06
			128.5		3.848E+07		4.02E+07	1.04		4.11E+07	1.07
			131.5		3.864E+07		4.07E+07	1.05		4.16E+07	1.08
			134.5		3.843E+07		4.05E+07	1.05		4.13E+07	1.08
			137.5		3.811E+07		3.94E+07	1.03		4.03E+07	1.06
			141.5		3.508E+07		3.65E+07	1.04		3.73E+07	1.06
			145.5		3.090E+07		3.30E+07	1.07		3.37E+07	1.09
			149.5		2.545E+07		2.66E+07	1.05		2.72E+07	1.07
			153.5		1.974E+07		2.05E+07	1.04		2.10E+07	1.07
Core Barrel	-18.27	-47.25	106.5		3.421E+07		3.45E+07	1.01		3.49E+07	1.02
			110.5		4.652E+07		4.87E+07	1.05		4.92E+07	1.06
			114.5		5.720E+07		5.97E+07	1.04		6.03E+07	1.05
			118.5		6.502E+07		6.87E+07	1.06		6.95E+07	1.07
			122.5		7.095E+07		7.58E+07	1.07		7.67E+07	1.08
			125.5		7.478E+07		7.92E+07	1.06		8.01E+07	1.07
			128.5		7.515E+07		8.11E+07	1.08		8.20E+07	1.09
			131.5		7.681E+07		8.14E+07	1.06		8.22E+07	1.07
			134.5		7.491E+07		7.98E+07	1.07		8.07E+07	1.08
			137.5		7.236E+07		7.68E+07	1.06		7.76E+07	1.07
			141.5		6.641E+07		7.02E+07	1.06		7.09E+07	1.07
			145.5		5.715E+07		6.11E+07	1.07		6.18E+07	1.08
			149.5		4.667E+07		5.04E+07	1.08		5.10E+07	1.09
			153.5		3.445E+07		3.59E+07	1.04		3.63E+07	1.06
Core Barrel	-0.63	-49.77	106.5		4.321E+07		4.46E+07	1.03		4.53E+07	1.05
			110.5		5.814E+07		6.26E+07	1.08		6.35E+07	1.09
			114.5		7.080E+07		7.58E+07	1.07		7.69E+07	1.09
			118.5		8.203E+07		8.73E+07	1.06		8.85E+07	1.08
			122.5		8.938E+07		9.63E+07	1.08		9.77E+07	1.09
			125.5		9.403E+07		1.01E+08	1.07		1.02E+08	1.09
			128.5		9.540E+07		1.03E+08	1.08		1.04E+08	1.09
			131.5		9.618E+07		1.03E+08	1.08		1.05E+08	1.09
			134.5		9.429E+07		1.01E+08	1.07		1.03E+08	1.09
			137.5		9.057E+07		9.72E+07	1.07		9.86E+07	1.09
			141.5		8.207E+07		8.88E+07	1.08		9.00E+07	1.10
			145.5		7.174E+07		7.72E+07	1.08		7.83E+07	1.09
			149.5		5.807E+07		6.41E+07	1.10		6.50E+07	1.12
			153.5		4.317E+07		4.62E+07	1.07		4.69E+07	1.09

*   - The axial extent of the fuel in the TORT model is from 105 cm to 155 cm.

** - The measurement uncertainty for all the ^{58}Ni(n,p)^{58}Co was 5.7% at the one-sigma level.

Table 4.14. Calculated-to-Measured (C/M) Ratios for the VENUS-3 Benchmark Experiment
^{115}In(n,n')^{115m}In Equivalent Fission Fluxes using TORT with BUGLE-96 and BUGLE-B7 Cross-Sections

Measurement Zone	Position (cm)				Measured Equivalent Fission Flux**		TORT with BUGLE-96			TORT with BUGLE-B7	
	X	Y	Z*				Equivalent Fission Flux	C/M		Equivalent Fission Flux	C/M
Inner Baffle	-4.41	-4.41	131.5		2.713E+09		2.65E+09	0.98		2.64E+09	0.97
Inner Baffle	-4.41	-0.63	131.5		2.249E+09		2.22E+09	0.99		2.21E+09	0.98
Outer Baffle	-39.69	-0.63	106.5		1.189E+08		1.22E+08	1.03		1.22E+08	1.03
			110.5		1.698E+08		1.81E+08	1.07		1.82E+08	1.07
			114.5		2.181E+08		2.30E+08	1.06		2.31E+08	1.06
			118.5		2.657E+08		2.82E+08	1.06		2.82E+08	1.06
			122.5		3.256E+08		3.40E+08	1.04		3.40E+08	1.04
			125.5		3.871E+08		4.02E+08	1.04		4.01E+08	1.04
			128.5		4.859E+08		4.99E+08	1.03		4.97E+08	1.02
			131.5		6.112E+08		6.10E+08	1.00		6.06E+08	0.99
			134.5		6.915E+08		6.84E+08	0.99		6.79E+08	0.98
			137.5		7.196E+08		7.08E+08	0.98		7.03E+08	0.98
			141.5		6.894E+08		6.82E+08	0.99		6.76E+08	0.98
			145.5		6.182E+08		6.09E+08	0.99		6.04E+08	0.98
			149.5		5.062E+08		5.04E+08	0.99		5.00E+08	0.99
			153.5		3.614E+08		3.44E+08	0.95		3.41E+08	0.94
Water Gap	-44.73	-0.63	106.5		3.767E+07		3.83E+07	1.02		3.86E+07	1.02
			110.5		5.187E+0		5.39E+07	1.04		5.42E+07	1.05
			114.5		6.610E+07		6.89E+07	1.04		6.93E+07	1.05
			118.5		8.268E+07		8.50E+07	1.03		8.54E+07	1.03
			122.5		9.990E+07		1.05E+08	1.05		1.05E+08	1.06
			125.5		1.187E+08		1.20E+08	1.01		1.20E+08	1.01
			128.5		1.405E+08		1.43E+08	1.01		1.43E+08	1.02
			131.5		1.553E+08		1.57E+08	1.01		1.57E+08	1.01
			134.5		1.725E+08		1.76E+08	1.02		1.75E+08	1.02
			137.5		1.835E+08		1.79E+08	0.98		1.79E+08	0.97
			141.5		1.786E+08		1.75E+08	0.98		1.75E+08	0.98
			145.5		1.596E+08		1.57E+08	0.99		1.57E+08	0.98
			149.5		1.344E+08		1.32E+08	0.98		1.31E+08	0.98
			153.5		1.003E+08		9.09E+07	0.91		9.08E+07	0.91
Core Barrel	-49.77	-9.45	114.5		3.114E+07		3.21E+07	1.03		3.24E+07	1.04
			131.5		6.647E+07		6.54E+07	0.98		6.57E+07	0.99
			145.5		6.490E+07		6.30E+07	0.97		6.31E+07	0.97

Table 4.14. Calculated-to-Measured (C/M) Ratios for the VENUS-3 Benchmark Experiment
^{115}In(n,n')^{115m}In Equivalent Fission Fluxes using TORT with BUGLE-96 and BUGLE-B7 Cross-Sections

Measurement Zone	Position (cm)				Measured Equivalent Fission Flux**		TORT with BUGLE-96			TORT with BUGLE-B7	
	X	Y	Z*				Equivalent Fission Flux	C/M		Equivalent Fission Flux	C/M
Core Barrel	-49.77	-0.63	106.5		1.898E+07		1.97E+07	1.04		1.99E+07	1.05
			110.5		2.632E+07		2.78E+07	1.06		2.81E+07	1.07
			114.5		3.364E+07		3.60E+07	1.07		3.64E+07	1.08
			118.5		4.168E+07		4.43E+07	1.06		4.47E+07	1.07
			122.5		5.081E+07		5.29E+07	1.04		5.34E+07	1.05
			125.5		5.862E+07		6.08E+07	1.04		6.12E+07	1.04
			128.5		6.611E+07		6.91E+07	1.05		6.95E+07	1.05
			131.5		7.527E+07		7.42E+07	0.99		7.46E+07	0.99
			134.5		7.857E+07		8.03E+07	1.02		8.06E+07	1.03
			137.5		8.181E+07		8.17E+07	1.00		8.20E+07	1.00
			141.5		7.946E+07		7.94E+07	1.00		7.97E+07	1.00
			145.5		7.187E+07		7.19E+07	1.00		7.21E+07	1.00
			149.5		6.074E+07		6.06E+07	1.00		6.08E+07	1.00
			153.5		4.538E+07		4.34E+07	0.96		4.36E+07	0.96
Core Barrel	-47.25	-18.27	114.5		3.145E+07		3.32E+07	1.06		3.34E+07	1.06
			131.5		6.527E+07		6.64E+07	1.02		6.65E+07	1.02
			145.5		6.317E+07		6.29E+07	1.00		6.29E+07	1.00
Core Barrel	-45.99	-22.05	114.5		2.916E+07		3.10E+07	1.06		3.11E+07	1.07
			131.5		5.782E+07		5.90E+07	1.02		5.91E+07	1.02
			145.5		5.406E+07		5.47E+07	1.01		5.47E+07	1.01
Core Barrel	-44.73	-24.57	106.5		1.616E+07		1.65E+07	1.02		1.66E+07	1.03
			110.5		2.251E+07		2.30E+07	1.02		2.32E+07	1.03
			114.5		2.843E+07		2.93E+07	1.03		2.95E+07	1.04
			118.5		3.422E+07		3.51E+07	1.03		3.53E+07	1.03
			122.5		4.037E+07		4.12E+07	1.02		4.14E+07	1.03
			125.5		4.450E+07		4.58E+07	1.03		4.60E+07	1.03
			128.5		4.936E+07		5.06E+07	1.03		5.08E+07	1.03
			131.5		5.326E+07		5.37E+07	1.01		5.38E+07	1.01
			134.5		5.578E+07		5.68E+07	1.02		5.68E+07	1.02
			137.5		5.706E+07		5.71E+07	1.00		5.71E+07	1.00
			141.5		5.482E+07		5.47E+07	1.00		5.47E+07	1.00
			145.5		4.892E+07		4.90E+07	1.00		4.91E+07	1.00
			149.5		4.325E+07		4.04E+07	0.94		4.05E+07	0.94
			153.5		3.041E+07		2.86E+07	0.94		2.87E+07	0.94

Table 4.14. Calculated-to-Measured (C/M) Ratios for the VENUS-3 Benchmark Experiment
^{115}In(n,n')^{115m}In Equivalent Fission Fluxes using TORT with BUGLE-96 and BUGLE-B7 Cross-Sections

Measurement Zone	Position (cm)				Measured Equivalent Fission Flux**		TORT with BUGLE-96			TORT with BUGLE-B7	
	X	Y	Z*				Equivalent Fission Flux	C/M		Equivalent Fission Flux	C/M
Core Barrel	-42.21	-28.35	106.5		1.696E+07		1.71E+07	1.01		1.74E+07	1.02
			110.5		2.323E+07		2.38E+07	1.02		2.41E+07	1.04
			114.5		2.884E+07		3.02E+07	1.05		3.06E+07	1.06
			118.5		3.446E+07		3.57E+07	1.04		3.62E+07	1.05
			122.5		3.955E+07		4.10E+07	1.04		4.15E+07	1.05
			125.5		4.336E+07		4.47E+07	1.03		4.53E+07	1.04
			128.5		4.667E+07		4.81E+07	1.03		4.87E+07	1.04
			131.5		4.954E+07		5.02E+07	1.01		5.07E+07	1.02
			134.5		5.079E+07		5.18E+07	1.02		5.23E+07	1.03
			137.5		5.121E+07		5.15E+07	1.01		5.20E+07	1.02
			141.5		4.861E+07		4.88E+07	1.00		4.92E+07	1.01
			145.5		4.393E+07		4.37E+07	0.99		4.41E+07	1.00
			149.5		3.846E+07		3.59E+07	0.93		3.63E+07	0.94
			153.5		2.700E+07		2.59E+07	0.96		2.62E+07	0.97
Core Barrel	-38.43	-33.39	114.5		2.928E+07		2.92E+07	1.00		2.97E+07	1.01
			131.5		4.457E+07		4.40E+07	0.99		4.46E+07	1.00
			145.5		3.611E+07		3.66E+07	1.01		3.72E+07	1.03
Core Barrel	-35.91	-35.91	114.5		3.187E+07		3.23E+07	1.01		3.28E+07	1.03
			131.5		4.601E+07		4.61E+07	1.00		4.68E+07	1.02
			145.5		3.651E+07		3.69E+07	1.01		3.75E+07	1.03
Core Barrel	-18.27	-47.25	114.5		7.292E+07		7.40E+07	1.01		7.43E+07	1.02
			131.5		1.001E+08		1.01E+08	1.01		1.02E+08	1.02
			145.5		7.480E+07		7.57E+07	1.01		7.60E+07	1.02
Core Barrel	-0.63	-49.77	106.5		5.576E+07		5.01E+07	0.90		5.05E+07	0.91
			110.5		7.180E+07		7.17E+07	1.00		7.22E+07	1.01
			114.5		8.627E+07		8.79E+07	1.02		8.85E+07	1.03
			118.5		9.990E+07		1.02E+08	1.02		1.02E+08	1.02
			122.5		1.101E+08		1.12E+08	1.02		1.13E+08	1.03
			125.5		1.140E+08		1.17E+08	1.03		1.18E+08	1.04
			128.5		1.168E+08		1.20E+08	1.03		1.21E+08	1.04
			131.5		1.159E+08		1.21E+08	1.04		1.21E+08	1.05
			134.5		1.154E+08		1.18E+08	1.02		1.19E+08	1.03
			137.5		1.111E+08		1.13E+08	1.02		1.14E+08	1.03
			141.5		1.006E+08		1.03E+08	1.03		1.04E+08	1.03
			145.5		8.685E+07		8.96E+07	1.03		9.02E+07	1.04
			149.5		7.624E+07		7.35E+07	0.96		7.40E+07	0.97
			153.5		5.050E+07		5.18E+07	1.03		5.22E+07	1.03

* - The axial extent of the fuel in the TORT model is from 105 cm to 155 cm.
** - The measurement uncertainty for all the ^{115}In(n,n')^{115m}In was 5.5% at the one-sigma level.

Table 4.15. Calculated-to-Measured (C/M) Ratios for the VENUS-3 Benchmark Experiment
^{27}Al(n,α)^{24}Na Equivalent Fission Fluxes using TORT with BUGLE-96 and BUGLE-B7 Cross-Sections

Measurement Zone	Position (cm)				Measured Equivalent Fission Flux**	TORT with BUGLE-96			TORT with BUGLE-B7	
	X	Y	Z*			Equivalent Fission Flux	C/M		Equivalent Fission Flux	C/M
Inner Baffle	-4.41	-4.41	131.5		1.561E+09	1.89E+09	1.21		1.94E+09	1.24
Inner Baffle	-4.41	-0.63	131.5		1.927E+09	1.58E+09	0.82		1.62E+09	0.84
Outer Baffle	-39.69	-0.63	114.5		1.852E+08	1.94E+08	1.05		1.99E+08	1.08
			131.5		4.788E+08	4.76E+08	0.99		4.87E+08	1.02
			145.5		4.765E+08	4.68E+08	0.98		4.78E+08	1.00
Water Gap	-44.73	-0.63	114.5		8.376E+07	8.28E+07	0.99		8.54E+07	1.02
			131.5		1.871E+08	1.71E+08	0.91		1.76E+08	0.94
			145.5		1.782E+08	1.70E+08	0.95		1.74E+08	0.98
Core Barrel	-49.77	-9.45	114.5		3.197E+07	3.49E+07	1.09		3.60E+07	1.13
			131.5		6.316E+07	6.17E+07	0.98		6.36E+07	1.01
			145.5		6.026E+07	5.95E+07	0.99		6.13E+07	1.02
Core Barrel	-49.77	-0.63	114.5		4.110E+07	4.10E+07	1.00		4.24E+07	1.03
			131.5		7.669E+07	7.33E+07	0.96		7.55E+07	0.98
			145.5		7.270E+07	7.11E+07	0.98		7.32E+07	1.01
Core Barrel	-47.25	-18.27	114.5		3.159E+07	3.25E+07	1.03		3.35E+07	1.06
			131.5		6.022E+07	5.76E+07	0.96		5.94E+07	0.99
			145.5		5.705E+07	5.45E+07	0.95		5.61E+07	0.98
Core Barrel	-45.99	-22.05	114.5		3.051E+07	2.98E+07	0.98		3.08E+07	1.01
			131.5		5.328E+07	5.03E+07	0.94		5.18E+07	0.97
			145.5		4.801E+07	4.66E+07	0.97		4.80E+07	1.00
Core Barrel	-44.73	-24.57	114.5		2.753E+07	2.77E+07	1.01		2.86E+07	1.04
			131.5		4.977E+07	4.51E+07	0.91		4.65E+07	0.93
			145.5		4.330E+07	4.14E+07	0.96		4.26E+07	0.98
Core Barrel	-42.21	-28.35	114.5		3.168E+07	3.36E+07	1.06		3.47E+07	1.10
			131.5		5.149E+07	4.96E+07	0.96		5.13E+07	1.00
			145.5		4.350E+07	4.31E+07	0.99		4.45E+07	1.02
Core Barrel	-38.43	-33.39	114.5		3.683E+07	3.45E+07	0.94		3.57E+07	0.97
			131.5		5.481E+07	4.86E+07	0.89		5.02E+07	0.92
			145.5		4.279E+07	4.24E+07	0.99		4.38E+07	1.02
Core Barrel	-35.91	-35.91	114.5		3.807E+07	3.96E+07	1.04		4.09E+07	1.08
			131.5		5.532E+07	5.27E+07	0.95		5.45E+07	0.98
			145.5		4.231E+07	4.39E+07	1.04		4.54E+07	1.07

Table 4.15. Calculated-to-Measured (C/M) Ratios for the VENUS-3 Benchmark Experiment
^{27}Al(n,α)^{24}Na Equivalent Fission Fluxes using TORT with BUGLE-96 and BUGLE-B7 Cross-Sections

Measurement Zone	Position (cm)				Measured Equivalent Fission Flux**		TORT with BUGLE-96			TORT with BUGLE-B7	
	X	Y	Z*				Equivalent Fission Flux	C/M		Equivalent Fission Flux	C/M
Core Barrel	-18.27	-47.25	114.5		6.806E+07		6.48E+07	0.95		6.67E+07	0.98
			131.5		8.915E+07		8.70E+07	0.98		8.95E+07	1.00
			145.5		6.547E+07		6.64E+07	1.01		6.83E+07	1.04
Core Barrel	-0.63	-49.77	114.5		9.554E+07		8.70E+07	0.91		8.96E+07	0.94
			131.5		1.202E+08		1.17E+08	0.97		1.20E+08	1.00
			145.5		8.848E+07		8.86E+07	1.00		9.12E+07	1.03

* - The axial extent of the fuel in the TORT model is from 105 cm to 155 cm.

** - The measurement uncertainty for all the ^{27}Al(n,α)^{24}Na was 7.2% at the one-sigma level.

4.6   Conclusions from Verification and Validation Tests

The VITAMIN-B7 and BUGLE-B7 libraries have been verified and validated by an extensive set of tests and by comparison to benchmark experiments. Although these libraries were not developed for criticality applications, the results of the critical benchmark analyses help to verify the VITAMIN-B7 library by demonstrating agreement with experimental data that is consistent with results obtained using the VITAMIN-B6 library and with results using continuous energy data based on ENDF/B-VII.

The primary application for which the VITAMIN-B7 and BUGLE-B7 libraries were developed is use in LWR shielding analyses, including pressure vessel dosimetry calculations. The shielding benchmarks in Sections 4.4 and 4.5 provide an extensive set of tests of both the VITAMIN-B7 and BUGLE-B7 libraries. These tests include Monte Carlo calculations, two-dimensional and three-dimensional deterministic transport calculations, and the hybrid MAVRIC sequence in SCALE. The results of the shielding benchmarks demonstrate that the VITAMIN-B7 and BUGLE-B7 libraries are appropriate for use in LWR shielding applications.

The calculated dosimetry responses for the pressure vessel dosimetry benchmarks in Section 4.5 using the VITAMIN-B7 and BUGLE-B7 libraries are typically equal to or slightly higher (by up to about 4%) than the responses calculated using VITAMIN-B6 and BUGLE-96. In all the benchmark analyses, the calculated reaction rates are within 20% of the measured data, which is consistent with the calculational uncertainty criterion in Regulatory Guide 1.190.

The differences in the calculated responses for the shielding benchmarks using the VITAMIN-B7 and BUGLE-B7 libraries compared to VITAMIN-B6 and BUGLE-96 are not as pronounced as the changes that occurred when the VITAMIN-B6 and BUGLE-96 libraries were developed. VITAMIN-B6 and BUGLE-96 included significant changes in some ENDF evaluations (particularly iron) which had a considerable effect on pressure vessel dosimetry applications. In comparison, there were no substantial changes to the cross-section data for many of the structural elements (e.g., Fe, Cr, and Ni) in ENDF/B-VII.0 compared to ENDF/B-VI.3.

The results of the benchmark evaluations suggest that VITAMIN-B6, VITAMIN-B7, BUGLE-96, and BUGLE-B7 are all suitable for LWR shielding analyses. While the new libraries do not provide a demonstrable improvement for LWR shielding applications, they provide validated libraries based on the latest version of the Evaluated Nuclear Data File, which enables adherence to Regulatory Guide 1.190.

5 REFERENCES

1) J. E. White et al., *Production and Testing of the Revised VITAMIN-B6 Fine-Group and the BUGLE-96 Broad-Group Neutron/Photon Cross-Section Libraries Derived from ENDF/B-VI.3 Nuclear Data*, NUREG/CR-6214 Revision 1 (ORNL-6795/R1), prepared for the U.S. Nuclear Regulatory Commission by Oak Ridge National Laboratory (April 2000).

2) *Nuclear Data Sheets*, Volume 107, Issue 12, pp. 2931–3060, December 2008.

3) R. W. Roussin et al., *VITAMIN-C: The CTR Processed Multigroup Cross-Section Library for Neutronics Studies*, ORNL/RSIC-37 (1980). Available from the Radiation Safety Information Computational Center at Oak Ridge National Laboratory as DLC-041/VITAMIN-C.

4) D. R. Harris et al., "MINX: A Modular Code System for Processing Multigroup Cross Sections from Nuclear Data in ENDF/B Format," LA-UR-1766 (1973).

5) R. E. MacFarlane and D. W. Muir, "The NJOY Nuclear Data Processing System – Version 91," LA-1270-M (1994).

6) N. M. Greene, W. E. Ford, III, L. M. Petrie, and J. W. Arwood, "AMPX-77: A Modular Code System for Generating Coupled Multigroup Neutron-Gamma Cross-Section Libraries from ENDF/B-IV and/or ENDF/B-V," ORNL/CSD/TM-283, Oak Ridge National Laboratory, October 1992.

7) C. R. Weisbin et al., *VITAMIN-E: An ENDF/B-V Multigroup Cross-Section Library for LMFBR Core and Shield, LWR Shield, Dosimetry, and Fusion Blanket Technology*, ORNL-5505 (February 1979). Available from the Radiation Safety Information Computational Center at Oak Ridge National Laboratory as DLC-113/VITAMIN-E.

8) *SCALE: A Modular Code System for Performing Standardized Computer Analyses for Licensing Evaluation*, ORNL/TM-2005/39, Version 6, Vols. I–III, Oak Ridge National Laboratory, Oak Ridge, Tenn., January 2009. Available from the Radiation Safety Information Computational Center at Oak Ridge National Laboratory as CCC-750.

9) R. W. Roussin, "BUGLE-80: Coupled 47 Neutron, 20 Gamma-Ray, P3, Cross-Section Library for LWR Shielding Calculations," Informal Notes (1980). Available from the Radiation Safety Information Computational Center at Oak Ridge National Laboratory as DLC-075/BUGLE-80.

10) G. L. Simmons, "Analysis of the Browns Ferry Unit 3 Irradiation Experiments," EPRI NP-3719 (November 1984). Available from the Radiation Safety Information Computational Center at Oak Ridge National Laboratory as DLC-076/SAILOR.

11) Regulatory Guide 1.190, *Calculational and Dosimetry Methods for Determining Pressure Vessel Neutron Fluence*, U.S. Nuclear Regulatory Commission (March 2001).

12) ANSI/ANS-6.1.2-1999, *American National Standard Neutron and Gamma-Ray Cross Sections for Nuclear Radiation Protection Calculations for Nuclear Power Plants*, American Nuclear Society, La Grange Park, Illinois.

13) M. E. Dunn and N. M. Greene, "AMPX-2000: A Cross-Section Processing System for Generating Nuclear Data for Criticality Safety Applications," *Trans. Am. Nucl. Soc*., **86**, 118-119 (2002)

14) http://www.nndc.bln.gov

15) Chart of the Nuclides, 16th ed., KAPL, Inc., 2002.

16) ANSI/ANS-6.4-2006, *Nuclear Analysis and Design of Concrete Radiation Shielding for Nuclear Power Plants,* American Nuclear Society, La Grange Park, Illinois.

17) International Reactor Dosimetry File 2002 (IRDF-2002), International Atomic Energy Agency (2006).

18) P. J. Griffin et al., "SNL RML Recommended Dosimetry Cross Section Compendium," SAND92-0094 (November 1993). Available from the Radiation Safety Information Computational Center at Oak Ridge National Laboratory as DLC-178/SNLRML.

19) P. J. Griffin and R. Paviotti-Corcuera, "Summary Report of the Final Technical Meeting on 'International Reactor Dosimetry File: IRDF-2002,'" International Atomic Energy Agency (2003).

20) X-5 Monte Carlo Team, "MCNP—A General Monte Carlo N-Particle Transport Code, Version 5," Los Alamos National Laboratory, LA-UR-03-1987 (2003).

21) *International Handbook of Evaluated Criticality Safety Benchmark Experiments*, NEA/NSC/DOC(95)03, Organization for Economic Co-operation and Development–Nuclear Energy Agency (OECD-NEA) (September 2009).

22) E. Sajo, M. L. Williams, and M. Asgari, "Comparison of Measured and Calculated Neutron Transmission through Steel for a ^{252}Cf Source," *Annals of Nuclear Energy* **20** (9), 585–604 (1993).

23) G. Manturov, Y. Rozhikhin, and L. Trykov, "Neutron and Photon Leakage Spectra from Cf-252 Source at Centers of Six Iron Spheres of Different Diameters" (ALARM-CF-FE-SHIELD-001), *International Handbook of Evaluated Criticality Safety Benchmark Experiments*, *Volume VIII—Criticality Alarm/Shielding Benchmarks*, NEA/NSC/DOC/(95)03, Organization for Economic Cooperation and Development–Nuclear Energy Agency (OECD-NEA) (September 2007).

24) N. E. Hertel, R. H. Johnson, B. W. Wehring, and J. J. Dorning, "Transmission of Fast Neutrons through an Iron Sphere," *Fusion Technology* **9**, 345–361 (March 1986).

25) SINBAD Abstract NEA-1553/26 SBE 13.001.

26) B. Jansky, Z. Turik, E. Novak, J. Kyncl, F. Cvachovec, and P. Tiller, "Comparison of Measured and Calculated Neutron Transmission through Heavy Water for ^{252}Cf Source Placed in the Center of 30 cm Diameter Sphere," *Annals of Nuclear Energy*, **24** (15), 1189-1212 (1997).

27) K. Ueki, A. Ohashi, N. Nariyama, S. Nagayama, T. Fujita, K. Hattori, and Y. Anayama, "Systematic Evaluation of Neutron Shielding Effects for Materials," *Nuclear Science and Engineering* **124**, 455–464 (1996).

28) D. E. Peplow, T. M. Evans and J. C. Wagner, "Simultaneous Optimization of Tallies in Difficult Shielding Problems," *Nuclear Technology* **168** (3), 785−792 (2009).

29) I. Remec and F. B. K. Kam, *H. B. Robinson-2 Pressure Vessel Benchmark*, NUREG/CR-6453 (ORNL/TM-13204), prepared for the U.S. Nuclear Regulatory Commission by Oak Ridge National Laboratory, October 1997.

30) P. Chowdhury, M. L. Williams, and F. B. K. Kam, *Development of a Three-Dimensional Flux Synthesis Program and Comparison with 3-D Transport Theory Results*, NUREG/CR-4984 (ORNL/TM-10503), prepared for the U.S. Nuclear Regulatory Commission by Oak Ridge National Laboratory, January 1988.

31) I. Remec and F. B. K. Kam, *An Update of the Dosimetry Cross-Section Data Base for the Adjustment Code LSL-M2*, ORNL/NRC/LTR-95/20, June 1995.

32) I. Remec and F. B. K. Kam, *Pool Critical Assembly Pressure Vessel Facility Benchmark*, NUREG/CR-6454 (ORNL/TM-13205), prepared for the U.S. Nuclear Regulatory Commission by Oak Ridge National Laboratory, July 1997.

33) R. E. Maerker, *Analysis of the VENUS-3 Experiments*, NUREG/CR-5338 (ORNL/TM-11106), prepared for the U. S. Nuclear Regulatory Commission by Oak Ridge National Laboratory, August 1989.

34) Prediction of Neutron Embrittlement in the Reactor Pressure Vessel, OECD/NEA report 2000.

35) W. A. Rhodes and D. B. Simpson, *The TORT Three-Dimensional Discrete Ordinates Neutron/ Photon Transport Code*, ORNL/TM-13221, October 1997.

NRC FORM 335 (12-2010) NRCMD 3.7	U.S. NUCLEAR REGULATORY COMMISSION	1. REPORT NUMBER (Assigned by NRC, Add Vol., Supp., Rev., and Addendum Numbers, if any.)
	BIBLIOGRAPHIC DATA SHEET *(See instructions on the reverse)*	NUREG/CR-7045

2. TITLE AND SUBTITLE	3. DATE REPORT PUBLISHED	
Production and Testing of the VITAMIN-B7 Fine-Group and BUGLE-B7 Borad-Group Coupled Neutron/Gamma Cross Section Libraries Derived from ENDF/B-VII.0 Nuclear Data	MONTH September	YEAR 2011
	4. FIN OR GRANT NUMBER J4234	

5. AUTHOR(S)	6. TYPE OF REPORT
J. M. Risner, D. Wiarda, M. E. Dunn, T. M. Miller, D. E. Peplow, and B. W. Patton	Technical
	7. PERIOD COVERED *(Inclusive Dates)*

8. PERFORMING ORGANIZATION - NAME AND ADDRESS *(If NRC, provide Division, Office or Region, U.S. Nuclear Regulatory Commission, and mailing address; if contractor, provide name and mailing address.)*

Oak Ridge National Laboratory
Managed by UT-Battelle, LLC
PO Box 2008, Bldg. 5700, MS-6170
Oak Ridge, TN

9. SPONSORING ORGANIZATION - NAME AND ADDRESS *(If NRC, type "Same as above"; if contractor, provide NRC Division, Office or Region, U.S. Nuclear Regulatory Commission, and mailing address.)*

Division of Safety Systems
Office of Nuclear Reactor Regulation
U.S. Nuclear Regulatory Commission
Washington, DC 20555-0001

10. SUPPLEMENTARY NOTES
Bernard Grenier, NRC Project Manager

11. ABSTRACT *(200 words or less)*

New coupled neutron-gamma cross-section libraries have been developed for use in light water reactor (LWR) shielding applications, including pressure vessel dosimetry calculations. The libraries, which were generated using EValuated Nuclear Data File/B Version VII Release 0 (ENDF/B-VII.0), use the same fine-group and broad-group energy structures as the VITAMIN-B6 and BUGLE-96 libraries. The processing methodology used to generate both libraries is based on the methods used to develop VITAMIN-B6 and BUGLE-96 and is consistent with ANSI/ANS 6.1.2. The ENDF data were first processed into the fine-group pseudo-problem-independent VITAMIN-B7 library and then collapsed into the the broad-group BUGLE-B7 library. The VITAMIN-B7 library contains data for 391 nuclides. This represents a signficicant increase compard to the VITAMIN-B6 library, which contained data for 120 nuclides. The BUGLE-B7 library contains data for the same nuclides as BUGLE-96, and maintains the same numeric IDs for those nuclides. The broad-group data includes nuclides which are infinitely dilute and group collapsed using a concrete weighting spectrum, as well as nuclides which are self-shielded and group collapsed using weighting spectra representative of important regions of LWRs. The verification and validation of the new libraries includes a set of critical benchmark experiments, a set of regression tests that are used to evaluated multigroup cross-section libraries in the SCALE code system, and three pressure vessel dosimetry benchmarks. Resuylts of these tests confirm that the new libraries are appropriate for use in LWR shielding analyses and meet the requirements of Regulatory Guide 1.190.

12. KEY WORDS/DESCRIPTORS *(List words or phrases that will assist researchers in locating the report.)*	13. AVAILABILITY STATEMENT unlimited
radiation, shielding, neutron, gamma, cross section, dosimetry, fluence	14. SECURITY CLASSIFICATION
	(This Page) unclassified
	(This Report) unclassified
	15. NUMBER OF PAGES
	16. PRICE

NRC FORM 335 (12-2010)

Printed
on recycled
paper

Federal Recycling Program

NUREG/CR-7045

Production and Testing of the VITAMIN-B7 Fine-Group and BUGLE-B7 Broad-Group Coupled Neutron/Gamma Cross-Section Libraries Derived from ENDF/B-VII.0 Nuclear Data

September 2011